Multi-Response Optimization of Process Parameter during Machining of C69300 Lead-Free Copper Alloy Using Multi-Objective Grey Wolf Algorithm

Etafa Abera Merga

A Thesis Submitted to Department of Mechanical Engineering

School of

Mechanical, Chemical and Materials Engineering

Presented in Partial Fulfillment of the Requirement for the Degree of

Master's in Manufacturing Engineering

Office of Graduate Studies

Adama Science and Technology University

June-2023

Adama, Ethiopia

Multi-Response Optimization of Process Parameter during Machining of C69300 Lead-Free Copper Alloy Using Multi-Objective Grey Wolf Algorithm

Etafa Abera Merga

Under the Supervision and Guidance of

Dr. Moera Gutu Jiru (Associate professor)

A Thesis Submitted to Department of Mechanical Engineering

School of

Mechanical, Chemical and Materials Engineering

Presented in Partial Fulfillment of the Requirement for the Degree of

Master’s in Manufacturing Engineering

Office of Graduate Studies

Adama Science and Technology University

June, 2023

Adama, Ethiopia

DECLARATION

I hereby declare that this Master Thesis entitled **"Multi-Response Optimization of Process Parameter during Machining of C69300 Lead-Free Copper Alloy using multi-objective Grey Wolf Algorithm"** is my original work. That is, it has not been submitted for the award of any academic degree, diploma or certificate in any other university. All sources of materials that are used for this thesis have been duly acknowledged through citation.

Etafa Abera Merg ___________ _________

Candidate Signature Date

RECOMMENDATION

We, the advisors of this thesis, hereby certify that we have read the final version of the thesis entitled **"Multi-Response Optimization of Process Parameter during Machining Of C69300 Lead-Free Copper Alloy using multi-objective Grey Wolf Algorithm"** prepared under our guidance by **Etafa Abera Merga** submitted in partial fulfillment of the requirements for the degree of Mater's of Science in **Manufacturing Engineering**. Therefore, we recommend the submission of the final revised version of the thesis to the department following the applicable procedures.

____________________________	________________________	________________
Advisor	**Signature**	**Date**
____________________________	________________________	________________
Co-advisor	**Signature**	**Date**

APPROVAL SHEET

We, the advisors of the thesis entitled "**Multi-Response Optimization of Process Parameter during Machining of C69300 Lead-Free Copper Alloy using multi-objective Grey Wolf Algorithm**" and developed by **Etafa Abera**, hereby certify that the recommendation and suggestions made by the board of examiners are appropriately incorporated into the final version of the thesis.

______________________	______________________	______________
Major Advisor/Supervisor	Signature	Date
______________________	______________________	______________
Co-advisor/ Co-supervisor	Signature	Date

We, the undersigned, members of the Board of Examiners of the thesis by **Etafa Abera** have read and evaluated the thesis entitled "**Multi-Response Optimization of Process Parameter during Machining Of C69300 Lead-Free Copper Alloy using multi-objective Grey Wolf Algorithm** " and examined the candidate during open defense. This is, therefore, to certify that the thesis is accepted for partial fulfillment of the requirement of the degree of Master of Science in **Manufacturing Engineering.**

______________________	______________________	______________
Chairperson	Signature	Date
______________________	______________________	______________
Internal Examiner	Signature	Date
Dr. Endalkachew Mosisa	[signature]	08/12/15
External Examiner	Signature	Date
______________________	______________________	______________
Department Head	Signature	Date
______________________	______________________	______________
School Dean	Signature	Date
______________________	______________________	______________
Office of Postgraduate Studies, Dean	Signature	Date

ACKNOWLEDGEMENT

Throughout every step of preparing this thesis, I would like to thank God as without his help nothing can be done. Furthermore, I am grateful to my advisor Dr. Moera Gutu (Associate professor) in the Department of Mechanical Engineering, Adama Science and Technology University for his tremendous assistance and suggestions. Working with him has been a rewarding experience, and I feel extremely fortunate to have had such a dedicated and experienced Advisor. My heartfelt gratitude also goes out to my Teacher, Dr.Devendra Kumar Sinha, Assistant Professor in the Department of Mechanical Engineering, Adama Science and Technology University, for his help in facilitating materials for this study from India.

Furthermore, I'd like to thank Adama Science and Technology University for giving the financing for my study work, as well as Ethiopian Technical University for kindly providing lab facilities to conduct the necessary experiments. Finally, I'd like to express my appreciation and admiration to everyone who has contributed directly or indirectly to the accomplishment of this thesis.

TABLE OF CONTENTS

LIST OF FIGURES PAGE

LISTS OF TABLE PAGE

LIST OF ACRONYMS AND ABBREVATION

CNC:	Computer Numerical Control
PB:	Lead Element
OA:	Orthogonal array
GWO:	Grey Wolf Algorithm Optimization
GA:	Genetic Algorithm
MRR:	Material Removal Rate
DOE:	Design Of Experiment
CVD:	Chemical Vapor Deposition
MQL:	Minimum Quantity Lubrication
PCD:	Polycrystalline Coated Diamond
MOPSO:	multiple objective particle swarm optimization
2D:	Two dimension
HSS:	High speed steel
LCD:	Liquid Crystal Display
ASTM:	American Society for Testing and Materials
ANN:	Artificial Neural Network
S/N:	Signal to Noise Ratio
V:	Cutting Speed
F:	Feed rate
D:	depth of cut
AGOA:	Artificial grey wolf optimization algorithm

ABSTRACT

In machining processes, limiting the use of resources such as energy, tools, price, and production time while maximizing process outputs such as surface quality and productivity has a substantial impact on the environment, process sustainability, and profit. This study addresses the use of advanced multi-objective Grey Wolf optimization Algorithm to optimize turning-process parameters, specifically cutting speed, feed rate, and depth of cut, in the dry machining of C69300 lead-free copper alloy for a high-efficiency process. The C69300 Lead-Free copper alloy has strong corrosion resistance and resistance to stress related corrosion cracking which makes this material applicable in many areas. Since C69300 is lead-free, this material conforms to the International safety regulations. However, the machining of this material is difficult due to the absence of lead in the materials. In this study, the L16 Taguchi Orthogonal Array design was used to conduct sixteen experimental tests on a CNC machine in which cutting temperatures, material removal rate and surface roughness was determined as main responses characteristics from range of input cutting parameters (cutting speed, Feed rate and depth of cut). The level of significance of machining parameters was determined using analysis of variance (ANOVA). It has been determined that the most significant factor influencing surface roughness was feed rate, whereas the most significant factor influencing the cutting temperature was cutting speed. The feed rate was the most significant factor affecting the Material removal rate. Next, the regression model was developed for each responses using Minitab software to formulate the relationships between the process parameters and the considered three response parameters. The multi-objective Grey wolf optimization (MOGWO) technique was employed to simultaneously optimize surface roughness, material removal rate and cutting temperature. The full range of objective functions was covered by MOGWO, and the produced Pareto front was quite close to the real Pareto front. Using the Multi-Criteria Decision Making (MCDM) technique (VIKOR method), the best choice from the Pareto solution set was selected based on the higher level information. Higher-level information was implemented by giving equal preference for three responses and the obtained solution was given as: surface roughness 3.7µm, Cutting temperature 45.2^{0}C and material removal rate 11859.85mm^3/min. The corresponding input cutting parameters were cutting speed 64.6 m/min, Feed rate 0.15 mm/rev and depth of cut 1.24 mm. In addition, three confirmatory tests were performed to evaluate the performance of the derived Pareto front solutions. The percentage error between predicted and experimental values was less than 10% for all responses investigated, indicating that the acquired real Pareto front solutions were encouraging in enhancing machining performance during dry turning of C69300 lead-free copper alloy.

Keywords: *Surface Roughness; Material Removal Rate; Cutting Temperature; Grey Wolf Optimization; VIKOR; Lead-Free Brasses; Environmentally Friendly; Machinability.*

CHAPTER ONE

1. INTRODUCTION

1.1 Background of the Study

It is challenging to machine pure copper because of its high ductility, plasticity, and toughness. Copper's machinability is enhanced by alloying it with zinc, tin, lead, silicon, or nickel, making copper alloys even simpler to machine than the majority of other metallic materials (Chruściński et al., 2021). When compared to machining steels or aluminum alloys of comparable strength, these alloys require significantly less cutting force. Among those elements alloyed with copper, lead has traditionally been used to lubricate cutting tools and allow chips to flow freely to enhance the machinability of copper alloys and other metals. Copper alloys frequently contain lead (Pb) to ensure pressure tightness and enhance machinability, both of which have a direct impact on cutting tool life. As a result, these lead particles increase the machinability of copper alloy by serving as both a stress concentration point and a lubricant, encouraging the formation of small discontinuous chips and reducing tool wear (Johansson et al., 2022; Toulfatzis et al., 2016; Pantazopoulos, 2002). As a result, leaded copper has been utilized extensively in plumbing projects as well as the base material for architectural hardware, bearings, gears, shafts, worm gears, bushings, corrosion-resistant/pressure-tight castings, high-speed/high-pressure bearings, impellers, pumps, cosmetics, musical instruments, screw machine parts, valves, pipe fittings, and general fasteners.

For free-machining additions to brasses and bronzes, lead was the preferred material until recently. Over 90% of the machinability of copper alloys is related to lead alloys (Johansson et al., 2022)and extensive research has been carried out to find out how lead affects the machinability of copper alloys. The two main copper alloys, bronze and brass, are made easier to process by the addition of lead. However, it was determined that lead in the alloys may poison any humans who come into contact with them. Lead poisoning is frequently linked to developmental abnormalities of the mind and behavior. It can also result in gastrointestinal difficulties, blood illnesses, and other issues.

All cast members have to comply with the federal Safe Drinking Water Act (2011). According to the federal Safe Drinking Water Act of 2011, all cast copper parts used in potable water applications have to have a lead content of less than 0.25%. To support global public health objectives, the copper alloy industry actively developed several "lead-free" alloys that are suited for a variety of products. Even though the fact that lead helps copper alloys to machine more easily, environmental health and safety rules have recently banned the use of dangerous elements like lead in critical manufacturing processes and consumer goods. Hence, replacing it immediately is important (Schultheiss et al., 2018). The evaluation concentrated on two main strategies to recapture the lead's advantageous effects. The first one is the development of novel copper compositions as well as a route that is compositionally invariant, and the second approach is based on a series of heat treatments.

The objective of compositional modification is to replicate the beneficial effects of Pb by incorporating particles from the second phase, whereas the objective of the alternative method is to stabilize the β -phase. In general, it has been demonstrated that novel compositions outperform conventional ones in terms of their mechanical properties. The ability to incorporate a wide range of alloying elements allows for a variety of strengthening mechanisms to emerge. In a similar vein, when compared to conventional leaded compositions, the β -stabilized heat treated Pb-free conventional compositions exhibited an increase in strength and hardness at the expense of ductility (Schultheiss et al., 2018 ; Oishi et al., 2023). The majority of the new compositions, however, lacked machinability when compared to conventional lead-based copper alloys, and only a small minority of them did so while maintaining acceptable mechanical qualities. So, it is believed that producing alloys that may include both design characteristics will be the most effective way to create the next generation of lead-free copper alloys.

Considering the aforementioned restrictions and the environmental needs of the current legislation, several recent recommendations for a variety of design combinations as alternatives to traditional leaded copper alloy have been reported in the preceding sentence. Hence, it shouldn't be surprising that using lead-free alloys with the same conventional machining settings, cutting tools, and production techniques that were designed to perform best for free-machining leaded copper alloy might result in production issues and increase operating costs. Nevertheless, many of the common challenges posed by the materials can be addressed by using quicker, more potent machine tools and aggressive machining conditions.

In comparison to alternatives like steel and stainless steel, shops can use the high-speed machining capabilities of lead-free alloys with contemporary machining solutions to offset the costs of raw materials with higher throughput, increased production capacity, longer tool life, lower costs per part, and a higher scrap value. The following pathways are therefore recommended for further applicable research. The use of cutting parameter optimization techniques like the genetic algorithm (GA) and Grey Wolf algorithm (GWO) to improve the significant quality attributes (chip morphology, power utilization, cutting power, and surface roughness) for the process ability of nonleaded copper combinations has become a crucial strategy to overcome difficulties during the machining of this alloy. It is crucial to optimize and validate industrial-scale cutting conditions, a growing area of research, for the production of model final copper alloy industrial components using intricate machining techniques like CNC machining centers. This thesis primarily focuses on the lead-free copper alloy's machinability and process parameter optimization to overcome the aforementioned difficulties.

1.2 Outline of the elements used to replace lead in copper alloys.

One of the most common lead substitutes used as a free machining addition in lead-free copper alloys is bismuth. It has a low melting point and is practically insoluble in copper, much like lead. Although it isolates near the grain limits due to its lower dissolving point and dissolvability in copper, bismuth replaces lead in the mentioned sans-lead combinations, increases the machinability and strained snugness features, and is not known to be harmful to human beings (Chruciski et al., 2021; Tesfay Reda et al., 2021). Due to its effect on machinability, selenium is also used as an alloying element in several lead-free alloys. Initial research conducted at the Asarco Technical Center in Salt Lake City revealed that the alloy's machinability is significantly improved and the amount of bismuth in the alloy is decreased when selenium and bismuth are combined in brass casting applications.

To achieve acceptable machinability in lead-free copper alloys, Si can also be used in place of Pb (Oishi et al., 2023 ; Chruściński et al., 2021; Tesfay Reda et al., 2021). However, their high price, complex technology, and poor cutting ability due to silicon's abrasive properties may be drawbacks. Additionally, recent research concentrated on employing a powder metallurgical method to create lead-free, graphite-infused brass that can be utilized in machines. This is how the idea works: A common solid lubricant with an abrasive character is graphite. Because it is affordable and environmentally friendly, it can be used as an element that can be machined in brass alloys. However, utilizing the ingot metallurgy method, it is challenging to equally distribute graphite particles throughout the brass matrix because of the significant density difference between graphite and brass alloy (Zhao et al., 2007). Several patented lead-free copper alloys are available on the market. However, it's crucial to remember that the majority of them almost always contain bismuth. Bismuth silicon and selenium were often the only choices available to replace lead.

1.3 Application Area of lead-free copper alloy

Lead-free copper alloys are becoming more and more useful in the manufacturing and engineering sectors due to their improved mechanical qualities, corrosion resistance, and cost. Lead-free bronze and brass are the two primary subtypes of lead-free copper alloys. Depending on the use, the ratio of the two major metals (copper and zinc or copper and tin) will change in both bronze and brass. For machining applications with lead-free brass, for example, a high copper percentage and some other metals are recommended, but higher zinc content is preferable for applications requiring strength. Other metals, such as manganese and aluminum, can be applied to improve certain qualities (e.g., corrosion resistance). The elemental composition of lead-free brass is crucial. This alloy's affordability, machinability, and light weight are comparable to those of conventional metals. Lead-free brass's composition is important. Lead is not used in great amounts to make lead-free brass, yet this alloy is still as cost-effective, Machine able, and light as traditional leaded brasses. Lead-free brass frequently has more copper and less zinc than leaded varieties, creating a stronger component that might be better able to resist corrosion. Lead-free brass is less malleable than lead-containing brass; nevertheless, because of its reduced lead concentration. Lead-free copper alloy is not only a better option for the environment, but it can also be used in applications such as food packaging where lead could create safety risks.

Figure 1.1: Some Applications area of lead-free copper alloys

Alloys of copper sans lead provide further advantages besides safety. They have great thermal conductivity and a high level of corrosion resistance, making them the perfect choice for applications that need heat exchange or electrical conductivity. Moreover, they are reasonably simple to manufacture into complex shapes and have excellent abrasion resistance. Lead-free brass alloys can be easily soldered or welded with conventional procedures, however it should be kept in mind that due to heat treatment, these processes will somewhat reduce the alloy's strength. Lead-free brass alloys often cost less than regular brass alloys because lead cannot be removed from the alloy without further processing (like smelting). As a result, bushings, bearings, gears, shafts, worm gears, architectural hardware, corrosion-resistant/pressure-tight castings, high-speed/high-pressure bearings, impellers, pumps, cosmetics, musical instruments, screw machine parts, and other components are commonly produced of leaded free copper.

1.4 Machining process

A wide range of production-related technologies and techniques are referred to as "machining." It can be broadly defined as the process of removing material from a work piece using machine tools that are powered by an external source to shape it into the desired form. A controlled material-removal approach enables material (usually metal) to be shaped and sized to the proper final form throughout the machining process. Nowadays, machining is necessary for the vast majority of metal parts and components. The fabrication of additional materials using machining procedures, such as plastics, rubber, and paper goods, is also a prevalent activity.

1.4.1 Types of machining processes

Machining processes are mainly divided into three types traditional, abrasive and non-traditional.

- **Traditional machining** techniques are those that have been in use since the dawn of time. They are employed in the production of practically every common type of product. These procedures include turning, drilling, lapping, and others.
- **Abrasive machining** is a type of machining in which a large number of tiny abrasive particles are used to remove material from a workpiece. Examples frequently used are polishing, honing, and grinding. Although expensive, abrasive methods can produce parts with tighter tolerances and a better surface polish than other machining techniques.
- **Non-traditional machining** techniques are those that aren't commonly employed and are only applied to really high-quality engineering projects. Electric discharge machining (EDM), electrochemical machining (ECM), and other non-traditional material removal techniques are examples.

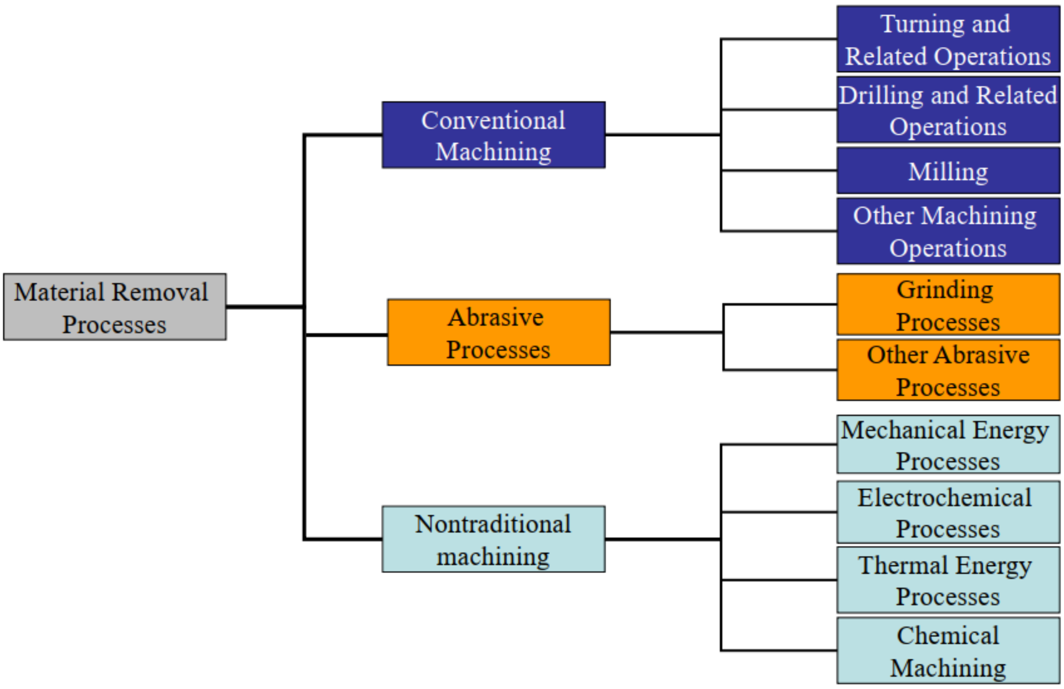

Figure 1.2: Classification of the material removal process

The three primary types of machining are turning, drilling, and milling. Shaping, planning, drilling, broaching, and sawing are other processes that can be broken down into numerous categories.

- **Turning operations** are those in which the primary means of advancing metal against the cutting tool is the rotation of the work pieces. The main piece of machinery used for turning is a lathe.
- **Milling operations** involve rotating the cutting tool to press the cutting edges against the work piece. The main piece of machinery used in milling is a milling machine.
- **Drilling operations** are those in which holes are created or honed by contacting the work piece with a spinning cutter that has cutting edges at the lower extremity. Although occasionally on lathes or mills, drill operations are mostly performed in drill presses.
- Although not precisely machining because they don't necessarily produce dwarf, auxiliary operations are still carried out on a standard machine tool. A lathe, mill, or drill press can be used for burnishing, which creates no swarf. These operations are called Miscellaneous operations

1.4.2 Cutting conditions

The tool and the work must move relative to one another to carry out a machining operation. The main action is carried out at a set cutting speed. Moreover, the tool must be lateralized across the work piece. The term for this noticeably slower activity is the feed. How deep the cutting tool penetrates below the initial work surface is measured by the depth of cut, also known as the remaining dimension of the cut. The combination of speed, feed, and cut depth is referred to as the cutting parameters. They design the three machining axes, and for specific procedures, users may use their product to figure out how much material is removed per unit of time. According to the intended use and the cutting conditions, machining processes are typically divided into two categories, Final cuts and Rough cuts. To produce a shape that is close to the desired shape, roughing cuts are used to remove a significant amount of material from the starting work part as quickly as possible, i.e., with a large Material Removal Rate (MRR), while still leaving some material on the piece for a subsequent finishing operation. To provide the product with the desired final dimension, tolerances, and surface quality, finishing cuts are employed. During production machining operations, the item frequently goes through one or more roughing cuts followed by one or two finishing cuts.

Turning operations

A turning operation is employed when the surface of a work piece needs to be machined to the required diameter. In other words, excess material is removed from the external diameter of a work piece or cylindrical surface.

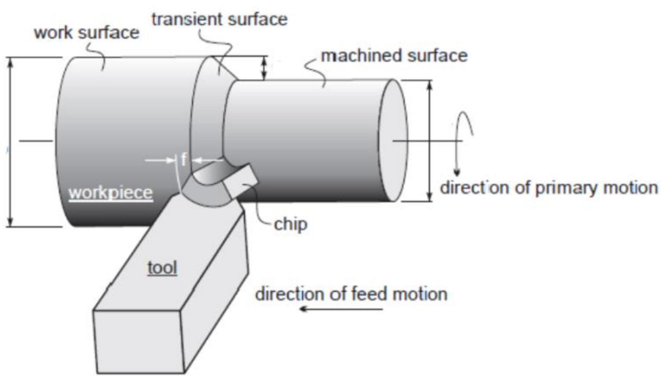

Figure 1.3: Turning operation on a round work piece

A. Cutting Parameters in Turning Operation

Many parameters are used to specify the cutting tool speed and turning speed. These parameters are chosen for each operation depending on the material of the work piece, the tool, the tool size, and other factors.

- **Cutting Feed:** The cutting feed is the movement of the work piece or cutting tool during one spindle rotation, and it is typically measured in inches per revolution (IPR). For a multi-point tool, the cutting feed, which is expressed in inches per tooth, is also equal to the feed per tooth (IPT).
- **Cutting speed**: which is expressed in surface feet per minute (SFM), refers to how quickly the work piece's surface is being sliced in relation to the cutting tool's edges.
- **Spindle Speed:** This refers to how quickly the spindle and work piece rotate in revolutions per minute (RPM). Calculating spindle speed involves dividing the cutting speed by the work piece's circumference.
- **Feed Rate:** Measured in inches per minute, this is the rate at which the cutting tool moves with respect to the work piece as it cuts (IPM).
- **Axial Depth of Cut:** During a facing operation, the tool's depth along the work piece's axis is measured. A lower feed rate will be necessary for a deeper axial cut. If not, it will lead to a heavier tool load and a shorter tool life.

Table 1.1: Summary of turning equations

Parameters	**Equations**	**Description**
Rotational Speed: N(RPM's)	$N = \frac{V}{\pi DO}$	N= Rotational Speed (RPM's), v= Cutting Speed (SFPM), DO=Original Diameter.
Feed Rate: f_r (Dist/Min)	$f_r = N\ f$	f_r = Feed Rate (Dist/Min) N = Rotational Speed (RPM's) f = Feed (Dist/Rev)
Machining Time (Min.)	$Tm = \frac{L}{fr}$	Tm = Machining Time (Min.) L = Length of Cut f_r = Feed Rate (In./Min.)
Material Removal Rate (in. cu./Min)	MRR = v f d	MRR = Material Removal Rate (in.cu./Min), v = Cutting Speed (SFPM), f = Feed (Dist./Rev.) d = Depth of Cut

Depth of Cut	$d = \frac{Do - Df}{2}$	DO = Original Diameter, Df = Final Diameter d = Depth of Cut

A. Overview of Quality/Performance characteristic to be optimized in this study

- **Material removal rate**

The volume of material removed per unit of time during the machining process is referred to as the material removal rate (MRR). The material removal rate (MRR) of a turning operation measures how well the work piece is cut on the lathe. Also, the amount of material removed (MRR) is a clear indication of how effectively cutting machines are used in industrial activities. The profit increases as more material is removed. Consequently, it is important to enhance the rate of material removal during the machining process to increase profit. The Material removal rate is measured in mm^3/s, cm^3/min or in^3/min. The following table provides a common calculation of material removal.

- **surface roughness**

Surface roughness is a good way to judge how well a part has been machined. The relative smoothness of a surface's profile is calculated as surface roughness. The Ra surface finish chart displays the geometric mean of surface heights obtained across a surface. Surface roughness, in this example after CNC machining, is a measurement of the typical texture of a part's surface. To define surface roughness, various criteria are utilized. One of them that is used the most frequently is Ra (Roughness average), which is generated from the variations in heights and depths on a surface. Microscopically, Ra surface roughness is measured in micrometers (x 10^{-6} m), typically you should be aware that surface roughness in this context differs from surface polish. Several finishing techniques, including anodizing, bead blasting, and electroplating, can be used to increase the surface finish of a machined object. As machined surface texture of a part is referred to as surface roughness in this context. Certain Ra values are defined in ISO4287 as industry standards for the manufacturing sector. These values can be entered during CNC machining. All types of manufacturing and post-processing processes can use them; their range is 25 um to 0.025 um. We can produce more high-quality goods the less surface roughness there is. Hence, if you want to produce high-quality products, you should minimize this parameter.

- **Cutting temperature.**

During machining operations, a large amount of heat is created as a result of plastic deformation, which takes place in a very small area of the cutting tool. The work piece surface integrity and quality, chip formation mechanisms, tool wear, and tool life are all significantly impacted by this high temperature. It is essential to be aware of the temperature at various locations on the tool, chip, and work piece during the machining processes to properly optimize cutting parameters, improve machinability and product quality, and decrease machining costs, and increase tool life and productivity. In general, high cutting temperatures are bad for the tool and the work, especially when they are high. The heat is largely absorbed by the chips. But it doesn't matter because the chips are hurled. Hence, efforts should be taken such that the heat is gradually removed by the chips, leaving just a tiny quantity of heat to injure the tool and the work piece. Reduce the cutting temperature as much as possible to produce high-quality goods. The following are some potential consequences of a high cutting temperature on a cutting edge:

- Rapid tool wear, which reduces tool life
- Plastic deformation of cutting edges if the tool materials are not enough hard and strong
- Thermal flaking and fracturing of cutting edges due to thermal shocks
- Builti-up edge formation

The possible detrimental effects of cutting temperature on the machined work piece are

- Dimensional inaccuracy of the job due to thermal distortion and expansion-contraction during and after machining
- Surface damage by oxidation, rapid corrosion, burning etc.
- Induction of tensile residual stresses and micro-cracks at the surface and sub-surfaces

1.5 Problem Statement

The development of lead-free copper alloys is a key area of research due to the environmental and health hazards associated with lead. However, the amount of lead in a copper alloy greatly influences its machinability. Lead is added to copper alloys to improve its machinability. Lead plays two roles in copper alloys: it works as a lubricant and in free machining grades, it facilitates in chip break apart (Amaral et al., 2018). However, lead cannot be used in any material in some applications, such as those involving parts that come into contact with drinking water. Therefore, Copper alloys manufacturers have developed a number of "without lead" and "low lead" combinations that can be used in many applications. Since the use of environmentally acceptable lead-free copper alloys is becoming a requirement in many industries, manufacturers must adapt their machining processes immediately to this new reality. Bismuth, silicon, and selenium are elements that are utilized to replace lead in lead-free copper alloys to improve machinability (Oishi et al., 2023). In contrast to typical leaded copper alloys, the majority of the new compositions experienced machinability concerns, and only a small number of them have good machinability properties while keeping acceptable mechanical properties (Adineh et al., 2019). When lead-free copper alloys are machined with parameters optimized for leaded copper alloys, the material's machinability suffers, resulting in higher cutting force, longer chips, and increased tool wear (Amaral et al., 2018).

Many of the challenging issues associated with the materials can be resolved by employing faster, more powerful machine tools and more aggressive machining parameters. Simultaneous "multi-objective" optimization of the major quality characteristics (chip morphology, power consumption, material removal rate, cutting force, and surface roughness) by utilizing advanced optimization techniques, for the machining of lead-free brass alloys has become a future research area due to the continuous production of the lead-free brass and bronze alloy by copper alloy industry. This study explored the machinability and simultaneous "multi-objective" optimization of the major quality characteristics (material removal rate, cutting temperature and surface roughness) of C69300 lead-free copper alloy to solve those issues raised above.

1.6 Objectives of the Study

1.6.1 General Objectives

The general objective of this study was to simultaneously optimize the material removal rate, cutting temperature, and surface roughness during machining of the C69300 lead-free copper alloy using multi-objective Grey Wolf Algorithm.

1.6.2 Specific Objectives

The followings are the specific objectives of this research:

1. To investigate the machinability of lead-free C69300 copper alloy and, using DOE, determine the most significant factors affecting surface roughness, cutting temperature and material removal rate during CNC turning of C69300 Lead-Free Copper Alloy.

2. To Simultaneous optimize the major quality characteristics (material removal rate, cutting temperature and surface roughness) using multi-objective Grey Wolf Algorithm (MOGA).
3. To select the best solution from the set of multi-objective solutions by using VIKOR Multi-Criteria Decision Making Techniques.
4. To analyze chip morphology while CNC machining C69300 Lead-Free Copper Alloy (brass alloy).

1.7 Significance of the Study

To support global programs for general well-being, the copper alloy industry actively produced various "lead-free" and "low lead" combinations that are suitable for numerous applications. Comparing produced the new compositions to conventional leaded copper alloys, the majority of them lacked machinability, and just a few of them did so while also exhibiting acceptable mechanical properties. As a result, it shouldn't come as a surprise that using lead-free alloys with the same standard machining parameters, cutting tools, and manufacturing procedures that were developed to work well for free-machining leaded copper alloy can result in higher production costs. To reduce the challenges involved with the machining of the lead-free copper alloy, which is produced to adhere to strict regulations, the proposed study investigated the machinability of the C69300 lead-free silicon brass and multi-objective optimization of cutting parameters. As a result, it offers enormous individual and organizational benefits for people and other stakeholders. It will help me better understand the theoretical and applied knowledge in the research field. Also, this study has benefits for future researchers, manufacturing firms that need this lead-free copper alloy material, and students studying this topic.

1.8 Motivations

Companies are obligated by international safety standards to remove lead from material compositions because lead absorption causes a possible health risk. Lead-free copper alloys are becoming increasingly popular, which puts manufacturers under pressure to change their casting and machining techniques as soon as possible. Lead has been used in machining to help with chip control, acting as a natural chip breaker and lowering tool wear. As a result, the decreased lead content in copper alloys causes the materials to be less Machine able, which increases cutting forces, lengthy chips, and tool wear. Numerous recent proposals for a variety of design combinations as well as real legislation have been made in conformity with the aforementioned restrictions and environmental standards. In general, when transitioning from leaded copper alloys to lead-free alloys, it is crucial to consider the differences in their properties and adjust machining settings, cutting tools, and production techniques accordingly. Employing the same conventional methods designed for free-machining leaded copper alloys can lead to production issues and increased operating costs. Optimization of the machining process for lead-free alloys requires careful evaluation and adjustment to ensure efficient and cost-effective production.

In addition, many of the normal challenges posed by the materials can be solved by using quicker, more potent machine tools and aggressive machining conditions. Since cutting temperature is vital sign for the sustainability of any machining system whereas the productivity index includes material removal rate (MRR) and surface roughness (Ra), these major output characteristics must be optimized simultaneously. This study is based on the concept that to increase the productivity, efficiency, and sustainability of machining processes, these major output characteristics must be optimized simultaneously. To fully take use of the optimized values of other machining parameters, dry-cutting circumstances are invested as an input variable. Due to the nature of individual responses, the multi-objective Grey Wolf optimization technique is used to emphasize the significance of Multi-Objective Optimization (MOGA) .This method has already been used with various materials or a different set of parameters (Abbas et al., 2023 ; Kumar et al., 2022 ; Fountas et al., 2019 ; Subbaiah, 2022). The purpose is to develop and optimize a multi-objective function in terms of input parameters that are concurrently sustainable, productive, and efficient. Generally, the main motivation for doing this study is to show how industries must modify machining processes to reflect the fact that using green lead-free copper alloys is increasingly required in many applications. To increase production capacity, extend tool life, reduce cost per part, and increase throughput, it is crucial to optimize and validate the cutting conditions on an industrial scale when fabricating an example of a final lead-free copper alloy industrial component using sophisticated machining operations (like a CNC machining center). This study examines the processing-ability and parameter optimization of silicon brass lead-free copper alloy to address the aforementioned issues in general.

1.9 The Expected outcome of the study

This exploration essentially focuses on researching machinability and enhancement of the cutting parameter of C69300 lead-free silicon brass sans lead copper alloy.

In this research paper number of outcomes will be expected such as:-

- To investigate the cutting parameters that have the greatest impact on surface finish and material removal while machining lead-free brass alloy.
- This study will also be important to obtain the best cutting parameters that produce a high surface finish and material removal rate while machining lead-free brass alloy to make high-quality products with greater amount of production.
- To inform the metal product industry of the ideal cutting parameters that result in a high surface finish and simplify the process in terms of both cost and quality while machining C69300 lead-free brass alloy.

1.10 Scope of the Study

The scope of this study is to identify the most significant cutting parameters that affect surface roughness , cutting temperature and material removal rate and Simultaneous "multi-objective" optimization of the major quality characteristics (material removal rate, cutting temperature and surface roughness) during CNC turning of the C69300 lead-free silicon brass alloy. Moreover, Chip morphology will be also analyzed in this study.

1.11 Structure of the Thesis

This study entitled experimental and numerical investigation of dry machining of C69300 lead-free copper alloy using CNC lathe machine and is organized into five chapters.

- ✓ Chapter one of the thesis is an introduction with an overview of the chosen work piece and cutting condition, the statement's problem, its significance and objectives, and finally its scope and limitations.
- ✓ Chapter two provides an overview of previous research work related to this research, and the summary of the literature with the research gap is described.
- ✓ Chapter three discusses the materials and methodologies used in this research study. This includes detailed information about the work piece and cutting tool used machines and equipment used, and the experimental procedure followed.
- ✓ In Chapter four, the main results of experimental studies and predictions are presented together with a detailed discussion. This chapter examines the effects of cutting parameters (spindle speed, depth of cut, and feed rate) on surface roughness, material removal rate, tool temperature and flank wear.
- ✓ At the last the whole study's conclusion, recommendations, and future research directions were given

CHAPTER TWO

2. LITERATURE REVIEW

2.1 Introduction

Until recently, lead was the free-machining addition material of choice for brasses and bronzes. Lead alloys account for about 90% of the machinability of copper alloys (Stoddart et al., 1979) and a great deal of research has been conducted to learn more about how lead affects the ease with which copper alloys can be machined. Even though lead plays an important role to make copper alloys to be machined easily, the use of hazardous materials like lead in essential manufacturing fields and consumer goods was recently restricted by environmental health and safety regulations. The idea of removing lead (Pb) from brass and bronze alloys has had a significant effect on their machinability, overall quality, and manufacturing process efficiency. The replacement of lead-containing copper alloy with a lead-free alternative does not appear to be economically viable from a manufacturing–economic standpoint; however, it is technically possible and satisfies the requirements of the enforced legislation (Schultheiss et al., 2018). Adjusting novel materials and handling courses in the green economy is a crucial choice for competitive business and industry development, according to a global perspective with significant modern and social impact.

To improve the machinability of lead-free copper alloys, a lot of recent proposals for various design combinations as alternatives to standard leaded copper alloy have been reported in the literature in accordance with the aforementioned limitations and environmental requirements of actual legislation. As a free machining additive in lead-free copper alloy, bismuth and silicon are the main lead replacements. Bismuth has a low melting point and is nearly insoluble in copper, just like lead (Chruściński et al., 2021; Tesfay Reda et al., 2021). In lead-free copper alloys, Si can also replace Pb to achieve good machinability (Taha et al., 2012). However, their high cost, intricate technology, and weak cutting properties due to the abrasive nature of silicon may be disadvantaged. The copper alloy industry proactively made various "without lead" and "low lead" combinations that are suitable for many parts to help general well-being programs all over the world. However, unlike conventional leaded copper alloy, the majority of the novel compositions faced in challenge machinability, and only a few of them combined machinability with acceptable mechanical properties. As a result, a variety of studies on machinability of lead-free copper alloys (brass) and related alloys are included in the following articles to learn about their successes in resolving machining issues in this area. There have been numerous studies regarding to the machinability study of lead-free copper alloys and some advancements have been achieved in this area. Some of these studies are presented in the following section and they are categorized according to their specific study area.

2.2 Machinability review of lead-free copper alloy

The factors affecting the machining of lead-free copper alloys are reviewed in this chapter. These factors are the machining responses produced and the cutting variables employed during the machining of lead-free copper alloys. The cutting parameters (cutting speed, feed rate, and depth of cut), coolant, and cutting tools are the primary cutting factors during machining. Surface roughness, tool wear, and cutting forces are the three major machining responses. The following major topics will be explored in this chapter:

- Chip Formed and the recommended cutting tool and tool wear when machining lead-free copper alloys.
- When cutting lead-free copper alloy, cutting force developed and achievable surface roughness.
- Suggestions for dry machining when working with the lead-free copper alloy.

The viewpoints of various researchers are provided and thoroughly reviewed in each subtopic.

2.2.1 Cutting Force and Surface Roughness

Morteza Adineh. (2021) used a novel technology, an artificial neural network, and the cuckoo algorithm, to forecast and optimize the major cutting forces when turning various Si brass alloys. As part of his research, he examined the principal cutting forces of various as cast Si brass alloys under a variety of operational situations, including cutting speed, feed rate, and depth of cut. The ANN-COA technique was shown to be beneficial for modeling and optimizing the principal cutting force. To apply the ANN-COA model and obtain the least quantities of main cutting force, the genetic algorithm (GA) was applied to discover the best condition of the input parameters. When the input variables Cu = 68.5 wt%, Zn = 28.78 wt%, Si = 2.72 wt%, CS = 86.78 m min-1, FR = 0.18 mm rev-1, and Doc = 0.66 mm are combined, the main cutting force can be reduced as little as feasible.

Ebrahim et al. (2020) used surface roughness as response parameters to investigate the machinability Free Cutting Brass (CuZn35Pb3) .Using Taguchi Method and dry turning operation he also optimize surface roughness as well. According to his study, the optimum surface roughness was obtained at higher cutting speed (50 m/min), lower feed (0.3 mm/rev) and higher depth of cut (3.5 mm). The minimum surface roughness at optimum turning parameters was obtained as 1.63 µm. The Result of variance indicates the contribution of cutting speed; feed and depth of cut were 88.74%, 1.13% and 6.46% respectively. Among which cutting speed was the most significant factor for improving surface roughness.

S/N ratio and ANOVA Were employed to obtain the optimum cutting parameter in turning of C352 Brass Alloy bars using HSS cutting tools. Based on S/N ratio and ANOVA analyses, it is concluded that, the optimum value for cutting force (CF), surface roughness (SR) and cutting temperature (CT) are 9.4 kgf, 1.9 mm and 59 C respectively and corresponding cutting parameters are, cutting speed (s) = 900 rpm, depth of cut (d) = 0.15 mm and feed rate (f) = 0.3 mm/rev (Yadu Krishnan et al., 2020) .

Mer Seçgin. (Seçgin, 2021) used a Multi-axis CNC Lathe to perform a multi-objective optimization of the Ms58 Brass Machining Operation. As machining parameters in this study, rotation speed, feed rate, and tool diameter were used. These parameters' effects on average surface roughness (Ra), cutting time (t), and dimensional deviation (dev) have been determined using the surface response method. The feed rate was shown to be the most influential factor in reducing time. The optimal machining parameter combination was 10 mm tool diameter, 150 mm/min feed rate, and 1000 rev/min rotation speed. The parameters chosen are determined by the requirements for improved surface roughness, reduced cutting time, and reduced dimensional deviation. Only 10 mm tool diameter, 50 mm/min feed rate, and 1000 rev/min rotation speed optimize surface roughness. Only 8 mm tool diameter, 143 mm/min feed rate, and 1525 rev/min rotation speed optimize cutting time. Only the following parameters optimize cutting time: 10.31 mm tool diameter, 50 mm/min feed rate, and 1000 rev/min rotation speed.

Research was conducted by N. A. Fountas et al., conducted on the Multi-response optimization of CuZn39Pb3 brass alloy turning by implementing the Grey Wolf algorithm. In his work he performed experimental study on machinability parameters in turning of CuZn39Pb3 brass alloy. Machinability was investigated with reference to arithmetic mean surface roughness Ra (µm), maximum height of the profile Rt (µm) and main cutting force Fc (N) which were considered as dependent responses affected by the cutting conditions; rotational speed n (rpm); feed rate f (mm/rev) and depth of cut a (mm). An L18 mixed-level Taguchi orthogonal design of experiments was set to build the design space according to the operational range of cutting conditions as well as their corresponding levels. The results obtained suggest that cutting conditions and their interactions differently affect the responses of Ra, Rt and Fc. Main cutting force is minimized by applying low speeds and moderate feeds whereas roughness parameters Ra and Rt are minimized by using high speeds combined to moderate feeds for a depth of cut equal to 1.0 mm. An advanced multi-objective intelligent algorithm following the behavior and social activity of grey wolves was applied to solve the problem. It was revealed that the algorithm is efficient in its heuristic search during all independent algorithmic runs with emphasis to the final recommended optimal parameters to solve the optimization problem(Fountas et al., 2019).

K Venkata Rao et al. (Rao, 2019) used tool vibration and surface roughness as response parameters to investigate the machinability of silicon bronze alloy in orthogonal turn milling. To optimize process parameters in Silicon Bronze orthogonal turn milling, an advanced teaching -learning based optimization (TLBO) technique was introduced in this research effort. By using the amplitude of cutter vibration and surface roughness 60µm (ISO 10816) and 3 µm respectively as constraints, it has been demonstrated that the three optimal combinations of cutting speed, feed, and depth of cut were obtained for least surface roughness and amplitude of cutter vibration. Nonetheless, the combination of 54.7 m/min cutting speed, 3.9 m/min feed rate, and 1.08 mm depth of cut has a low surface roughness and a tool vibration of 30.95 m.

Vilarinho et al. (Vilarinho et al., 2005) investigated a few relationships relating to the influence of chemical composition and hardness on several cutting power components. The proposed empirical connections took into account the effects of several alloying elements that are normally present in the composition of brass as well as the influence of Pb, which has been shown by a number of writers to have an impact on the machinability behavior. Cutting forces (Fz) were discovered to be lower in traditional alloys (CuZn36Pb3, CuZn39Pb3) compared to contemporary brass alloys of the ternary systems under consideration (Cu-Sn-Zn, Cu-Al-Zn, and Cu-Fe-Zn) (Vilarinho et al., 2005)(Vilarinho et al., 2005). However, in some instances, traditional alloys showed feed rate and depth of cut that were comparable to or even greater than those of current brasses.

Additionally, machinability of various lead-free brass alloys were investigated by Vilarinho et al. CuZn21Si3P and CuZn39Pb3 brasses were compared for the advancement of residual stresses, and the results showed that the Si-containing alloy preserved lower residual stresses and achieved improved abrasion resistance despite requiring higher cutting forces. This work examined modern brass alloys of the ternary systems. This may also indicate improved fatigue and stress-corrosion cracking resistance, however more research is needed (Tam et al., 2016). When typical leaded brasses and Pb-free brasses are compared for their machinability, the two most important factors that determine the cutting force and surface roughness are the depth of cut and feed rate. Because of the capacity to control both machinability criteria through the optimization of these variables, their examination is crucial (Gaitonde et al., 2008).

Cutting forces and surface quality were used by Taha et al. to investigate the machinability of lead-free silicon brass alloys (Taha et al., 2012). This piece was simple to process thanks to the high quality of the machined surface. To evaluate this, the average surface roughness (Ra) of the machined surfaces was evaluated using H20 and H123 tools under varied cutting parameters. For all of the Si-containing brass alloys examined, Ra was indubitably almost independent depth of cut. Ra kept going up as cutting feed kept going up, and as speed increased, Ra decrease progressively.

The alloys containing 1% and 2% Si, leaded brass C37700, and leaded brass had the alloys with the lowest Ra values. Even higher Ra values were found in alloys containing 3 and 4 weight percent Si (Taha et al., 2012). A rise in Ra was observed. Ra was discovered to rise by 40% as the silicon percentage increased from 1% to 4% Si. For both leaded and unleaded alloys, the relationship between cutting forces and cut depth was inverse. In both cases, the machining behavior was linked to an increase in chip formation resistance brought on by an increase in the amount of material removed. The cutting speed increased the cutting force up to a speed of 50 m/min. This was attributable to the higher friction on the tool face caused by the chip flow. High speeds caused the cutting temperature to rise, which in turn decreased the material's friction forces and shear strengths due to thermally induced softening. This decreased cutting force in turn caused the cutting temperature to rise. Furthermore, the lubricating action of Pb decreased the coefficient of friction between the chip and the tool face, resulting in the lowest cutting force value in leaded brass. For 1% Si, the source of the greatest cutting force was found to be the strongest alloy (Taha et al., 2012).

2.2.2 Chip Formation and Tool Wear

Li et al.(2012) study the effect of incorporation of a soft intermetallic phase that is uniformly distributed throughout the material of lead-free copper alloys and found that this process is frequently used as a design requirement for Pb-free brasses. This study work concluded that, incorporating a uniformly distributed soft intermetallic phase is a common design requirement for Pb-free brasses to enhance machinability. This study work focused on, the effect of Ti addition to lead-free brasses was investigated and found that the BS40-2.2Bi alloy had superior machinability compared to standard leaded brass Cu40Zn3.2Pb. The machining method produced varied chip morphologies for evaluating the alloys' machinability. The brittleness of Bi affected the chip's fracture behavior in BS40-2.2Bi, and adding Ti changed the chip's geometry, causing it to take on the shape of a continuous spiral at 0.5 wt% Ti content, making its chip shape distinct from that of conventional leaded brass.

G. Adinamis. (2019) used contemporary machine tools to undertake comprehensive testing on representative leaded and non-leaded brass rod alloys in laboratory and production environments. Machinability data acquired for turning, drilling, and milling provides new insights into the implications of increasing tool life, efficiency, surface integrity, and chip formation on tool life, feed rate, and depth of cut. The findings indicate that advances in machine tool technology, along with the untapped high-speed machining capabilities of brass, provide new potential for manufacturers to become more efficient and profitable (Speed et al., 2019).

Toulfatzis et al.(2018) conducted a study on lead-free CuZn42, CuZn38As, and CuZn36 brasses, and confirmed that an increased volume fraction of the β-phase improves the machinability of the alloys by enabling the creation of micro-cracks during the machining process. However, the control of chip segmentation process was dominated by the distribution of Pb particles. The study also found that the CuZn38As alloy exhibited superior surface quality compared to its typical leaded counterpart. Further research on processing parameters and their impact on the microstructure and properties of lead-free copper alloys could lead to further improvements in their machinability(Abbas et al., 2018; Toulfatzis et al., 2018).

The influence of artificial wear and cutting speed on vibration and chip form characteristics was explored by Peter Pavol Monka (Pavol Monka, 2023). In the trials, three different types of brass alloys were used as machining materials. The measured data was statistically examined before the appropriate dependencies were plotted. Chips were collected for each machining situation, and the report contains a database of the resulting chip morphologies at varied cutting speeds, allowing them to be compared and classified. The results show that the brass alloys CW510L and CW614N have three times the vibration damping of the CW724R alloy, and that chip formation is relatively good in the evaluated machining settings even without the use of a chip breaker. An undesirable chip shape resulted.

Furthermore, the dispersion of Pb particles dominated the chip segmentation process. Extending on this concept, a higher volume proportion of the β -phase would be stabilized at room temperature by performing a series of heat treatments on the Pb-free alloys (at 775 °C for 60 minutes for CuZn42 and at 850 °C for 2 hours for CuZn38As). As a result, a small improvement in machinability was anticipated. With a higher volume fraction of the β-phase, the alloys showed an improvement in machinability, and in the case of the CuZn38As alloy, they outperformed their standard leaded counterpart in terms of surface quality (Toulfatzis et al., 2018)Nobel et al. studied the machinability of numerous lead-free copper alloys, including CW510L, CW511L, and CW724R, and discovered a link between machinability and the use of different cutting tool materials. The chip formation machinability of the lead-free silicon brass CW724R outperformed that of other lead-free brasses such as CuZn42 (CW510L) and CuZn38 (CW511L) (Nobel et al., 2016)

Laakso et al. (2018) used simulations and experiments to conduct their research to find out how different cutting parameters affect the morphology of a low-lead brass chip (Laakso et al., 2013).Although this low-lead brass is not standardized, its composition is comparable to that of the standard lead-free brass CuZn38As (CW511L).A positive rake angle (+5), a high cutting speed (300 m/min), and a low cutting feed rate (0.1 mm/rev) were found to improve chip breakage from a continuous chip to a chip with an average length of 4 mm, according to these simulations and experiments. Chip breakage is favored by high cutting speeds because they suppress softening effects at high strain rates, making chips more brittle. Using a positive rake angle (like +5) reduces friction force and cutting force to a minimum. By reducing the feed rate and/or the depth of cut, one could reduce friction by decreasing the tool–chip contact area. The aforementioned findings were confirmed by FEM simulations. In addition, the addition of Pb replacers Si and Al elements) was used in a recent study to investigate the effect of Zn equivalent on the evaluation of chip morphology and machining surface quality of free cutting silicon brasses

Based on the information provided, it appears that the inclusion of alloying elements such as Si can achieve the equilibrium stability of various main phases in the Cu-Zn alloy system. The Chemical Thermo Mechanical Pulp (TMP) process may increase this effect even further and have a direct impact on fracture behavior, chip-breaking characteristics, and machinability performance(Doostmohammadi & Moridshahi, 2015; Rajabi & Doostmohammadi, 2018). Taha and colleagues discovered that as the Si percentage in modern lead-free brasses (CuZn40) grew from 0% to 1%, tool wear increased marginally. This increase in tool wear was related to an increase in hard-phase volume fractions and a decrease in soft β-phase volume fractions(Taha et al., 2012). The β-phase was discovered to be damaging to tool wear in Si-containing brass alloys. The increasing volume of the brittle and intermetallic phases induced a minor increase in tool wear, but no significant changes in hardness or microstructure were found when the Si concentration was increased from 1% to 4%. Understanding the impact of alloying elements on tool wear and microstructure can help optimize cutting parameters and improve machinability performance overall.

Taha et al.(2012) found that as the cutting speed reduced, chip formation changed from continuous to discontinuous, although decreasing the cutting speed may reduce productivity. Adding 4% Si to unleaded CuZn40 brass, on the other hand, produced acceptable long bevel and cylindrical chip forms. The production of hard secondary-phase precipitates, rather than mechanical qualities, influenced the kind of chip. Furthermore, using recycled bismuth-tin (Bi-Sn) solder in the lead-free brass alloy Cu-38Zn-0.5Si resulted in smaller chip size morphology. When compared to CuZn38, the presence of the β-phase in CuZn21Si3P improved chip-breaking efficiency, while the high proportion of β-phase in the CuZn41.5 microstructure affected chip shape. Overall, these findings imply that a variety of strategies can be employed to enhance machining operations for lead-free copper alloys, increasing productivity while minimizing concerns such as excessive tool wear rates (Rojananan et al., 2017).

Klocke et al. (2016) investigate the machinability of low-lead brass alloys ys (CuZn38As, CuZn42, and CuZn21Si3P) with various coatings and tools. A diamond-like carbon coating (Ti, V, Zr, Hf, Nb, and Ta) minimized machining challenges. Tool wear was measured while cutting lead-based and lead-free brass alloys, pointing to coating carbide tools as a potential solution for high tool wear rates (Schultheiss et al. (2021). It was later discovered that brasses with high Si content typically produce discontinuous chip types, whereas low-Si brasses are associated with superior surface quality and improved mechanical properties, but the low-Si brasses studied in their study still produced discontinuous chips(Taha et al., 2012)

2.2.3 Suggestions for dry machining when working with copper alloy

Under dry or MQL cutting circumstances, copper alloys are simple to cut with a machine. They are suited for the majority of machining operations due to their low cutting temperatures and short, controlled chip forms. Brass turning was researched by Davim et al. under MQL and flood and cooling circumstances. They concluded that the performance of MQL machining was on equivalent to or better than flood coolant machining(Gaitonde et al., 2008). The severe chip adhesion to the tool rake face and built-up edge, which is especially obvious at low cutting speeds, makes pure copper difficult to machine. Ni and

Alpas investigated how dry machining of commercially pure copper led to the creation of sub-micron grain structures. They reported that the secondary shear zone material had significantly distorted and elongated grains(Ni & Alpas, 2003).

2.3 Summary of Literature Review

According to the literature reviewed above and summarized in Table 2.1, most researchers focused on a comparative study of leaded and non- leaded copper alloys. For a variety of materials, many researchers have identified the optimum cutting parameter; however, the same methodology has not yet been employed for lead-free brass alloys.

Table 2.1: Summary of Literature Work

No	Reference	Material under study	Tool material	Parameter of study	Analysis Method	Outcome/result obtained
1	(Adineh & Doostmohammadi, 2021)	Different casted samples by adding different amounts of high purity Si to Cu65Zn35 and Cu70Zn30 base brasses.	HSS	Chemical composition (Cu, Zn and Si contents) and parameters (v, d and f)	Artificial neural network and cuckoo algorithm have	Minimum cutting force was obtained at Cu = 68.5 wt%, Zn = 28.78 wt%, Si = 2.72 wt%, CS = 86.78 m min-1, FR = 0.18 mm rev-1, and Doc= 0.66
2	(Ebrahim et al., 2020)	Free Cutting Brass (CuZn35Pb3).	Ceramic coated-carbide tool	(cutting speed, feed rate and depth of cut)	Taguchi and ANOVA	According to this study minimum surface roughness obtained at higher cutting speed, lower feed and higher depth of cut a was 1.63 µm.
3	(Fountas et al., 2019)	CuZn39Pb3 brass alloy	A SECO® coated tool insert	(cutting speed, feed rate and depth of cut)	The Artificial grey wolf optimization algorithm	According to the outputs, the best point of alpha wolf is for surface roughness, cutting force and height of the profile were obtained.
4	(Seçgin, 2021)	Ms58 Brass	HSS	(Tool diameter, cutting speed, feed rate and depth of cut)	Taguchi and Response surface method	The best combination of machining parameters was 10 mm tool diameter, 150 mm/min feed rate and 1000 rev/min rotation speed.

5	(Rao, 2019)	ASTM B98 Silicon Bronze metal.	HSS	(Tool diameter, cutting speed, feed rate and depth of cut)	Teaching-learning based optimization (TLBO) technique	Minimum surface roughness and amplitude were obtained at V= 54.7m/min, f= 3.9m/min and d= 1.08mm , tool vibration of 30.95µm.
6	(Taha et al., 2012)	Alloy prepared using Cu 60/Zn 40 and Cu 80/Si 20	H20 and H123	Cutting tool, Cutting speed, feed rate and depth of cut	-	In the 1 wt% Si alloy, the maximum cutting force is measured and undesirable continuous chip type is produced.
8	(Toulfatzis et al., 2018)	CuZn39Pb3 , CuZn42 and CuZn38As	Uncoated cemented	Materials, Cutting speed , feed rate and depth of cut	-	The results were very promising concerning the chip breaking performance.

2.4 Research Gap

As explained in the literature, the copper alloy industry proactively made various "without lead" and "low lead" combinations that are suitable for many parts to help general well-being programs all over the world. However, unlike conventional leaded copper alloy, the majority of the novel compositions faced in challenge machinability, and only a few of them combined machinability with acceptable mechanical properties. As tried to be explained in the literature review, there hasn't been much done on simultaneous multi-objective optimization and validation of cutting conditions on an industrial scale for newly fabricated lead-free copper alloy especially brass alloys. From varieties of newly developed lead-free brass alloys, Lead-free C69300 Silicon Brass alloy is the one that is used in various applications in industry. From the literature review it clearly stated that, multi-objective optimization of process parameters during machining of C69300 lead-free silicon brass alloy was not studied yet. Therefore, this study will focus on machinability study and simultaneous multi-objective optimization of cutting parameter during CNC turning of C69300 lead-free silicon brass.

CHAPTER THREE

3. MATERIALS AND METHODS

3.1 Introduction

The experimental procedures that were used for this study being described in this section. This section specifically begins with a brief overview of the material selected, including its chemical composition, mechanical and physical properties. After that, the machining setup and list of equipment used which includes the CNC machine, the cutting tools, measurement devices and characterization instruments used are given. The section then describes the experiment design that was used to carry out the trial runs. Finally, a detailed description of the optimization algorithms used for this study and their working principle was also given in this section.

3.2 Materials

Taking into account the aforementioned restrictions and the environmental requirements of the actual legislation, numerous recent recommendations for a variety of design combinations as alternatives to conventional leaded copper alloy materials have been published in the literature review. From a variety of design combinations, Silicon brass is a special type of lead-free copper alloy developed by the copper industry which has extensive use in a variety of industrial applications. C69300 lead-free silicon brass round bar with 900mm length and 25mm diameter was the material used for this study. Automatic screw machines, parts bolts, condenser tube plates, nuts, pneumatic fittings, pump parts, screw machine products, valve stems, water valve bodies, marine products, and propeller shafts are some of the applications where this material is most commonly used. This work piece's material was chosen because it is one of the copper alloys developed without lead to replace leaded alloys and is utilized in many applications where turning operations are necessary to produce the components. Additionally, to improve and validate cutting conditions on an industrial scale during the machining of newly created C69300 lead-free silicon brass, a machinability study and simultaneous optimization of major quality characteristics (cutting temperature, material removal rate, and surface roughness) during CNC turning operation is needed as explained by different researchers. For each experimental run, the material was cut into five equal lengths (180mm) in length and machining length was 30mm for each run.

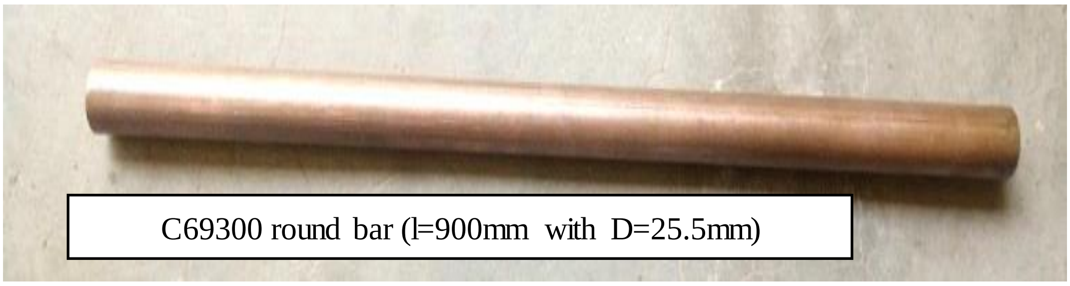

Figure 3.1: C69300 lead-free copper alloy round bar prepared samples for turning

3.2.1 Chemical Composition of C69300 Lead-Free copper alloy according to ASTM B371/B371M-19 C69300

The paragraph describes the work piece material used in the experiment, which is C69300 without lead copper alloy, also known as silicon red brass. This material is commonly used for underground service lines due to its corrosion resistance and moderate strength and spring retention qualities. Silicon brasses contain less than 20% zinc and less than 6% silicon, making them strong and somewhat corrosion-resistant. The C69300 used for turning operations had a diameter of 25mm and 30mm of length was allotted for each run at dry machining conditions. The chemical composition of C69300 was analyzed using spectrometry in Figure 3.4 and the mechanical and physical properties of the material are provided in Table 3.1 and Table 3.2.

Table 3.1: Standard Chemical Composition of C69300 Lead-Free Brass

Cu%	Pb%	Sn%	Zn%	Fe%	P%	Ni%	Mn%	Si%
73.00-79.00	0.02-0.09	0.2	Rem	0.10	0.04-0.15	0.10	0.10	2.70-3.40

3.2.2 Properties of C69300 Lead-Free Brass

3.2.2.1 Physical Properties of C69300 Lead-Free Brass

The Physical Properties of C69300 Lead-Free Brass according to ASTM B371/B371M-19 are summarized in table 3.2.

Table 3.2: Physical Properties of C69300 Lead-Free Brass

Properties	Unit in metric system
Melting point in liquidus	880 ˚C
Melting point in solidus	855 ˚C
Density	8.3 gm/cm3 at 20 ˚C
specific gravity	8.3
Electrical Conductivity	0.046 Mega Siemens/cm at 20 ˚C
Thermal Conductivity	37.76 W/mat 20 ˚C
Coefficient of Thermal Expansion 68-212	17.8 $\cdot 10^{-6}$ per ˚C (20-100 ˚C)
Specific Heat Capacity	377.1 J/kg at 20 ˚C
Modulus of Elasticity in Tension	104801MPa

3.2.2.2 Mechanical Properties of C69300 Lead-Free Brass

Mechanical Properties of C69300 Lead-Free Brass according to ASTM B371/B371M-19 C69300 are listed in Table 3.3.

Table 3.3: Mechanical Properties of C69300 Lead-Free Brass

Size range	Tensile strength (MPa)	Yield Strength (MPa)	Elongation, in 4x Diameter or Thickness of Specimen, min (%)	Rockwell "B" hardness (max HRB approx.)
up to 1/2" inclusive	585	310	5	85
over 1/2" to 1" inclusive	515	240	10	80
over 1" to 2 1/2" inclusive	480	205	10	75

3.3 Cutting Tool Material selection

The Cutting Tool material for used this study was M -2 type High-Speed Steel (HSS). M-2 type high-speed steel is a tungsten-molybdenum high-speed steel with a well-balanced combination of toughness, wear resistance, and red-hardness qualities. Because of its remarkable properties and low cost, M-2 is one of the most popular and widely utilized high speed steels in the world. According to the literature review, using the hardest and most abrasion-resistant cutting tool materials improved cutting performance due to the abrasive qualities of silicon found in lead-free silicon brass alloy. M-2 type (HSS) is one of the toughest and most wear-resistant materials utilized in cutting tools today. Carbon, chromium, vanadium, molybdenum, and sometimes cobalt are the principal alloying elements in this HSS. Positive clearance and rake angle were used to prevent friction heating, which wears out tooling and creates potential damage to the part as the emperature rises. As illustrated in figure 3.2, a fixed angle was adopted (side relief angle (8°), side back rake angle (9°), end relief angle (7°), and nose radius (0.75mm).

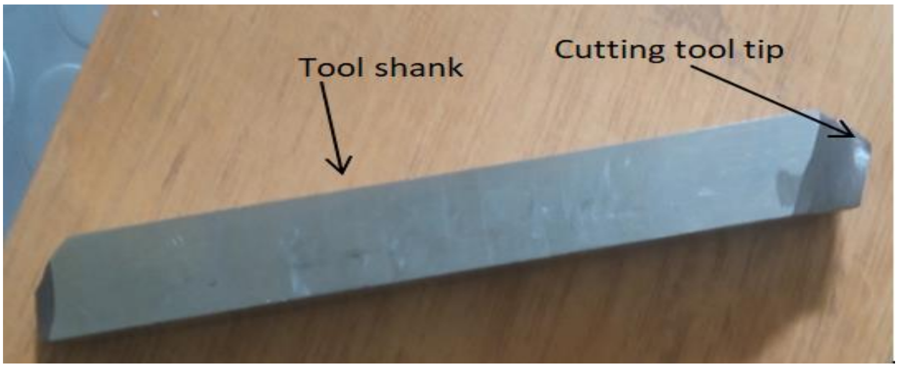

Figure 3.2: HHS Cutting tool after gridding

3.4 Lists of Equipment used for this study

Generally, the following equipment was used in this study work.

- CNC lathe machine.
- MM-2 HSS cutting tool.
- Contact type Surface Profilo-meter
- SPECTROTEST TXCO2 Machine

3.4.1 Specifications of the CNC Machine Tool used for this study

CNC lathe machine was used for the experimental study of C69300 Lead-Free Brass alloy. The machine tool was manufactured by Dalian Machine Tool Group Corporation and its model is CKE6150 and its main technical specifications are reported in table 3.4.

Table 3.4: Main Technical Specifications of the CNC Machine Tool

Description	Dimension
Maximum work piece length	1000 mm
Spindle center height	250 mm
Power	24 KVA
Voltage rating	380 V
Power frequency	50 Hz
Full load current	34 A
Spindle speed range	45 RPM – 2000 RPM
Overall dimension (L×W×H)	2830 × 1750 × 1620
Machine weight	2600 Kg

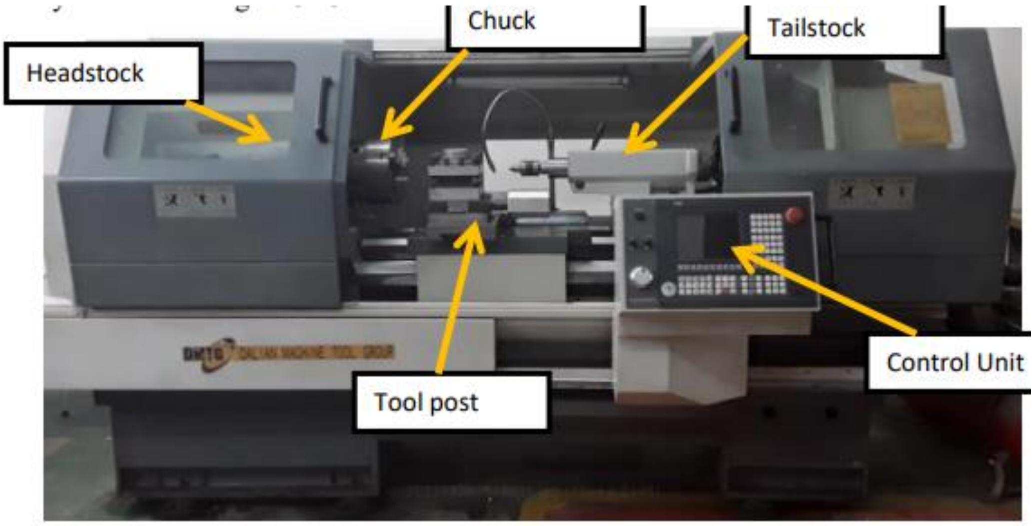

Figure 3.3: CNC Machine Tool

For turning process to be performed by CNC lathe part program needs to be developed. In this study part program was inserted by using program input device of the CNC machine tool.

3.4.2 Spectrometers

Numerous metals and alloys' elemental compositions was easily determined by spectrometry analysis. The chemical makeup of C69300 brass material was tested using Txc02-type spark spectroscopy equipment as shown in Figure. 3.4 and results of the test was attached in the appendix.

Figure 3.4: Material composition testing machine (spectroscopy)

3.4.3 Infrared thermometer

The Infrared thermometer was used to measure the cutting temperature during the machining process. The thermometer records the surface temperature of the contact between the cutter and work piece in dry conditions. The unit optics transmits, reflect and sense energy that is concentrated onto a detector, which converts the information into a temperature reading. The thermometer is activated by pulling and holding the trigger, while focusing the laser pointer onto the cutting zone. The temperature reading is displayed on an LCD with units available in degrees Celsius. Figure 3.5 shows the infrared thermometer used to measure tool and surface contact temperature.

Figure 3.5: Infrared thermometer for measure temperature

3.4.4 Surface Roughness Tester

The German-made VOGEL Surface Roughness Tester which is depicted in Figure 3.6, was used to measure surface roughness. The micrometer (m) value of surface roughness is displayed on this tester. The VOGEL Surface Roughness Tester 65711 measures between 0.02 and 50 micro meters. The surface imperfections of the work piece will be traced using a stylus attached to the tester's detecting unit. The instrument's liquid crystal display digitally displays the vertical stylus movement that occurred during the trace after being processed.

Figure 3.6: Surface-roughness testing equipment

3.5 Cutting condition selected

As stated in the literature review, under dry or MQL cutting circumstances, copper alloys are easier to cut with a machine. They are suited for the majority of machining operations due to their low cutting temperatures and short, controlled chip forms. Brass turning was researched by Davim et under MQL and flood and cooling circumstances. From this study, it was concluded that the performance of MQL machining was on equivalent to or better than flood coolant machining(Gaitonde et al., 2008). Therefore machining condition used in this study will be dry turning operation.

3.6 Methodology

The research approach was based on the experimental methodology applied aiming to evaluate the alloy performance in a more holistic view, which is presented schematically in the following flow chart as given in Figure 3.7.

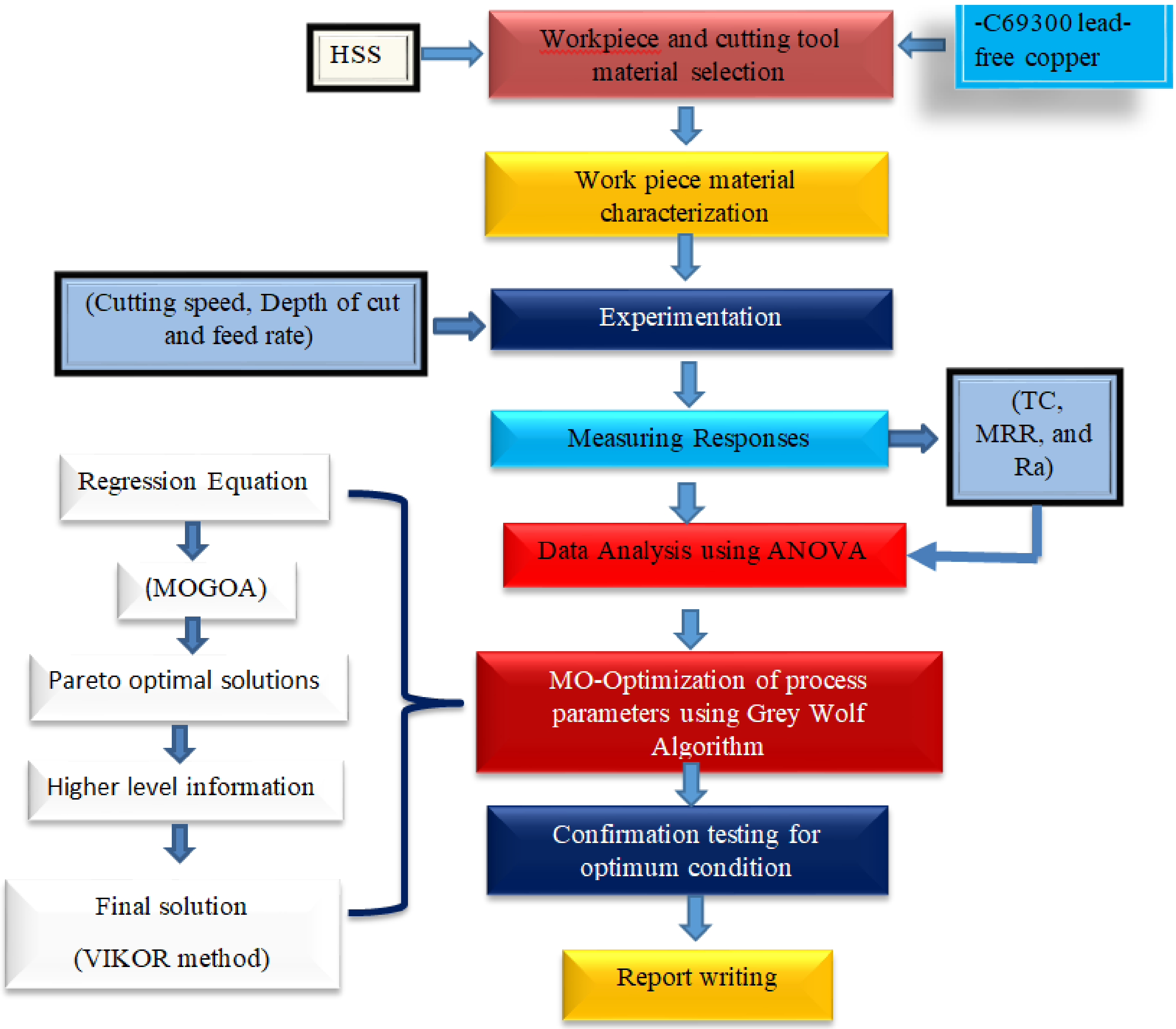

Figure 3.7: Flowchart of the experimental methodology applied for this research

3.7 Experimental Design

Setting levels for each factor is crucial for designing experimental runs. Hence, as indicated in Table 3.6, four levels of three process parameters (cutting speed, feed rate, and depth of cut) were used in this research. The ranges of the cutting conditions were determined by preliminary experiments and a review of the literature before levels were fixed. Table 3.5 shows process parameters with different leaded and lead-free brass materials used by different researchers.

Table 3.5: Summery Process parameters selected by various researchers

Researchers	Material	Cutting too	Process parameters		
			V(m/min)	Feed rate (mm/rev)	Depth of cut(mm)
(Peter Pavol Monka et al, 2023)	CW510L , CW724R(lead-free),(CW614N) leaded brass	Different cutting insert	100, 150, 225, and 337.5	0.06	1.0
(Schultheiss et al., 2021)	CuZn39Pb3 and CuZn21Si3P-lead-free	Coated cemented carbide	400	0.05-0.2	1.5
(Optimization et al., 2018)	CW510L,CW511 L C27450-Eco (lead-free) brass CW614N-leaded brass	Uncoated cemented	165, 192 ,220, 247	0.066,0.075, 0.085,0.1	0.5, 1.0 1.5, 2.0
(Yadu Krishnan et al., 2020)	C352 Brass Alloy	HSS	30, 53, 85	0.2 0.3 0.4	0.150.25 , 0.5
(Fountas et al., 2019)	CuZn39Pb3 (CW614N) alloy.	A SECO® coated tool insert	800(rpm), 1600(rpm)	0.1.0.18,0.33	0.5,1.0,1.5
(Speed et al., 2019)	C36000 ,C38500 – (leaded)C27450 ,C69240-(lead-free)	CCMT432 tungsten carbide	152,305, 610,914	0.08,0.13, 0.18,0.25,	0.51,1.14, 1.78,2.29
(Arun Vikram et al., 2015)	Brass (ISO:319)	HSS	560, 900, 1250(rpm)	0.14, 0.17, 0.2	0.5

The choice of cutting speeds (Vc), feed rates (f) and depth of cuts (Dc) to be used as input was made according to the studies previously performed on the machinability of brass alloys with similar compositions. It was decided to use cutting velocities between 40 and 350 m/ min. To guarantee those values, cutting speed of 40 m/min, , 60m/min ,80m/min and 100 m/min were combined with four different feed rates, 0.05 mm/rev, 0.10 mm/rev,0.15 mm/rev ,0.2 mm/rev, and four different depth of cut, 0.5 mm,0.75mm ,1.0 mm and 1.25(mm). Based on a literature review, cutting parameters and their level for CNC turning of C69300 lead-free silicon brass were chosen. Table 3.4 displayed the selected cutting parameters.

Table 3.6: List of parameters and their levels

Cutting Parameter	Units	Levels			
		1	2	3	4
Spindle speed	m/min	40	60	80	100
Depth of cut	mm	0.5	0.75	1	1.25
Feed rate	mm/rev	0.05	0.1	0.15	0.2

3.7.1 Selected Orthogonal Array

Turning experiments were performed on a CNC lathe utilizing an HSS cutting tool to machine a work piece made of lead-free copper alloy with chosen cutting parameters at one of four levels shown in Table 3.6. The number of factors and levels of various parameters determine which orthogonal array should be chosen. Three factors, each with four levels, were chosen in this experiment. Now, using the formula shown below, it is possible to determine the Degree of Freedom needed for the experiment (DOF).

$$\mathrm{DOF} = P\ (L\text{-}1) \qquad (3.1)$$

Where, P is the number of factors (p=3); L is the number of level (4) and DOF is the degree of freedom.

$$\mathrm{DOF} = 3^{*}\ (4\text{-}1) = 9$$

Degrees of freedom associated with the OA can be calculated by the number of rows in orthogonal array minus one. For the L16 orthogonal array, number of row is 16. Therefore, the Degree Of Freedom associated with the OA is 15. Since DOF of orthogonal array (OA) experiments should be larger than the total number of the DOF needed for the experiment, L16 orthogonal array was selected. Therefore, Taguchi orthogonal array L16 was created with the sixteen experimental runs as listed in Table 3.7. The related average values of the responses (surface roughness parameter (Ra), cutting temperature (Tc), and material removal rate (MRR)) are measured for each experimental run. The Taguchi method is commonly used in the design of the experiment (DOE) to optimize process parameters because it can shorten experimental runs and identify important factors more quickly. In addition, Taguchi uses orthogonal arrays to reduce the number of trials in comparison to the other approaches by analyzing the outcomes of experiments and determining the ideal conditions for a product or process, the Taguchi technique estimates the percent contribution of each factor and forecasts the response.

Table 3.7: Experimental Layout Using an L-16 Orthogonal Array

Exp. No	cutting speed(m/min)	Feed rate(mm/rev)	Depth of cut (mm)
1	40	0.05	0.50
2	40	0.10	0.75
3	40	0.15	1.00
4	40	0.20	1.25
5	60	0.05	0.75
6	60	0.10	0.50
7	60	0.15	1.25
8	60	0.20	1.00
9	80	0.05	1.00
10	80	0.10	1.25
11	80	0.15	0.50
12	80	0.20	0.75
13	100	0.05	1.25
14	100	0.10	1.00
15	100	0.15	0.75
16	100	0.20	0.50

3.7.2 Responses Measurement

3.7.2.1 Surface Roughness Measurement

The most important factor in the machining process is surface roughness because it is thought to be the foundation of product quality. It gauges how inadequately refined the surfaces are. Because a smooth surface (better-finished components) reduces the chance of surface damage caused by wear, corrosion, improves fatigue strength, reduces creep failure, and increases productivity & economics of the industry, the quality of the surface produced using conventional and non-conventional machining is important. The effectiveness of the surface for preventing wear and corrosion can also be influenced by the quality of a part produced by a machining operation. Depending on its uses, such as Ra, Rq, Rz, and Rt, surface roughness can be defined in a variety of ways. The average surface roughness, however Ra, also known as the arithmetic average (AA) or the center line average (CLA), is a measure of surface roughness that is frequently used in industry for mechanical components. For this reason, Ra was employed in this study to indicate surface roughness.

Figure 3.8: Measurement of surface roughness

3.7.2.2 Measurement of Tool tip work piece interface Temperature

To measure and analyze the relationship between cutting parameters (cutting speed, feed rate and depth of cut) and temperature, the infrared thermometer was used to capture the Tool-work piece interface cutting Temperature. The temperature of the cutting zone was measured during the machining time of every run. The basic working principle of infrared thermometer is, it measures the surface temperature of an object. The unit optics sense emitted, reflected, and transmitted energy, which is collected and focused onto a detector. The unit electronics translate the information into a temperature reading which is displayed on the unit. In units with a laser, the laser is used for aiming purposes only. By holding the meter by its handle grip and pointing it towards the surface to be measured. Pull and hold the trigger to turn the meter on and being tested. While continuing to push the trigger the laser pointer is concentrated at the cutting zone. Release the trigger and the hold, display will appear on the LCD indicating that the reading is being held.

We can select the temperature units 0C and 0F.The Infrared thermometer used for the temperature measurement was shown as in Figure 3.9 bellow;

Figure 3.9: Measurement of Tool-work piece interface Temperature

3.7.2.3 Calculation of Material Removal Rate (MRR)

The material removal rate is the volume of material removed per unit time which ultimately determines machining productivity. In roughing operations and the production of large batches, the material removal rate needs to be maximized. However, in finishing operations, it affects surface roughness, tool life, cutting temperature, and the overall economy of the machining process. In turning process for achieving low surface roughness, low tool wear, and low tooltip temperature, usually low cutting parameters are applied, as MRR is usually low for low cutting parameters. In the present investigation, the following formula has been used to compute the material removal rate.

$$\mathrm{MRR} = \mathrm{V} * \mathrm{f} * \mathrm{d} \qquad (3.2)$$

Where:

-f is the feed rate mm/rev

-V is the spindle speed in m/min and

-d is the depth of cut in mm for each turn.

3.7.3 Analysis of Variance (ANOVA)

Analysis of variance (ANOVA) was used to determine the significant factors affecting a quality characteristic. ANOVA is a statistical technique used to measure the influence of all control parameters, and in this case, the percentage contributions of each control factor were used to measure their corresponding effects on performance characteristics. The significance level of 5% was used for a 95% level of confidence. ANOVA results indicate whether there is a statistically significant difference in output characteristics when alpha values are below 0.05 (significant) or above 0.05 (not significant). The percentage contribution is an effective guide relative to the importance of each model term, and was calculated from the ANOVA analysis to determine the contribution of each influential parameter.

Each term that was used in ANOVA table were explained as follows:

- ✓ **Block:** The block row indicates how much variation in the response may be attributed to blocks. The analysis excludes block variation. Blocks are not tested (no F or p-value) since they are a non-replicable, difficult-to-change factor.
- ✓ **Model:** The model row displays how much variation in the response is explained by the model, as well as the overall model significance test.
- ✓ **Terms:** The model is broken down into distinct terms that are tested independently.
- ✓ **Residual**: The residual row indicates how much variation in the response remains unexplained.
- ✓ **Cor Total:** The amount of variation around the mean of the observations is shown in this row.
- ✓ Sum of Squares: The sum of the squared disparities between the overall average and the amount of variation described by the source of the rows.
- ✓ DOF: Degrees of Freedom: The number of estimated parameters needed to calculate the sum of squares of the source.
- ✓ The sum of squares divided by the degrees of freedom yields the mean square.
- ✓ **Mean**: The sum of squares for the effect of the mean. The column labeled "**df**" provides the degrees of freedom for each source. In response surface methodology, the total degrees of freedom equal the number of model coefficients added sequentially line by line.
- ✓ **For a mixture model**: let q be the number of components in a mixture. The degrees of freedom for the linear terms in a mixture model is (q-1), rather than q, because the sums of squares are corrected for the mean
- ✓ **F-Value:** A test for comparing the mean square of the source to the residual mean square.
- ✓ **Probability** > F: (p-value) The likelihood of seeing the observed F-value if the null hypothesis is true (no factor effects). Small probability values demand that the null hypothesis be rejected. The likelihood is equal to the integral under the F-distribution curve that lies beyond the observed F-value. In other words, if the Prob>F value is

very small (less than 0.05 by default), the source is found to be significant. Significant model terms are likely to effect on the response. The presence of a significant lack of fit shows that the model does not fit the data within the observed replicate variation.

3.7.4 Multi-response optimization used for this study

3.7.4.1 Introduction to Single and Multi-response optimization

Real engineering problems have a variety of challenges that must be solved and require a certain set of tools. Real-world problems are difficult because of their multi-objectivity, which is one of their most significant aspects. If several goals that need to be achieved, the problem is referred to as multi-objective. Without a doubt, the best approach to solving such issues is to use a multiple goal optimizer. For managing numerous objectives, there are two methods: a posteriori and a priori (Besharatnia et al., 2022; Makhadmeh et al., 2022; Marler & Arora, 2004).The former category of optimizers uses a single objective optimizer to solve a multi-objective problem by combining its objectives into a single goal and assigning each goal a weight (determined by decision-makers).A single solution can be identified as the best one since the combined search spaces are unary-objective. Contrarily, a posteriori approaches preserve the multi-objective formulation of the problems, enabling exploration of the behavior of the problems under a variety of design factors and operating settings. In this scenario, decision-makers will ultimately select one of the discovered solutions based on their requirements. There is no single solution when several objectives are the purpose of the optimization process, in contrast to single-objective optimization. Here, a set of answers to a multi-objective problem that illustrates different trade-offs between the objectives contains the best possible solutions (Besharatnia et al., 2022). In this study, non-dominated solutions were found using a posterior optimizer method so that decision-makers could ultimately select one of the solutions based on their requirements.

Numerous multi-objective optimization strategies that have shown reliability in locating the best solution during the past few decades, especially in the manufacturing sector, according to the literature. Via benchmarking issues, the researchers did introduce a number of unique alternatives that could outperform the established and traditional methods. That is, choosing among many multi-objective algorithms, such as the multi-objective grey wolf optimizer (MOGWO), the multi-objective genetic algorithm (MOGA), the multi-objective particle swarm optimization (MOPSO), etc. Four factors, namely simplicity, flexibility, derivation-free mechanism, and local optimum avoidance, explain why such algorithms have grown in popularity in terms of their application to addressing engineering problems. While simple ideas have largely served as their inspiration, meta-heuristic algorithms are typically relatively straightforward to use (Besharatnia et al., 2022; Marler & Arora, 2004).

The sources of inspiration resemble natural occurrences like animal behavior or evolutionary theories. Due to its simplicity, various natural notions can be simulated, new meta-heuristics can be proposed, multiple meta-heuristics can be hybridized, and existing meta-heuristics can even be improved. Also, this simplicity aids in the quick comprehension of metaheuristics for use in problem-solving. Flexibility refers to the capacity of the met heuristics to be applied to different problems without altering the fundamental structure of the algorithm. All that is involved in applying metaheuristics to problems are a system's inputs and outputs. Consequently, it is important to understand how to choose a metaheuristic to solve a certain problem. Moreover, most metaheuristics have derivation-free utilities. Metaheuristics stochastically optimize issues in contrast to gradient-based optimization approaches.

Optimization initializes randomly created candidate solutions, and there is no need to compute derivatives for search spaces to converge to optimal solutions. As a result, metaheuristics are ideally suited for solving practical problems involving expensive or unreliable derivative information. And finally, when compared to conventional optimization methods, metaheuristics are more adept at avoiding local traps. This happens as a result of the stochastic nature of metaheuristics, which enables them to avoid stagnation in local regions and exhaustively search the solution space. Metaheuristics are excellent mechanisms for optimizing such difficult real-world problems because solution spaces for real-world problems are typically unknown, extremely complicated, and include a large number of local optima. The No metaheuristic that is ideally suited for successfully resolving all optimization issues, according to the No-Free Lunch theorem (Fountas et al., 2019). This suggests that while a given metaheuristic may show extremely impressive results on a certain set of issues, it may perform poorly on a different set of problems of a different type. No-Free Lunch theorem, of course, makes this study area a particularly active one where contributions to improving existing algorithms and/or generating new ones are published very frequently.

- **Concept of Pareto dominance**

Multi-objective optimization finds applications in problems where more than one function needs to be optimized and the variations in design variables impact the objective. These problems have multiple solutions and the solution set is constituted based on Pareto dominance. One solution set is said to dominate another possible solution if it performs better or at least an equal value on all objectives, and at least a better value on one objective. This concept was mathematically formulated as Pareto dominance as.

Two vectors: $X = (x_1, x_2, x_3 \ldots\ldots, x_k)$ and $Y = (y_1, y_2, y_3 \ldots\ldots, y_k)$

X dominates Y iff :: $f(X_i) \geq f(Y_i)$ ¥ $_i = 1, 2\ldots\ldots\ldots k$ and any: $f(X_i) > f(Y_i)$

3.7.4.2 Ideal multi-objective optimization approach

An Ideal multi-objective optimization approach was used to obtain best parameters setting for optimum response performance. Multi-objective optimization grey wolf algorithm, which mimics the social hierarchy, hunting and prey exploration, is successfully implemented and Pareto optimal solutions are successfully recorded. VIKOR methodology was used to obtain the best solutions from Pareto lists.

Ideal multi-objective optimization approach can be summarized as follows:

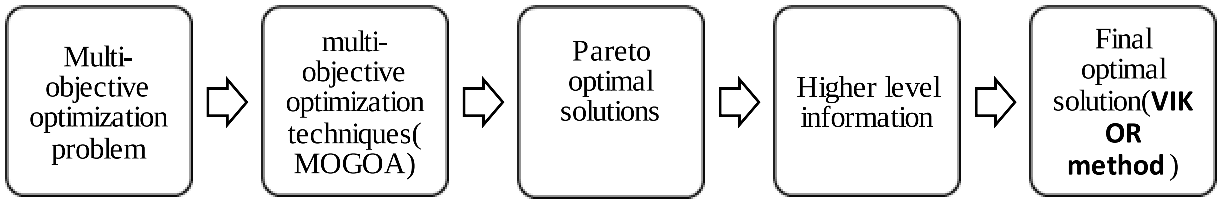

3.7.4.3 Grey Wolf algorithm (GWA) for multi-response optimization

This study uses a multi-objective grey wolf optimizer as its optimization technique (MOGWO). The GWO algorithm was proposed by Mirjalili in 2014 (Mirjalili et al., 2014). This method has already been used with various materials or a different set of parameters (Abbas et al., 2023; Fountas et al., 2019; Kumar et al., 2022; Seçgin, 2021; Subbaiah, 2022). Comparing to others optimization algorithms, GWO gives more feasible solutions and it has better performance. The purpose is to develop and optimize a multi-objective function in terms of input parameters that are concurrently sustainable, productive, and efficient. The social leadership and hunting technique of grey wolves were the main inspiration for this algorithm To mathematically model the social hierarchy of wolves when designing GWO, the fittest solution is considered as the alpha (α) wolf. Consequently, the second and third the best solutions are named beta (β) and delta (δ) wolves respectively. The rest of the candidate solutions are assumed to be omega (Ω) wolves. In the GWO algorithm the hunting (optimization) is guided by α, β, δ and Ω. The Ω wolves follow these three wolves to search the optimum solution.

➢ **Mathematical model and algorithm**

In this subsection the mathematical models of the social hierarchy, tracking, encircling, and attacking prey are provided. Then the GWO algorithm is outlined.

- **Social hierarchy:**

This algorithm was mostly inspired by the social leadership and hunting style of grey wolves. The fittest solution is taken into account as the alpha (α) wolf when building GWO to quantitatively describe the social structure of wolves. Consequently, the second and third best solutions are named beta (β) and delta (δ) wolves respectively. The rest of the candidate solutions are assumed to be omega (Ω) wolves. In the GWO algorithm the hunting (optimization) is guided by α, β, δ and Ω. The Ω wolves follow these three wolves to search the optimum.

- **Encircling prey:**

As mentioned above, grey wolves encircle prey during the hunt. To mathematically model encircling behavior the following equations are proposed:

$$\vec{D} = \left|\vec{C}\ .\overrightarrow{X_P}(t) - \vec{X}(t)\right| \qquad (3.3)$$

$$\vec{X}(t+1) = \left|\overrightarrow{X_P}(t) - \vec{A}.\vec{D}\right| \qquad (3.4)$$

Where t indicates the current iteration, $\vec{A}$ and $\vec{C}$ are coefficient vectors,

$\overrightarrow{X_p}$ is the position vectors of the prey, and $\vec{X}$ indicate the position vector of the GW.

Vectors $\vec{A}$ and $\vec{C}$ are calculated as follows:

$$\vec{A} = 2\vec{a}\overrightarrow{r_1} - \vec{a} \qquad (3.5)$$

$$\vec{C} = 2.\overrightarrow{r_1} \qquad (3.6)$$

Where components of $\vec{a}$ are linearly decreased from 2 to 0 over the course of iterartion and r_1, r_2 are random vectors in [0,1].

To see the effects of equations (3.1) and (3.2), a two-dimensional position vector and some of the possible neighbors are illustrated in Fig. 3. As can be seen in this figure, a grey wolf in the position of (X,Y) can update its position according to the position of the prey (X^*,Y^*). Different places around the best agent can be reached with respect to the current position by adjusting the value of A and C vectors.

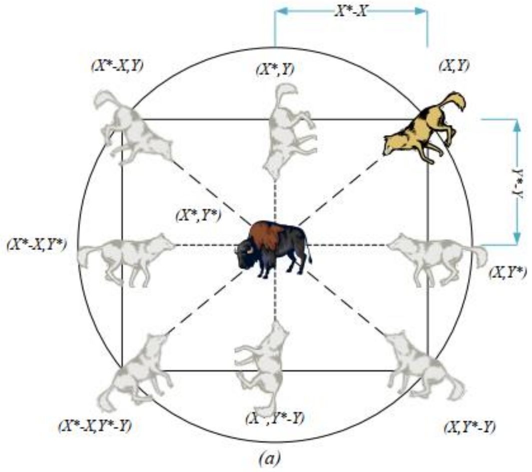

Figure 3.10: 2D a position vectors and their possible next location

- **Hunting:**

Grey wolves are known to be able to recognize the location of their prey and work together to encircle them during a hunt, usually guided by the alpha. However, when it comes to an abstract search space where the location of the optimum is unknown, the alpha, beta, and delta (best candidate solutions) are assumed to have better knowledge about the potential location of the prey. The first three best solutions obtained so far are saved, and the other search agents (including the omegas) are required to update their positions based on the position of the best search agent. The formulas proposed in this regard help to simulate this hunting behavior mathematically.

The following formulas are proposed in this regard.

$$\overrightarrow{D_\alpha} = \left|\overrightarrow{C_1}.\overrightarrow{X_\alpha} - \vec{X}\right| \quad (3.7)$$

$$\overrightarrow{D_\beta} = \left|\overrightarrow{C_2}.\overrightarrow{X_\beta} - \vec{X}\right| \quad (3.8)$$

$$\overrightarrow{D_\delta} = \left|\overrightarrow{C_3}.\overrightarrow{X_\delta} - \vec{X}\right| \quad (3.9)$$

$$\overrightarrow{X_1} = \overrightarrow{X_\alpha} - \overrightarrow{A_1}.\left(\overrightarrow{D_\alpha}\right) \quad (3.10)$$

$$\overrightarrow{X_2} = \overrightarrow{X_\beta} - \overrightarrow{A_2}.\left(\overrightarrow{D_\beta}\right) \quad (3.11)$$

$$\overrightarrow{X_3} = \overrightarrow{X_\delta} - \overrightarrow{A_3}.\left(\overrightarrow{D_\delta}\right) \quad (3.12$$

$$\vec{X}(t+1) = \frac{\overrightarrow{X_1} + \overrightarrow{X_2} + \overrightarrow{X_3}}{3} \quad (3.13)$$

- **Attacking prey (exploitation):**

As already said, the grey wolves attack their prey to put an end to the hunt after it stops moving To mathematically illustrate the prey getting closer, we reduce the value of $\boldsymbol{a}$. Keep in mind that this decrease also has an impact on the $\vec{A}$ fluctuation range. As a result, a decreases from 2 to 0 and takes on a random value in the range [-$\boldsymbol{a}$, $\boldsymbol{a}$] during the course of the iterations. The alpha, beta, and delta locations can now be used by the GWO algorithm's search agents to update their positions, which they can then use to launch an attack in the general direction of the prey using the previously suggested operators. However, the GWO algorithm is prone to stagnation in local solutions with these operators. It is true that the encircling mechanism proposed shows exploration to some extent, but GWO needs more operators to emphasize exploration.

The GWO algorithm starts optimization with generating a set of random solutions as the first population. During optimization, the three best obtained solutions so far are saved and considered as alpha, beta, and delta solutions. For every omega wolf (search agents except α, β, and δ), the position updating formula (3.5) to (3.11) are triggered. Meanwhile, parameters a and A are linearly decreased over the course of iteration. Therefore, Search agents tend to diverge from the prey when $|\vec{A}|>1$ and converge towards the prey when $|\vec{A}|<1$. Finally, the position and score of the alpha solution is returned as the best solutions obtained throughout optimization when an end condition is satisfied. To perform multi-objective optimization by GWO, two new components are integrated. The employed components are very similar to those of MOPSO (Coello et al., 2004). The first one is an archive, which is responsible for storing non-dominated Pareto optimal solutions obtained so far. The second component is a leader selection strategy that assists to choose alpha, beta, and delta solutions as the leaders of the hunting process from the archive. The archive is a simple storage unit that can save or retrieve non-dominated Pareto optimal solutions obtained so far. The key module of the archive is an archive controller, which controls the archive when a solution wants to enter the archive or when the archive is full. Note that there is a maximum member number for the archive. During the course of iteration, non-dominated solutions obtained so far are compared against the archive residents. There would be three different possible cases as follows:

- ✓ The new member is dominated by at least one of the archive residences. In this case the solution should not be allowed to enter the archive.

- ✓ The new solution dominates one or more solutions in the archive. In this case the dominated solution(s) in the archive should be omitted and the new solution will be able to enter the archive.
- ✓ If neither the new solution nor archive members dominate each other, the new solution should be added to the archive.

If the archive is full, it is advisable to start by using the grid technique to reorganize the segmentation of the objective space and locate the most crowded segment so that one of its solutions can be omitted. To increase the diversity of the final approximated Pareto optimum front, the new solution should then be introduced into the least congested segment. The multi-objective grey wolf optimizer's flowcharts are shown in Figures 6 (MOGWO). Except for the two additional components added to the method, the previously described concepts are applied to single objective optimization. An archive, the first new element, is in charge of keeping track of the existing non-dominated Pareto optimum solutions. Alpha, beta, and delta solutions are selected as the leaders of the hunting process from the archive using the second component, a leader selection approach. It is possible to save or recover non-dominated Pareto optimum solutions that have already been found using the archive, which is a straightforward storage unit. A population of 30 grey wolves and a maximum of 300 iterations were chosen to optimize the turning parameters.

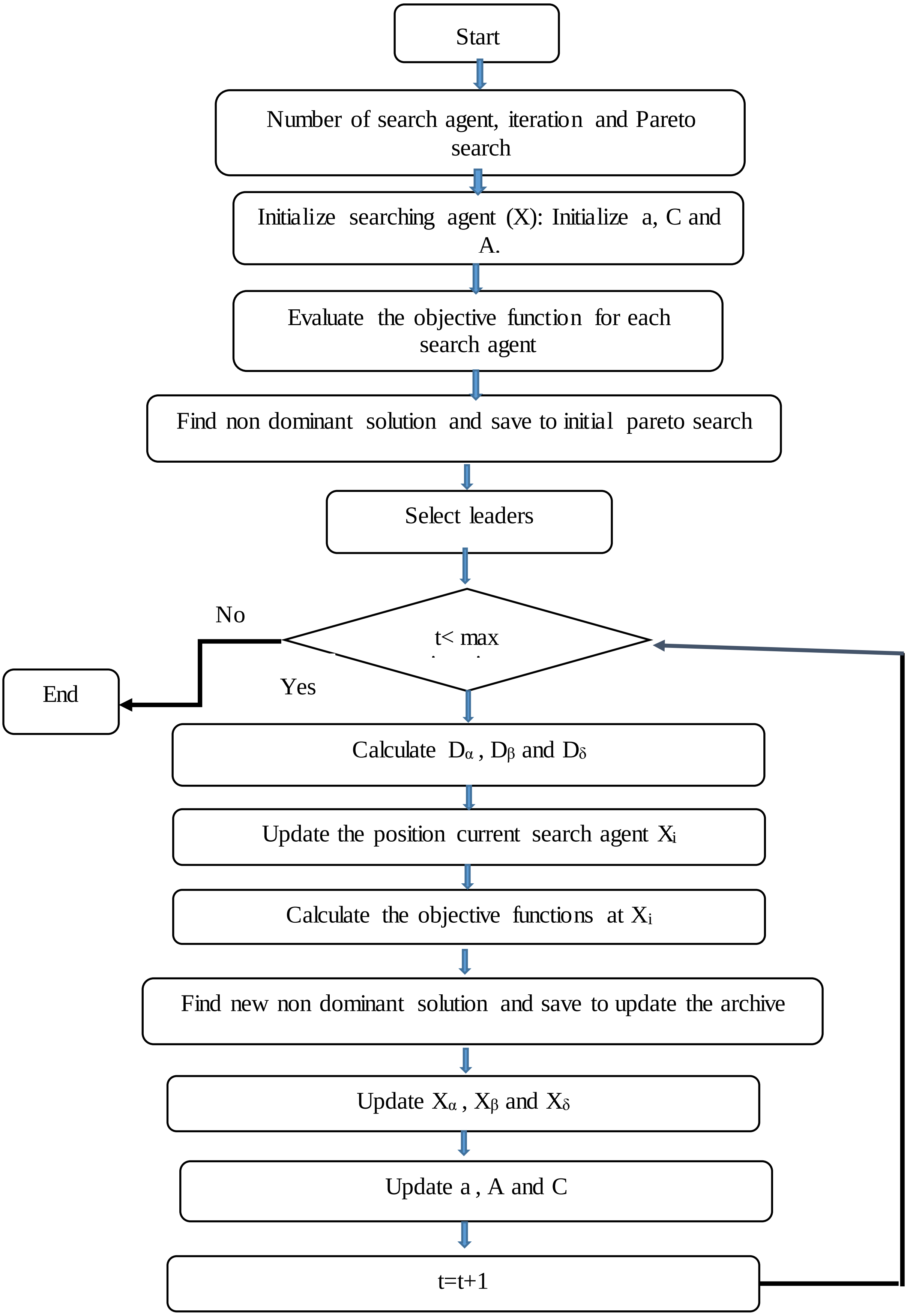

Figure 3.11: Illustrate the flowcharts of (MOGWO)

3.7.5 VIKOR method

Finally the VIKOR method was used to select the best solution from Pareto optimal set based on higher-level information. The VIKOR methodology is multi-criteria decision making (MCDM) or multi-criteria decision analysis method. Assuming that compromise is acceptable for conflict resolution, the decision maker wants a solution that is as close to the ideal as possible and the alternatives are evaluated following all established criteria. VIKOR was initially developed by Serafim Opricovic to resolve decision problems with conflicting and non-commensurable (different units) criteria (Mardani et al., 2016). The compromise option which is close to the optimal solution was identified by VIKOR after ranking the alternatives. The following is how the MCDM problem is stated: From the set of j feasible choices A1, A2... A_j, evaluated using the set of n criterion functions, choose the best (compromise) option in the multi-criteria sense. The performance (decision) matrix's elements f_{ij}, where f_{ij} is the value of the i^{th} criterion function for the option A_j, make up the input data.

The steps of the VIKOR method are as follows:

Step-1

- Establish matrix of criteria and different alternative: $f^+ = \max(f_{ij})$; $f^- = \text{Min}(f_{ij})$

step- 2

- Normalize the decision matrix (normalize S_i and R_j): $S_i = \sum\left[\frac{w_i(f^+_i - f_{ij})}{f^+_i - f^-_i}\right]$; $R_j = Max\left[\frac{w_i(f^+_i - f_{ij})}{f^+_i - f^-_i}\right]$

step -3

- Computation of for group utility function: $Q_j = \frac{v(S_j - S^+)}{S^+ - S^-} + \frac{v-1(R_j - R^+)}{R^- - R^+}$

step- 4

- Rank the alternatives: Ranking of Q_j , R_j and S_j are made from their minimum value. Hence the three ranking lists are obtained.

step- 5

- Acceptance of the ranking choice:-
- Case 1: Acceptable Advantage": Q (A (2) – Q (A (1)) >= DQ where: A (2) is the alternative with second position in the ranking list by Q; DQ = 1/(J-1).
- Case 2: Choice of random acceptance stability, where Q_j is the best from R_j and S_j, when v≥ 0.5

Where,

- ✓ f^+_i *and* f^-_i are the best (maximized responses) and the worst(minimized responses) values of all criterion functions respectively,

- ✓ w_i are the weights of criteria, expressing the DM's preference as the relative importance of the criteria.
- ✓ S_i and R_j are Normalized matrices and Q_j is the index for the group utility function.

CHAPTER FOUR

4. RESULTS AND DISCUSSION

4.1 Introduction

This Experimental study was conducted to evaluate the effects of the critical machining cutting parameters (cutting speed, feed rate, and depth of cut) on the surface roughness, material removal rate and cutting temperature during the CNC turning process of C69300 Lead-Free Copper alloy material. The trials were finished on a CNC lathe using an HSS cutting tool. The three main cutting parameters of Cutting speed (v), feed rate (f), and depth were carefully analyzed by building an experimental design employing a L16 Taguchi Orthogonal Array. Using the design of the experiment (DOE), the cutting parameters with the highest impact on surface roughness, material removal rate, and cutting temperature were identified. Regression models were successfully developed for surface roughness, material removal rate and cutting temperature.

After the regression models was developed, the aforementioned responses were simultaneously optimized using a sophisticated artificial grey wolf algorithm, which was quite successful in identifying the turning parameter values (values of cutting speed ,feed rate ,depth of cut)that were optimized. For simultaneous multi-objective optimization, Multi-optimization grey wolf algorithm (MOGWA) method coupled with the VIKOR (MCDM) method was utilized to optimize surface roughness, material removal rate, and cutting temperature. In this chapter the outcomes of the whole experiments were discussed in detail.

4.2 Samples after CNC Turning

The Turning operation was performed on a CNC lathe using various combinations of the cutting speed, feed rate and depth of cut. The work piece had been turned once before the experiment to remove any sharp edges and provide a smooth surface for the test, decreasing the diameter to 25 mm from the original 25.5mm. Sixteen experiments based on L16 orthogonal array were performed at different combinations of depth of cut, cutting speed and feed rate. The Sample after turning is given in the figure 4.1.

Figure 4.1: Samples after turning process

4.3 Result Values Obtained from Turning Experiment

In any field, data collecting is crucial to statistical analysis since it determines whether the study will advance to the best or worse outcomes. The findings of the analysis are improved by accurate and appropriate data collection. The selection of an appropriate data-gathering method for the analysis is crucial in this area of considered .Taguchi L16 Orthogonal array was used for conducting the experiment and then, from the studied set of input cutting parameters, material removal rate, cutting temperature and the achievable surface roughness were determined as response variables. In this study, each surface roughness (Ra) value is the average of three trial readings. The obtained results from each experimental test in turning C69300 Lead-Free copper alloy using an HSS cutting tool are listed in Tables 4.1 and Table 4.2.

Table 4.1: Experimental results of surface roughness

Exp. No	Cutting speed (m/min)	Feed rate (mm/rev)	Depth of cut(mm)	**Surface roughness (Ra) in(μm)**			
				Trial-I	**Trial-II**	**Trial-III**	**Average**
1	40	0.05	0.50	0.85	0.82	0.84	0.84
2	40	0.10	0.75	2.42	2.45	2.46	2.44
3	40	0.15	1.00	4.28	4.24	4.27	4.26
4	40	0.20	1.25	5.20	5.25	5.23	5.23
5	60	0.05	0.75	0.91	0.92	0.91	0.91
6	60	0.10	0.50	2.13	2.1	2.09	2.10
7	60	0.15	1.25	3.29	3.38	3.46	3.80
8	60	0.20	1.00	4.09	4.11	4.03	4.07
9	80	0.05	1.00	1.07	0.99	1.11	1.07
10	80	0.10	1.25	2.39	2.43	2.45	2.43
11	80	0.15	0.50	4.17	4.1	4.12	4.13
12	80	0.20	0.75	5.69	5.71	5.76	5.72
13	100	0.05	1.25	1.16	1.15	1.16	1.16
14	100	0.10	1.00	2.53	2.55	2.58	2.56
15	100	0.15	0.75	4.24	4.25	4.28	4.26
16	100	0.20	0.50	5.93	5.94	5.99	5.96

The results of the eight combinations of four depths of cut and feed rates for the turning experiments performed at cutting speeds of 40 m/min and 60 m/min are shown in Figure 4.2. The cutting temperature (^{0}C) and surface roughness (μm) are the reported as responses. According to this graph, the generated surface roughness and cutting temperature increased as the applied feed rate increased at four different levels of depth of cut. The same findings are shown in Figure 4.3, where proportionate trends between the applied feed rates and the attainable surface roughness and cutting temperatures were found. Additionally, it was discovered that while the feed rate and cutting speeds are held constant, an increase in the depth of cut causes an increase in all process responses. We can see from Figures 4.2, 4.3, and 4.3 that an increase in the three cutting parameters resulted in an obvious rise in cutting temperature and feasible surface roughness, as well as a significant increase in material removal rate.

Table 4.2: Experimental results of all three responses

Exp. No	Cutting speed (m/min)	Feed rate (mm/rev)	Depth of cut (mm)	Roughness in **(µm)**	MRR in (mm^3/min)	CT in (^{0}C)
1	40	0.05	0.50	0.84	1000	27
2	40	0.10	0.75	2.44	3000	28
3	40	0.15	1.00	4.26	6000	32
4	40	0.20	1.25	5.23	10000	35.4
5	60	0.05	0.75	0.91	2250	37
6	60	0.10	0.50	2.10	3000	39
7	60	0.15	1.25	3.80	11250	41.6
8	60	0.20	1.00	4.07	12000	45.5
9	80	0.05	1.00	1.07	4000	48
10	80	0.10	1.25	2.43	10000	51.7
11	80	0.15	0.50	4.13	6000	52.8
12	80	0.20	0.75	5.72	12000	54
13	100	0.05	1.25	1.16	6250	56
14	100	0.10	1.00	2.56	10000	57.3
15	100	0.15	0.75	4.26	11250	59
16	100	0.20	0.50	5.96	10000	61

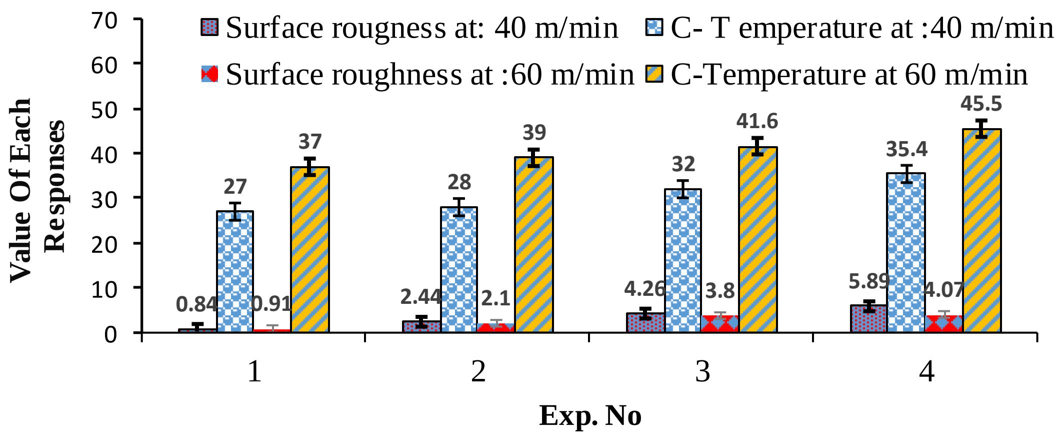

Figure 4.2: The results of the turning trials conducted at a cutting speed of 40 m/min, 60 m/min for cutting temperature and surface roughness

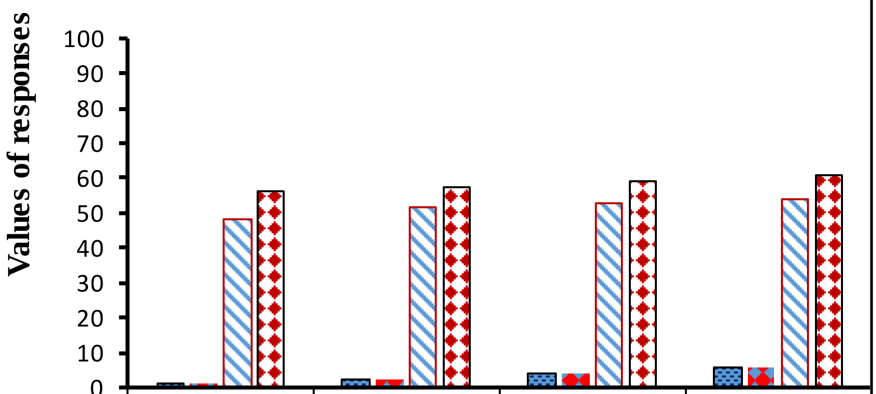

	1	2	3	4
Surface roughness at: 80 m/min	1.07	2.43	4.13	5.72
Surface roughness at 100 m/min	1.16	2.56	4.26	5.96
C- Temperature at: 80 m/min	48	51.7	52.8	54
C-Temperature at:100 m/min	56	57.3	59	61

Figure 4.3: The results of the turning trials conducted at a cutting speed of 80 m/min, 100 m/min Cutting temperature and surface roughness

One can observe from a comparison of the findings shown in the two figures that the increase in applied cutting speed has a negative impact, as a larger value causes both the surface roughness and the generated cutting temperature to rise. Nevertheless, as three cutting parameters increased, all three responses; cutting temperature, material removal rate and the achievable surface roughness were increased. This makes it obvious that there is a trade-off between the positive and negative effects of the process parameters, requiring the use of multi-objective optimization algorithms to increase process productivity while minimizing the other two responses, namely cutting temperature and surface roughness.

As can be seen from figure 4.4, keeping cutting speed at constant value, depth of cut, and feed rate all have a direct relation on the material removal rate. Therefore, increasing one of these factors or both of them, increases material removal rate. However, a high material removal rate alone does not necessarily indicate cost-effective machining, as this also calls for a good surface finish and lower cutting temperature. It is therefore important to optimize the machining parameters which can give us high material removal rate, good surface finish, less cutting temperature and etc

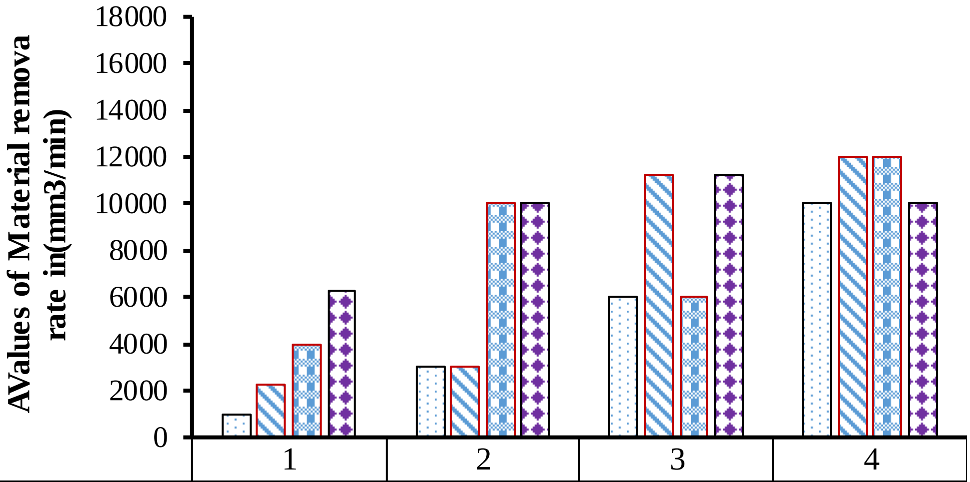

	1	2	3	4
MRR at :40 m/min	1000	3000	6000	10000
MRR at :60 m/min	2250	3000	11250	12000
MRR at : 80 m/min	4000	10000	6000	12000
MRR at :100 m/min	6250	10000	11250	10000

Figure 4.4: The results of the MRR turning trials conducted at a cutting speed of 40 m/min, 60m/min, 80 m/min and 100 m/min

4.4 Analysis of Surface Roughness

4.4.1 Analysis of Variance for Surface Roughness

ANOVA is utilized to identify how process parameters affect the observed outputs as well as how much of a role they played in affecting those outputs. The statistical test values of the machining parameters are used to calculate the Fisher value (F) and probability of confidence level (P), while the F-critical value is taken from a statistical data table. When the measured F-statistical value exceeds the F-critical value, the parameter is considered to have a degree of P-statistical significance for the response. Using Eq. (4.1), it is possible to determine the percentage of the process parameters that contributed to the response being generated. Table 4.3 displays the analysis of variance (ANOVA) of the process parameters on Surface Roughness. . Where DoF = degree of freedom, SS= Sum of squares, MSS = Mean Sum of squares, and F = F- Ratio generated by using Minitab 17 software.

$$\%\text{Contribution} = \text{Sum square of variable (SS)/Total Sum square (SST)} \tag{4.1}$$

Table 4.3: ANOVA process parameters on Surface roughness

Source	DF	Adj SS	Adj MS	F-Value	P-Value	% contribution	Remark
v	3	1.4113	0.4704	2.75	0.135	2.95	S
f	3	44.9784	14.9928	87.49	0.000	94.24	HS
d	3	0.3074	0.1025	0.60	0.639	0.6	LS
Error	6	1.0282	0.1714				
Total	15	47.7254					

S= 0.413975%, R-sq= 97.85%, R-sq(adj)=94.61%, R-sq(pred)=84.68 %

The ANOVA table consists of the F-values and P-values. By comparing the F-values with the tabulated ones (critical F-value), the significance of the factors can be understood. If the obtained F value of a parameter is greater than the tabulated (F- critical) one, then that particular parameter has a significant influence over the response variable. From standard table of F- statics, the F-critical value is $F_{3, 6} = 8.94$. From table 4.3, the F value of spindle speed is, $F=2.75 < F_{0.05, 3, 6} = 8.94$, depth of cut ($0.6 < F_{0.05, 3, 6} = 8.94$), (feed rate ($87.49$) $> F_{0.05, 3, 6} = 8.94$. Therefore, feed rate, have a significant influence over surface roughness.

According to Table 4.3, cutting speed and depth of cut have less effect on surface roughness than feed rate, which also has the highest sum of square (SS) value. Among the cutting parameters considered, feed rate was the most significant factor which affects surface roughness. Its percentage contribution was 94.24%. The Cutting speed was the second parameter that affects surface roughness and according to the ANOVA table, its percentage contribution was 2.95 %. Finally, since depth of cut has high p-value, it has low significant effect on the surface roughness with respect to feed rate and cutting speed. This experimental result was comparable while machining of lead-free copper alloys as reported in literature. According to literature, the obtained surface roughness while machining lead-free copper alloy is more dependent on feed rate than what is in the case for leaded copper alloy (Optimization et al., 2018); Schultheiss et al., 2021). Each of the cutting parameter possesses 3 degrees of freedom (DoF) and there are 15 degrees of freedom in total. The R^2 (adj) is 97.85% which indicates the amount of variation in the regression equation, and the R^2 (pred) which is 84.68 %, indicates how accurately the regression equation predicts the response

(Surface roughness) value. As the R^2 (adj) and R^2 (pred) value are greater than 84%, and they are also nearer to R^2 value (97.85%), it is established that the design models fit the experimental data very fine.

4.4.2 Normal probability plot

The graph of Normal Probability plot of surface roughness is represented in Figure 4.5. It was shown that, residuals follow a normal distribution, thus follow straight line. And the graph of Residuals vs. Predicted in Figure 4.6, which is a plot of the residuals versus the ascending predicted response values used to tests assumption of constant variance and the plot showed a random scatter or constant range of residuals across the graph that indicates there is no need for a transformation. So, the model is suitable to conduct analysis on effect of individual parameters on surface roughness.

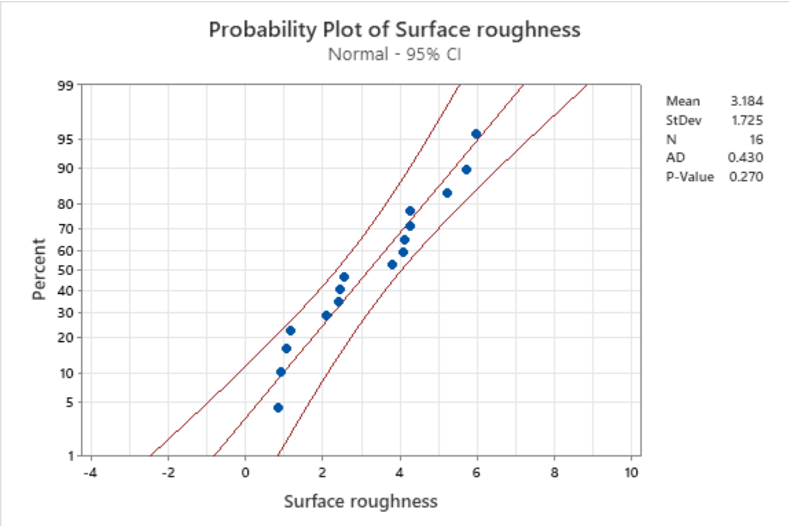

Figure 4.5: Normal Probability plot of surface roughness

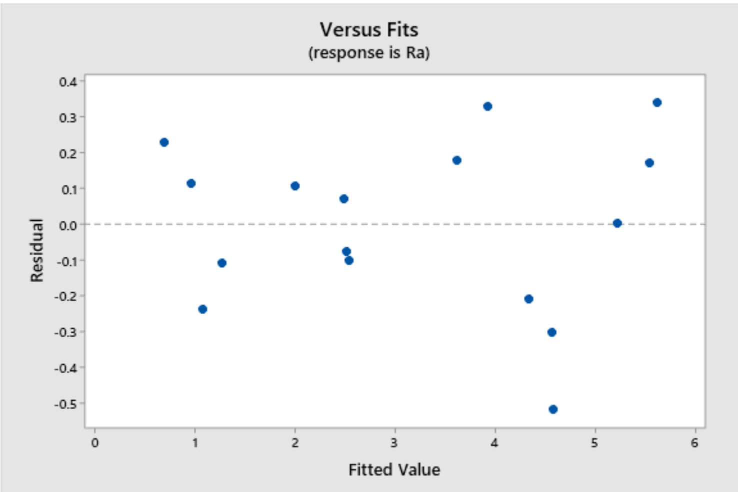

Figure 4.6: Residuals vs. fitted value plot

Main effect plots for means and SN ratios were generated to check the rank of cutting parameters affecting Surface Roughness. From Fig. 4.7, it has been noted that the Surface Roughness increased with an increase in feed rate. Surface Roughness measured at 0.2 mm/rev was higher compared to 0.05 mm/rev, 0.1 mm/rev and 0.15 mm/rev. There was an increase in Surface Roughness when the cutting speed increased as well, but not as that of feed rate. There was less difference for Surface Roughness as the depth of cut increased since it has less significant effect on surface roughness in this case.

Table 4.4: Response Table for Signal to Noise Ratios

Level	**v**	**f**	**d**
1	-8.2979	0.1142	-8.1885
2	-7.3532	-7.5173	-8.6662
3	-8.9417	-12.2728	-8.3831
4	-9.3868	-14.3037	-8.7417
Delta	2.0336	14.4179	0.5533
Rank	2	1	3

Table 4.5: Response Table for Means

Level	**v**	**f**	**d**
1	3.1925	0.9950	3.2575
2	2.7200	2.3825	3.3325
3	3.3375	4.1125	2.9900
4	3.4850	5.2450	3.1550
Delta	0.7650	4.2500	0.3425
Rank	2	1	3

Table 4.4 and Table 4.5 shows the response table for means and S/N ratios of surface roughness and it has been observed that the influence of each parameter on surface roughness was ranked as following order: Feed rate in the 1st place, cutting speed in the 2nd place and depth of cut 3rd place. The same conclusion can be drawn from figure 4.7 and figure 4.8, since the feed rate has the longest line (higher slope) when compared to depth of cut and cutting speed. According to the literature, a similar result was found as feed rate in the 1st place, cutting speed in the 2nd place and depth of cut 3rd place when their level of

significance is ranked on surface roughness during machining of lead-free copper alloy (Toulfatzis et al., 2018; Schultheiss et al., 2021).

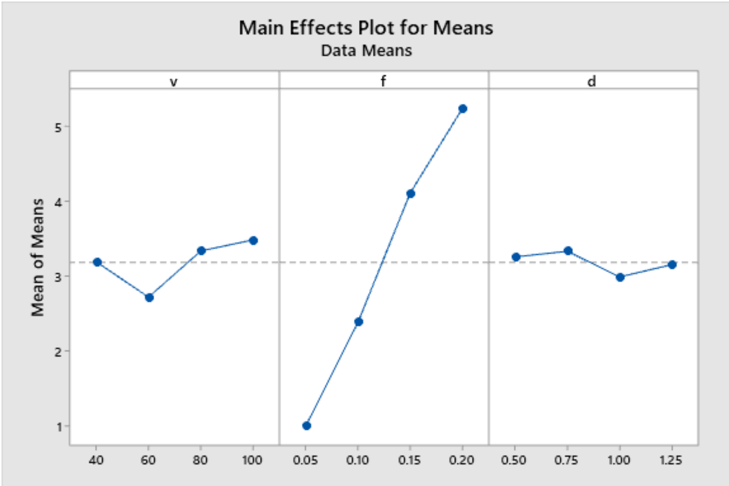

Figure 4.7: Main effect plot for means

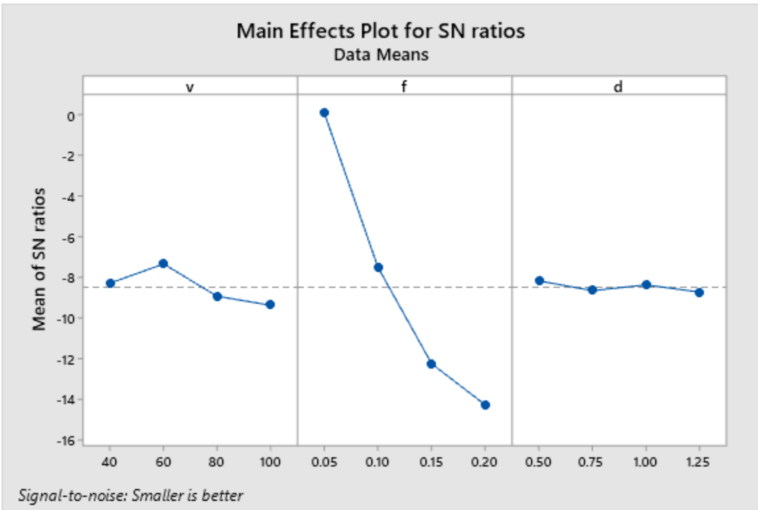

Figure 4.8: Main effect plot for SN ratios

4.4.3 Direct Effects of Machining Parameters on Surface roughness

According to Table 4.3, cutting speed and depth of cut have less effect on surface roughness than feed rate, which also has the highest sum of square (SS) value. Among the cutting parameters considered, the feed rate was the most significant factor affects on surface roughness. Depth of cut has high p- values when compare to feed rate and cutting speed so it is less significant as its p-values are greater than 0.05. Therefore ,lets leave behind the effect of depth of cut on surface roughness and analysis the direct effect of feed rate and cutting speed on surface roughness

4.4.3.1 Effect of feed rate on the surface roughness at constant cutting speed

From figure 4.9, it is evident that the feed rate has significant effect on the surface roughness. It was observed that, feed rate was directly propositional to the surface roughness at four different combination of constant cutting speed. The reason is that the area of contact and load carried by the cutter increases because of the increase in the feed rate. In this study work, increasing the feed rate increases the roughness of the machined surface. At a higher feed rate, the material removal rate is also high which results in the creation of friction between work and tool, leading to a pitting mark. A similar observation was made by (Toulfatzis et al., 2018; Schultheiss et al., 2021). Generally, increasing feed increase surface roughness during turning C69300 Lead-free copper alloy. This is mainly due to the increase in cutting force as the feed rate increases. Furthermore, as the feed rate increased, the plastic deformation also increases which increases cutting force. The increase of cutting force results in increase of machine tool vibration and tool wear which increases surface roughness.

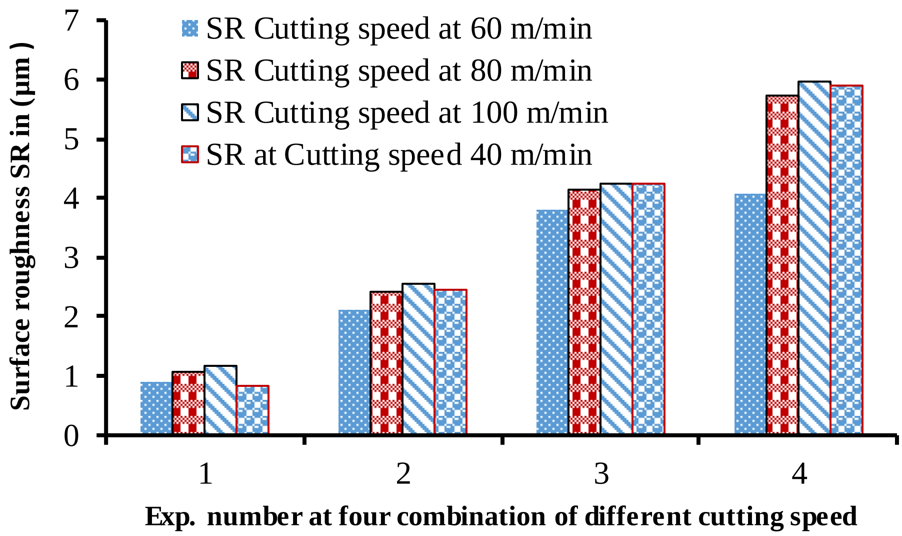

Figure 4.9: Effect of feed rate on the SR at different constant cutting speed

4.4.3.2 Effect of cutting speed on the surface roughness at constant feed rate

The effect of cutting speed on surface roughness is shown in Figure 4.10. It is clear that cutting speed affect surface roughness. Fig 4.10 shows the effect of cutting speed on surface roughness at four different feed rate values. From the graph it can be seen that at 0.05 mm/rev, the surface roughness increased from 0.84 to 1.16 µm. At all 0.1, 0.15 and 0.2 mm/rev, the surface roughness first slightly decreased as the cutting speed increased from 40 to 60 m/min and started to increase slowly as the cutting speed increased to 100 m/men.

The same conclusion was made by different researcher that, when machining lead-free copper alloy especially brass, the effect of cutting speed on the surface roughness fluctuates (Toulfatzis et al., 2018; Schultheiss et al., 2021).

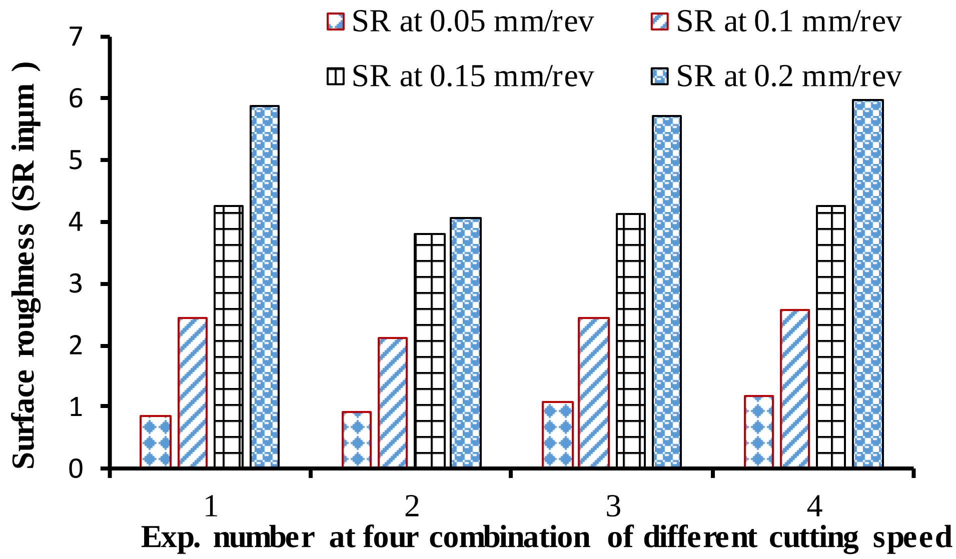

Figure 4.10: Effect of cutting speed on the SR at different constant values of feed rate

4.5 Analysis of Cutting temperature (CT)

4.5.1 Analysis of Variance for Cutting temperature

According to ANOVA in Table 4.6, Cutting speed has the greatest effect on the Cutting temperature and has the largest sum of square (SS) value, followed by feed rate and depth of cut. Among the cutting parameters considered, cutting speed was the most significant factor which effect cutting temperature and its percentage contribution is 93.73%. The feed rate was the second parameter that affects cutting temperature and according to the ANOVA table its percentage contribution was 5.71%. Finally, since the depth of cut has a high p-value, it has low significant effect on the cutting temperature with respect to feed rate and cutting speed. From table 4.6, the F value of spindle speed is, F=917.97 >F0.05, 3, 6 = 8.94, depth of cut (3.46< F0.05, 3, 6 = 8.94), (feed rate (F=55.92) > F0.05, 3, 6 = 8.94. Therefore, feed rate and cutting speed have a significant influence on cutting temperature. There are 15 degrees of freedom in total, with 3 degrees of freedom (DoF) for each cutting parameter. The adj-R^2, which measures the variance in the regression equation, is 99.49% and the pred-R^2, which measures how well the regression equation predicts the response (Cutting Temperature) value, is 98.55%. As the adj-$R^2$and pred-R^2 value is greater than 98%, and they are also nearer to R^2-value (99.80%), it is established that the design models fit the experimental data very fine.

Table 4.6: Analysis of Variance for cutting temperature (CT)

Source	DF	Adj SS	Adj MS	F-Value	P-Value	% contribution	Remarks
Cutting speed	3	1784.87	594.957	917.97	0.000	93.73	HS
Feed Rate	3	108.74	36.246	55.92	0.000	5.71	S
Depth of cut	3	6.74	2.246	3.46	0.091	0.35	LS
Error	6	3.89	0.648				
Total	15	1904.23					

S=0.805062, R^2= 99.80%, R^2(adj)=99.49%, R^2(pred)=98.55%

S-significant HS- highly significant, LS- less significant

,

A main effect plots for means and SN ratios were generated to check the influence of selected cutting parameters on cutting temperature as presented in Fig.4.11 and 4.12 respectively. From this graph, it has been noted that the cutting temperature increases with increases in cutting speed. Cutting temperature value at 100 m/min is higher compared to 40, 60 and 80 m/min. Cutting temperature increases when feed rate and depth of cut increase, resulting in poor surface finish due to high temperature

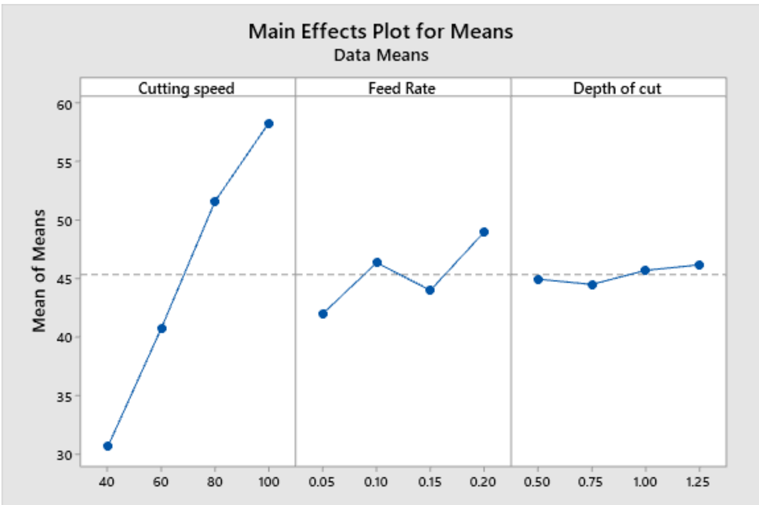

Figure 4.11: Main effect plot for means

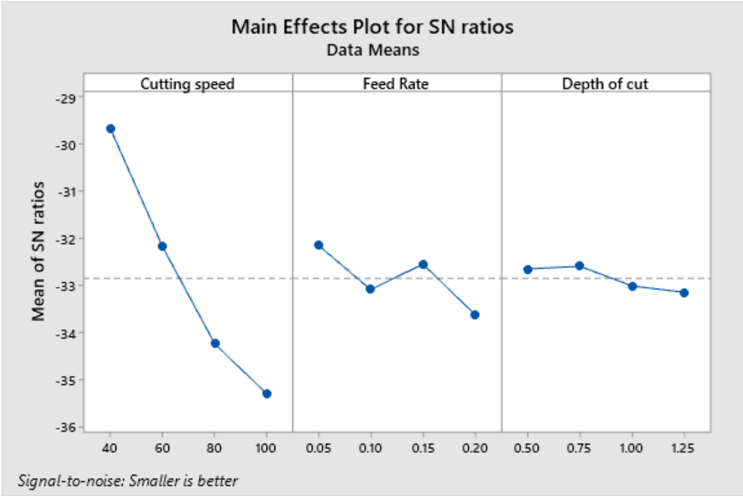

Figure 4.12: Main effect plot for SN ratio

Table 4.7: Response Table for means

Response Table for means			
Level	v	f	d
1	-29.66	-32.14	-32.65
2	-32.18	-32.55	-32.59
3	-34.25	-33.09	-33.01
4	-35.31	-33.62	-33.15
Delta	5.65	1.48	0.56
Rank	1	2	3

The response table for means and S/N ratios of Cutting temperature is shown in Table 4.7, and it has been noted that the order in which each parameter affects Cutting temperature is cutting speed 1st place, feed rate 2nd place, and depth of cut 3rd place. The same inference may be made from figure 4.9 and figure 4.10, where the cutting speed has a longer line or greater slope than the feed rate and depth of cut.

Table 4.8: For Signal-to-Noise Ratio

	Response Table for Signal to Noise Ratios		
Level	v	f	d
1	30.60	42.00	44.95
2	40.77	44.00	44.50
3	51.63	46.35	45.70
4	58.33	48.98	46.17
Delta	27.73	6.98	1.67
Rank	1	2	3

4.5.2 Normal probability plot

The graph of the Normal Probability plot of CT is represented in Figure 4.13. It is demonstrated that residuals follow a straight line since they have a normal distribution. And the graph of Residuals vs. Predicted in Figure 4.14 which is a plot of the residuals versus the ascending predicted response values used to tests assumption of constant variance and the plot showed a random scatter or constant range of residuals across the graph that indicates there is no need for a transformation. Therefore, the model can be used to analyses the impact of specific parameters on cutting temperature.

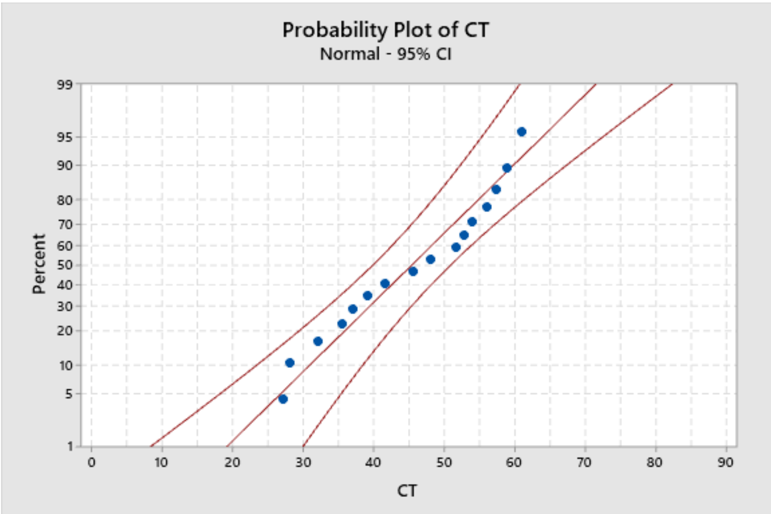

Figure 4.13: Normal probability plot for cutting temperature

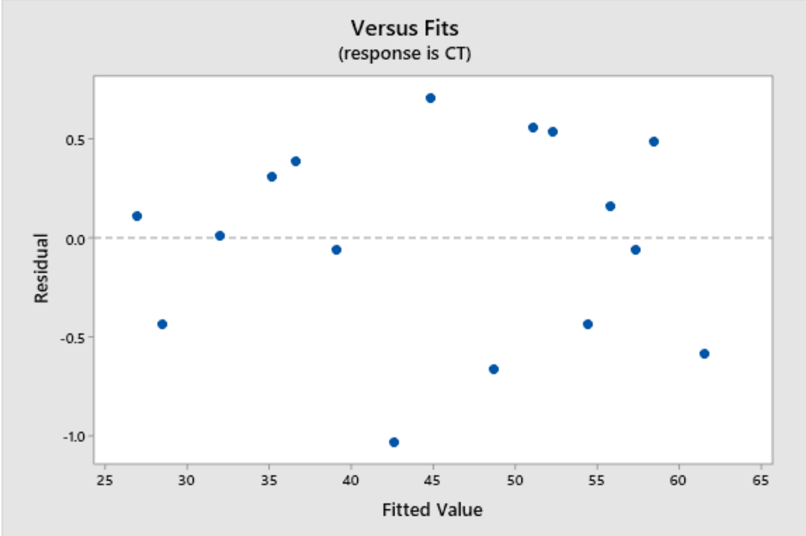

Figure 4.14: Residual vs fitted for cutting temperature

4.5.3 Direct Effects Of Machining Parameters On cutting temperature

4.5.3.1 Effect of feed rate on the cutting temperature

It is clear from Table 4.7 that the feed rate is listed as the second parameter which has significance effects on the cutting temperature. The cutting temperature is directly proportional to the feed rate.

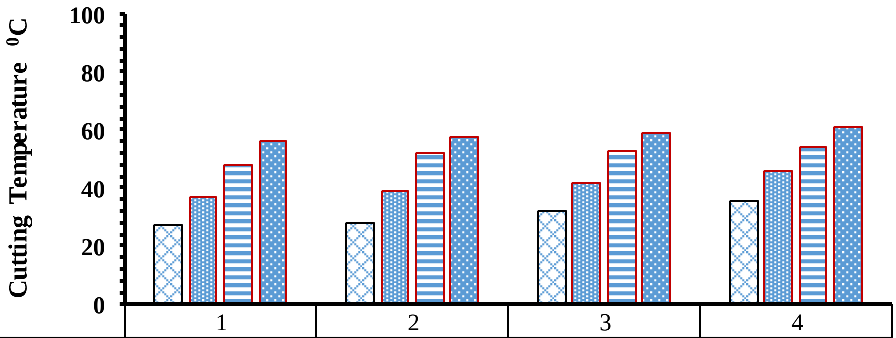

	1	2	3	4
CT- at 40 m/min	27	28	32	35.4
CT- at 60 m/min	37	39	41.6	45.5
CT- at 80 m/min	48	51.7	52.8	54
CT- at 100 m/min	56	57.3	59	61

Exp. number at four combination of different cutting speed

Figure 4.15: Effect of cutting speed on the CT at different constant feed rate

Fig. 4.15 displays that at 40 m/min Cutting temperature increased from 27 °C to 35.4 °C as the feed rate increased from 0.05 to 0.2 mm/rev. A S=similar trend was observed at 60 m/min ,80m/min 100 m/min in which Cutting temperature increased as the feed rate increased from 0.05 mm/rev to 0.2 mm/rev. The reason is that the area of contact and load carried by the cutter increases because of the increase in the feed rate. A faster feed rate leads to a higher rate of material removal, which increases friction between the work and the tool.

4.5.3.2 Effect of Cutting speed on the cutting temperature

From Fig. 4.16, it has been noted that the cutting temperature increased when the cutting speed increased. From the scientific background, as the cutting speed increases, there will be friction increases, which in turns increase the cutting temperature in the deformed zone. Cutting temperature value at 100 m/min is higher compared to 40, 60 and 80 m/min. Table 4.6 and Table 4.7 shows the response table for means and S/N ratios of cutting temperature and it has been observed that the influence of cutting speed on cutting temperature was ranked as: cutting speed in the 1st place. It also denotes that the cutting speed indicates the highest sum of square (SS) value and has also the biggest influence on the cutting temperature followed by feed rate and depth of cut.

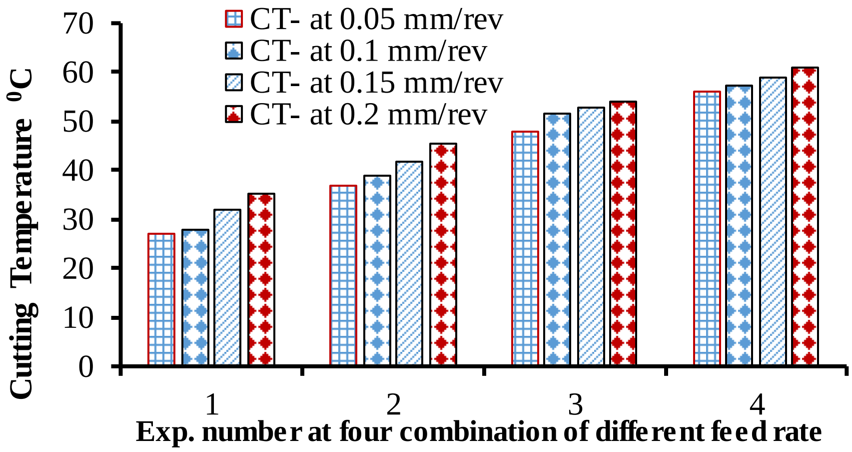

Figure 4.16: Effect of cutting speed on the CT at different constant feed rate

4.6 Analysis of Material Removal Rate (MRR)

In the machining process, the quantity of material removed per unit of time is called the material removal rate (MRR). Equation 4.2 was used to determine MRR in this study.

$$MRR = 1000v * f * d \tag{4.2}$$

As can be seen from equation 4.2, cutting speed, depth of cut, and feed rate all have a direct relation to the material removal rate. Therefore, increasing one of these factors increases the material removal rate. However, a high material removal rate alone does not necessarily indicate cost-effective machining, as this also calls for a good surface finish and lower cutting temperature. It is therefore important to optimize the machining parameters that can give us high material removal rate, good surface finish and less cutting temperature.

4.6.1 Analysis of Variance for Material removal rate (MRR)

Table 4.9 shows that the feed rate has the largest sum of square (SS) value and the greatest influence on Material removal rate**.** The material removal rate was also affected by cutting speed and depth of cut. Both Cutting speed and depth of cut equally affects Material removal rate**.** There are a total of 15 degrees of freedom, with 3 degrees of freedom (DoF) being shared by each cutting parameter. The adj- R^2 and R^2 were 93.07% and 82.69% respectively. Since adj- R^2 and R^2 are close to each other, it can be concluded that the design models fit the experimental data very fine.

Table 4.9: Analysis of Variance for material removal rate

Source	DF	Adj SS	Adj MS	P-Value	%contribution	Remarks
Cutting speed	3	40375000	13458333	0.041	18.18	S
Feed Rate	3	125875000	41958333	0.003	56.73	HS
Depth of cut	3	40375000	13458333	0.041	18.18	S
Error	6	15375000	2562500			
Total	15	222000000				

S= 1600.78 R-sq=93.07% R-sq(adj)= 82.69%

The effects of chosen cutting parameters on Material removal rate were investigated using main effect plots for means and SN ratios, as shown in Fig.4.17 and Fig. 4.18 respectively. Both figures illustrate how cutting parameters affects material removal rate. It was found that as cutting speed and depth of cut increased at constant feed rate, material removal rate also increased. In the study and from the ANOVA, it was found that feed rate was highly significant factor which affects MRR with percentage contribution of 56.73%. A higher Material removal rate results from deeper cuts because there is more material to be removed. Higher Material Removal Rate is achievable if the process is performed at high cutting speed.

Table 4.10: Response Table for means

Level	cutting speed	Feed Rate	Depth of cut

1	5000	3375	5000
2	7125	6500	7125
3	8000	8625	8000
4	9375	11000	9375
Delta	4375	7625	4375
Rank	2.5	1	2.5

Table 4.10 and Table 4.11 displays the response table for means and S/N ratios of Material removal rate and it can be seen that each parameter's influence on Material removal rate was ranked as follows: feed rate came in first, followed by depth of cut and cutting speed, which both had an equal impact. A similar conclusion may be taken from figure 4.17 since, in comparison to cutting speed and feed rate, the depth of cut has the longest line or highest slope.

Table 4.11: Response for Signal to Noise Ratio

Level	cutting speed	Feed Rate	Depth of cut
1	71.28	68.75	71.28
2	74.80	74.77	74.80
3	77.30	78.29	77.30
4	79.24	80.79	79.24
Delta	7.96	12.04	7.96
Rank	2.5	1	2.5

From Figure 4.16 it was observed that the material removal rate increased as cutting speed increased and it have a percentage of contribution of 18.83% in affecting material removal rate. From the experimental investigation it was observed that with too slow a cutting speed, time will be lost for the machining operation, resulting in low material removal rate or production rates.

Figure 4.17: Main effect plot for means

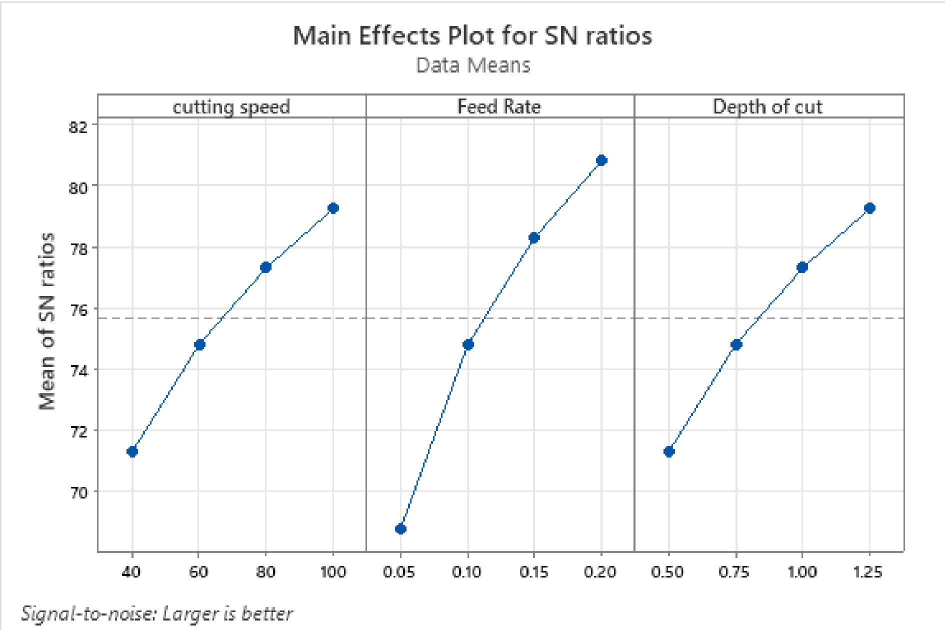

Figure 4.18: Main effect plot for SN ratio

Figure 4.17 also demonstrates that, when the cutting speed increases material removal rate also increases. The Cutting speed contributes 18.18% in affecting material removal rate. According to experimental study, a cutting speed that is too slow wastes time during the machining process and results in a less material removal rate or production. The effect of feed rate on material removal rate is also shown on the same Figure. It can be seen that, the highest material removal rate was found at the highest feed rate of 0.2 mm/rev, and the lowest material removal rate was found at 0.05 mm/rev. The ANOVA results showed that feed rate, with a percentage contribution of 18.18%, was the second major factor determining material removal rate. Increased feed rates result in more material coming into contact with the cutting tool, which increases the cutting force and speeds up the rate at which material is removed.

4.7 Multi-response optimization

The goal was simultaneous optimization of material removal rate (MMR), surface roughness (Ra), and cutting temperature (CT) using the Multi-objective optimization grey wolf algorithm (MOGWA). Since MOGWA requires the objective function of the responses considered, we were expected to develop a multiple regression model to predict three responses (material removal rate (MMR), surface roughness(Ra), and cutting temperature(CT)) by using a data set gathered during CNC turning of lead-free C69300 lead-free copper alloy. Models are used to determine how the responses change with cutting speed, feed rate, and depth of cut. After developing the mathematical function for the three responses, the Ideal multi-objective optimization approach was used to simultaneously optimize the following three responses as illustrated in the table below.

Responses	Independent Variables
Material removal rate(MMR)	Cutting speed (v), feed rate (f) and depth of cut (d).
Surface roughness(Ra)	
Cutting temperature(Tc)	

Surface roughness (Ra), material removal rate (MRR), and cutting temperature (Tc) are conflicting response characteristics. Any industrial engineer's job is to evaluate trade-offs critically because the output parameters are influenced by the machine tool selection, tool characteristics, machining environment, coolant application, and machining parameters. It is therefore essential to use multi-objective optimization approaches because the Taguchi method, which does single-objective optimization, is insufficient. To simultaneously optimize the above-listed three responses, the Ideal multi-objective optimization approach was used to obtain best parameters setting for optimum response performance. Multi-objective optimization grey wolf algorithm (MOGWA), which mimics the social hierarchy, hunting and prey exploration, is successfully implemented and Pareto optimal solutions are successfully recorded. VIKOR methodology was used to obtain the best solutions from Pareto lists.

Ideal multi-objective optimization approach can be summarized as follows:

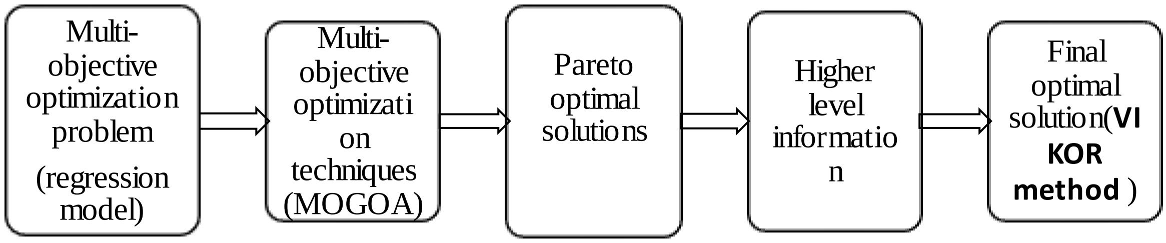

Ideal multi-objective optimization approach needs multiple objective functions. In this case, we have three responses, MRR, Ra and Tc as a function of Cutting speed (v), feed rate (f) and depth of cut (d). Therefore, we have to create a regression model for three responses so that we can use them as objective function for multi-objective optimization algorithm (MOGOA).

4.8 Regression Models for all responses

Regression models are mathematical function that describes the relationship between one or more independent variables and responses or dependent variable. To create mathematical models for three responses, MMR, surface roughness, and cutting temperature, multiple regression analysis was used. However, since material removal rate (MRR) is the deterministic formula, and its regression Equation is given in equation (4.6). Therefore, we developed a regression equation for the cutting temperature and surface roughness only. Although multiple regression analysis is one of the most popular statistical tools to develop mathematical models for dependent variables, it is also one of the most frequently misused.

Some assumptions that must be fulfilled, statistical tests that must be performed to evaluate the model's accuracy and the data's goodness of fit, as well as any issues that could arise with the model. How effectively analysts can use the methodologies to create suitable statistical models that are helpful to solve real problems is the first difficulty(Dietz et al., 1997). The second problem is figuring out how to use a good statistical software program, like Minitab, to implement the right methods and get the required output for evaluating and validating the proposed model. The regression models obtained from the experimental data by Stepwise regression in second-order models and the responses are written as a function of process parameters like cutting speed (v), tool feed (f) and depth of cut (d). For the Surface roughness (SR) and cutting temperature (CT), regression analysis was used to develop second-order regression models. First order, second-order, and interactions models between the various levels were taken into consideration to evaluate the impact of changing parameters (speed (v), tool feed (f) and depth of cut (d)) on the responses. The Regression model's general equation can be written as:

$$Y= \beta o + \sum_1^n \beta_i x_i + \sum_1^n \beta_{ii} x_{ii}2 + \sum_i \sum_j \beta_{ij} x_i x_j \quad (4.3)$$

Y is the response in Eq. (4.1), where x_i, x_j are variables for the cutting speed in (m/min), feed rate in (mm/rev), and depth of cut in (mm), respectively, and $\beta_{i,}$ $\beta_{ii}$and β_{ij} are the linear, quadratic, and interaction factors. The number of control elements in this relationship can range from i=1 to n, with n equivalent to 3 in this case. The MINITAB® 17 Software was used to calculate the coefficients for second-order regression models using experiential values of Ra and Tc and un-coded units (real experimental values of process parameters and responses). The insignificant terms can be removed either by using null hypothesis or by using stepwise procedure using p-values of different terms. On the other hand, the material removal rate (MRR) is deterministic formula, and its regression Equation is given in equation 4.6.

4.8.1 Regression Models for surface roughness (SR) and Cutting temperature (CT)

It is obvious that when developing a regression model, it is critical to include factors that have been specifically tested as well as other variables that influence the response. Minitab Statistical Software includes a number of statistical indicators and procedures that can assist in the development of appropriate regression models. In this study, first order, second-order, and two-way interaction models between different levels were explored to see how changes in factors like speed, feed rate, and depth of cut affected the responses. The MINITAB 17 Software was utilized in the study to compute coefficients for second-order regression models utilizing experiential values of Ra and Tc and un-coded units. Insignificant terms should be deleted when reducing models to simplify the model and increase its forecast accuracy. A model can be simplified by removing the term for a predictor variable or the interaction between predictor variables. This helps to improve prediction precision. Models can be reduced using Minitab software via a variety of procedures, including regression, ANOVA, DOE, and reliability.

To expand further, a term is regarded as statistically significant if the probability of observing a coefficient that is equal to or higher than the one in the model is less than 5%. Furthermore, step-wise regression avoids over fitting by only incorporating variables with a statistically meaningful impact on the result variable. This can help to increase the model's predicted accuracy while also making it more brief and understandable. Overall, these strategies are critical for constructing reliable regression models that may be utilized to make decisions based on data.

To construct a good model, stepwise regression model reduction employs P-values for predictors. Low p-values in regression indicate statistically significant terms. "Reducing the model" refers to the process of incorporating all possible predictors in the model and then methodically deleting the term with the highest p-value one at a time until only significant predictors are left. The adequate mode has a higher Adjusted R-squared and Predicted R-squared. In general, you select models with higher adjusted and forecast R-squared values. These statistics are intended to overcome a significant issue with normal R-squared—it increases with the addition of a predictor and can lead you to construct an unnecessarily complex model. The adjusted R squared increases only if the additional term improves the model more than would be anticipated by chance and it can also drop when the predictors are of poor quality. Predicted R-squared is a type of cross-validation that can decline. By splitting your data, cross-validation determines how well your model generalizes to other data sets.

By comparing the values of Adjusted R-squared and Predicted R-squared from the fit summary of both responses we can check the adequacy of developed model using the stepwise regression procedure. If a reasonable agreement is observed between the Adjusted R-squared and Predicted R-squared, we can say that data predicted by the developed models for each quality characteristic (output) are well-fitted. Furthermore, Residuals Plots, Normal Probability Plot and multi-collinearity was checked to test if any problems that affect the model. Residuals Plots were used to detect model lack of fit and unequal variances. Any trends or patterns in the plots indicate lack of fit and potential problems in the model. Normal Probability Plot is used to check the assumption of normality. A linear trend in the plot suggests that the normality assumption is nearly satisfied; nonlinear trend indicates that the assumption is likely violated.

In regression, multicollinearity occurs when some predictor variables in the model have a connection with other predictor variables. Severe multicollinearity can raise the variance of the regression coefficients, making them unstable.

Minitab software can determine the variance inflation factor (VIF) for a regression model. VIF's value starts at 1 and has no upper limit.

The following is a general rule of thumb for interpreting VIFs:

- ✓ A score of 1 show that there is no connection between any of the predictor variables in the model.
- ✓ A score between 1 and 5 shows a moderate correlation between a given predictor variable and other predictor variable in the model, but it is frequently not severe enough to warrant attention.
- ✓ A number greater than 5 suggests a potentially strong connection between a given predictor variable and the model's other predictor variables. The coefficient estimates and p-values in the regression output are most likely erroneous in this circumstance. The regression analysis for surface roughness and cutting temperature was performed using Minitab software.

Minitab was utilized in this case to create a regression model for the two responses using the Stepwise regression model reduction process. It develops a decent model by using P-values for predictors. Low p-values in regression indicate statistically significant terms. "Reducing the model" refers to the process of incorporating all possible predictors in the model and then methodically deleting the term with the highest p-value one at a time until only significant predictors are left. The following two parts show the ANOVA findings after model reduction for surface roughness and cutting temperature.

4.8.1.1 Regression analysis for Cutting temperature (CT)

Minitab software was used to perform a regression analysis for cutting temperature. In this case, Minitab was used to develop a regression model for cutting temperature by using Stepwise regression model reduction procedure. ANOVA results after model reduction for cutting temperature was displayed in Table 4.12.

Table 4.12: Analysis of Variance of cutting temperature

Source	DF	Adj SS	Adj MS	F-Value	P-Value
Regression	5	1894.24	378.85	378.95	0.000
V	1	1768.14	1768.14	1768.61	0.000
F	1	108.35	108.35	108.37	0.000
D	1	0.27	0.27	0.27	0.614
V*V	1	12.08	12.08	12.08	0.006
V*f	1	0.92	0.92	0.92	0.359
Error	10	10.00	1.00		
Total	15	1904.23			

S= 0.999868, R-sq= 99.47%, R-sq(adj)= 99.21%, R-sq(pred) =98.42%

Table 4.13: Coded Coefficients

Term	Coef	SE Coef	T-Value	P-Value	VIF
Constant	46.417	0.400	116.00	0.000	
V	0.4701	0.0112	42.05	0.000	1.00
F	46.55	4.47	10.41	0.000	1.00
D	0.78	1.51	0.52	0.054	2.04
V*V	-0.002172	0.000625	-3.48	0.006	1.00
V*f	-0.324	0.337	-0.96	0.359	2.84

4.8.1.2 Normal probability plot and residual vs fitted plot

The regression fit of the generated empirical models can be seen with normal probability plots as shown in figure 4.19. It is shown that, residuals following a normal distribution, thus follow straight line. And the graph of Residuals vs. Predicted in Figure 4.20 which is a plot of the residuals versus the ascending predicted response values used to tests assumption of constant variance and the plot showed a random scatter or constant range of residuals across the graph that indicates there is no need for a transformation. So, the model is suitable to conduct analysis on effect of individual parameters on Cutting temperature. If all of the residuals fall along a straight line drawn across the plotted points, it is assumed that the residuals/errors have a normal distribution.

Figure 4.19 demonstrates that the data points are pretty near to the fitted normal distribution line (the middle solid line of the graph). The normal probability plots of residuals show that the residuals are reasonably close to the normal probability lines, and the p-value is greater than the significance level of 0.05 in figure 4.19, showing that residuals are distributed normally (Suresha and Sridhara, 2012).

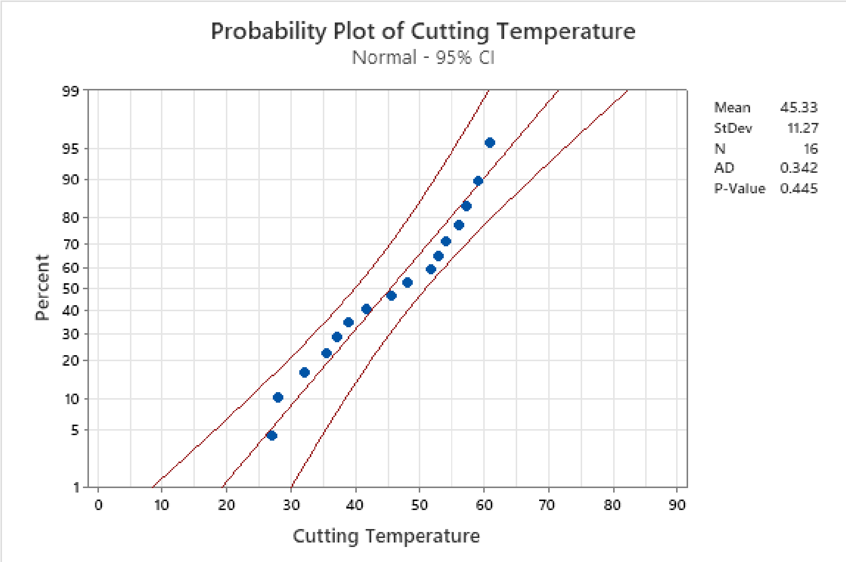

Figure 4.19: Normal probability plot

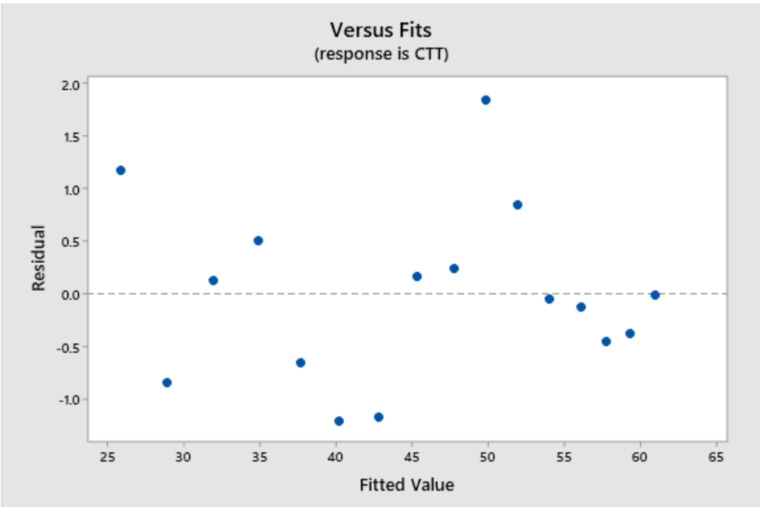

Figure 4.20: Residual vs fitted for cutting temperature

4.8.1.3 Model validation for cutting temperature

From the Analysis of Variance for cutting temperature in Table 4.12 it was observed that, the p-value of the regression model is equal to 0.000 implied that the model estimated by the regression procedure is significant at the level of 0.05.

The values of p for the terms included in the regression model are less than 0.05 indicating that all model terms are significant. In this case v, f, d, v^2 and v*f, were significant model terms and insignificant terms from the models have been removed by considering p-values. Here, we eliminate the variable (term) with the highest p-value for the test of significance of the variable, conditioned on the p-value being bigger than a predetermined level (0.05 or 95 % confidence level for this case). From Table 4.12 the difference between Predicted R-Squared and Adjusted R-squared is very small, then the model is fitting the data and it was reliably used to interpolate. Variance inflation factors (VIF) are all close to one which indicates that the predictors are not correlated (there is no multicollinearity).The R^2 Value indicates, the predictors explains 99.46% variance in the cutting temperature. The adjusted R^2 is account for several predictors in the model. Since the Predicted R-Squared (98.42%) is close to the Adjusted R-square (99.21%) and R-Squared (99.47%), the model does not appear to over fit and has adequate predictive ability. As it has been explained in this section, the model is valid and can be used for further optimization. The final models obtained for predicting cutting temperature (Tc) as the response was given as follows:

$$\mathrm{CT} = -6.47 + 0.8147\,v + 69.2\,\mathrm{f} + 0.78\,\mathrm{d} - 0.002172v^2 - 0.324\,v * \mathrm{f} \qquad (4.4)$$

4.8.2 Regression analysis for surface roughness (Ra)

Minitab software was used to perform a regression analysis for surface roughness. In this case, Minitab was used to develop a regression model for surface roughness by using Stepwise regression model reduction procedure. ANOVA results after model reduction for surface roughness are displayed in Table 4.14.

Table 4.14: Analysis of Variance

Source	DF	Adj SS	Adj MS	F-Value	P-Value
Regression	6	42.9841	7.1640	39.51	0.000
V	1	0.4470	0.4470	2.47	0.151
F	1	41.9341	41.9341	231.28	0.000
D	1	0.0015	0.0015	0.01	0.929
v*v	1	0.3844	0.3844	2.12	0.179
f*f	1	0.0650	0.0650	0.36	0.564
v*f	1	0.0691	0.0691	0.38	0.552
Error	9	1.6318	0.1813		
Total	15	44.6160			

S=0.42581 R-sq=96.34%. R-sq(adj)= 93.90% , R-sq(pred)= 90.51

Table 4.15: Coded Coefficients

Term	Coef	SE Coef	T-Value	P-Value	VIF
Constant	3.070	0.216	14.20	0.000	
V	0.00748	0.00476	1.57	0.151	1.00
F	28.96	1.90	15.21	0.000	1.00
D	0.059	0.642	0.09	0.929	2.84
v*v	0.000387	0.000266	1.46	0.179	1.00
f*f	-25.5	42.6	-0.60	0.564	1.00
v*f	0.089	0.144	0.62	0.552	2.84

4.8.2.1 Normal probability plot and residual vs fitted plot

The regression fit of the generated empirical models can be seen with normal probability plots as shown in figure 4.21. It is shown that, residuals follow a normal distribution, thus following a straight line. And the graph of Residuals vs. Predicted in Figure 4.22 which is a plot of the residuals versus the ascending predicted response values used to tests the assumption of constant variance and the plot showed a random scatter or constant range of residuals across the graph that indicates there is no need for a transformation. So, the model is suitable to analyze effect of individual parameters on Cutting temperature.

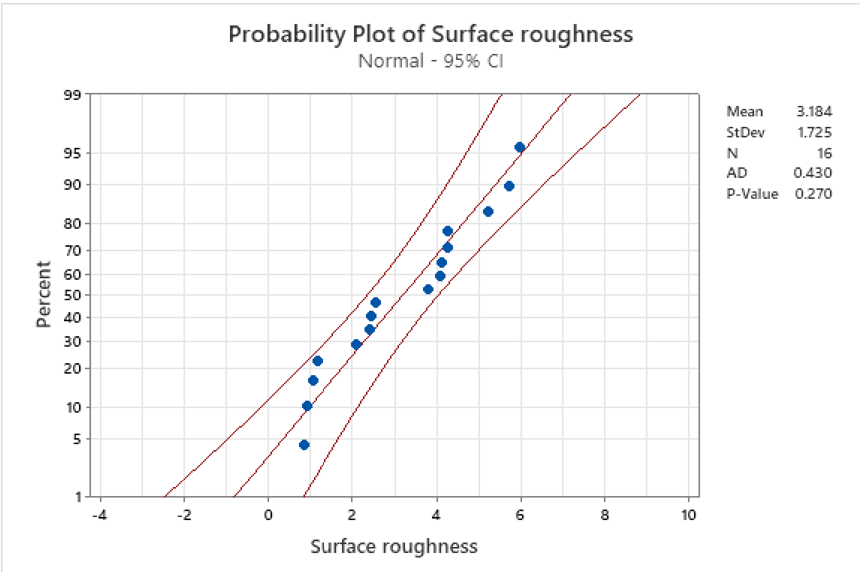

Figure 4.21: Normal probability plot for Surface roughness

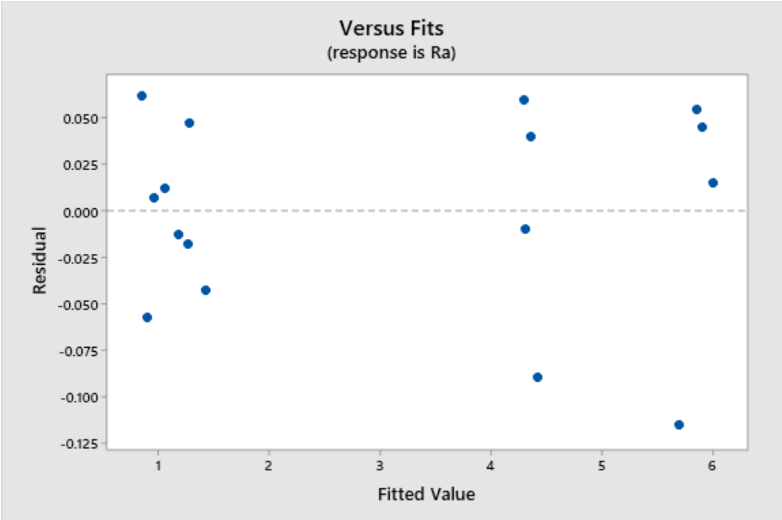

Figure 4.22: residual vs fitted plot for Surface roughness

4.8.2.2 Model validation for surface roughness

From Analysis of Variance for surface roughness on Table 4.14 it was observed that, the p-value of regression model is equal to 0.000 implied that the model estimated by the regression procedure is significant at the level of 0.05. In this case v, f, d, f^2,v^2 and v*f, were used as model terms and highly insignificant terms from the models have been removed by considering *p*-values. Here, we eliminate the variable (term) with the highest *p*-value for the test of significance of the variable, conditioned on the *p*-value being much bigger than a predetermined level (0.05 or 95 % confidence level for this case). From Table 4.14 the difference between Predicted R-Squared and Adjusted R-squared is very small, then the model is fitting the data and it was reliably used to interpolate. Variance inflation factors **(**VIF) are all close to one which indicates that the predictors are not correlated (there no multi-collinearity).The R^2 Value indicates, the predictors explains 94.24% variance in the cutting temperature. The adjusted R^2 is account for number of predictors in the model. Since Predicted R-Squared (90.51%) is close to Adjusted R-square (93.90%) and R-Squared (96.34%), the model does not appear to over fit and has an adequate predictive ability. As it has been explained in this section, the model is valid and can be used for further optimization. The final models obtained for predicting Surface roughness as response was given as follows:

$$Ra = 1.15 - 0.0579\,v + 29.1\,f + 0.059\,d + 0.000387\,v^2 - 25.5\,f^2 + 0.089\,fv \qquad (4.5)$$

On the other hand, the material removal rate (MRR) is deterministic formula with the actual variable values, and its regression Equation is given in equation:-

$$MMR = 1000 * v * f * d \quad (4.6)$$

4.9 Multi-Objective Grey Wolf Optimizer (MOGWO)

We can see from the experimental results in Table 4.1 that increasing the three cutting parameters increased the cutting temperature and the achievable surface roughness, and it also significantly increased the rate at which material was removed. This makes it obvious that there is a trade-off between the positive and negative effects of the process parameters, which requires the use of multi-objective optimization algorithms that increase process productivity while minimizing the other two responses (cutting temperature and surface roughness). From this we can understand that, Surface roughness, material removal rate (MRR), and cutting temperature are conflicting response characteristics. Any industrial engineer's job is to evaluate trade-offs critically because the output parameters are influenced by the machine tool selection, tool characteristics, machining environment, coolant application, and machining parameters. In this case, our goal is to simultaneously maximize material removal rate and minimizing surface roughness as well as cutting temperature.

We employed regression equations created for each response as the objective function to simultaneously optimize surface roughness, MRR, and cutting temperature using the Grey Wolf algorithm. A nonlinear multi-objective problem has been formulated as tried to be explained above. When using calculus based optimization techniques, it is important to verify the function's continuity and to consider the possibility of reporting local maxima or minima. Therefore, a nature-inspired MOGWO that is effective for numerous applications is chosen in this work.

The objective is to Minimize;

$$Ra = 1.15 - 0.0579\,v + 29.1\,f + 0.059\,d + 0.000387\,v*v - 25.5\,f*f + 0.089\,v*f$$

and

$$CT = -6.47 + 0.8147\,v + 69.2\,f + 0.78\,d - 0.002172\,v*v - 0.324\,v*f$$

Subject to Cutting parameter:

$40m/min \leq velocity \leq 100m/min$

$0.05mm/rev \leq feed \leq 0.2mm/rev$ and

$0.5mm \leq doc \leq 1.25mm$

And to Maximize of MMR=1000*v*f*d Subject to cutting parameters:

40m/min $\leq$ velocity $\leq$ 100m/min

0.05mm/rev $\leq$ feed $\leq$ 0.2mm/rev and

0.5mm $\leq$ doc $\leq$ 1.25mm

To optimize the three responses simultaneously, the multi-objective grey wolf optimization is run in MATLAB 2000 version using the following parameter. These initialization parameters were 30 grey wolves, 1000 maximum iterations, 50 for archive size, 0.1 for alpha, 4 for beta, and 2 for gamma. Equations 3.7, 3.8, and 3.9 were used to determine the distance vectors $D\alpha$, D_β and D_δ; these equations were presented in chapter three. Equations 3.10, 3.11, and 3.12 were used to calculate the position vectors. The next position of delta wolf was determined by Using Eq. 3.13. As objective functions, we utilize Equations 4.2, 4.3, and 4.4. The developed regression model for surface roughness, MRR, and cutting temperature are used as objective function in math lab software and the code is run multiple times to obtain the Pareto front. The obtained Pareto optimal solutions are shown In Table 4.16. The recommended convergence rate for grey wolf multi-objective optimization is between 0.01 and 0.05. This means that the algorithm should converge to the global best solution within 10% to 5% of the total number of iterations. The convergence rate of multi-objective grey wolf algorithm code used in this study was 7% which was found in the recommended range.

Table 4.16: Pareto optimal solutions with MOGWO for optimal machining condition

No	v	F	D	MRR	CT	Ra
1	82.62032	0.183127	1.25	18912.52	54.74071	4.902154
2	53.12969	0.0966	1.019093	5230.299	36.48821	2.256198
3	69.87453	0.082449	1.10098	6342.847	44.53367	1.79739
4	67.22859	0.169221	1.246924	14185.59	47.46561	4.286766
5	**64.60768**	**0.14834**	**1.237477**	**11859.85**	**45.20993**	**3.70616** ⟵
6	79.89106	0.113354	1.197401	10843.64	50.57985	2.841947
7	57.29791	0.126899	1.126029	8187.377	40.37051	3.098662
8	57.45348	0.128782	1.111374	8223.014	40.53588	3.14961
9	58.9111	0.118143	1.11988	7794.294	40.76735	2.849685
10	62.96019	0.08865	1.118908	6245.122	41.39838	1.980756
11	63.99755	0.08563	1.10355	6047.602	41.76908	1.887277
12	64.7004	0.155225	1.20326	12084.52	45.5604	3.891357

13	70.08904	0.098652	1.128509	7803.009	45.41222	2.297546
14	59.40567	0.110395	1.110542	7283.064	40.62983	2.627078
15	68.35536	0.098761	1.129152	7622.75	44.58256	2.293144
16	67.68958	0.108496	1.153744	8473.186	44.73769	2.582729
17	56.4844	0.092936	1.107562	5814.052	38.19935	2.130999
18	74.29801	0.156652	1.221258	14214.14	50.07552	4.025186
19	80.68575	0.147422	1.234894	14688.93	52.4169	3.865033
20	58.48961	0.095606	1.108284	6197.496	39.40616	2.199524
21	74.09645	0.161362	1.20397	14395.04	50.18591	4.151365
22	71.85993	0.114512	1.168245	9613.309	47.01121	2.786938
23	64.31781	0.126367	1.159778	9426.251	43.9457	3.088795
24	70.289	0.088584	1.119438	6970.2	45.03324	1.990169
25	72.51187	0.129641	1.205923	11336.32	48.03446	3.238184
26	62.38441	0.10732	1.120673	7502.998	42.01866	2.535367
27	69.03104	0.171151	1.209329	14287.94	48.36248	4.353672
28	59.85755	0.106187	1.108143	7043.444	40.65317	2.504418
29	52.33401	0.107279	1.090455	6122.205	36.66093	2.572164

The obtained real Pareto front is shown in Figure 4.23. The full range of objective functions is covered by MOGWO, and the produced Pareto front is quite close to the real Pareto front. Pareto front plays a role in the distribution of responses to reach a state where it is difficult to improve a particular situation without worsening another. Because connection with other MCDM techniques is necessary to identify the best optimal point, the VIKOR method was used.

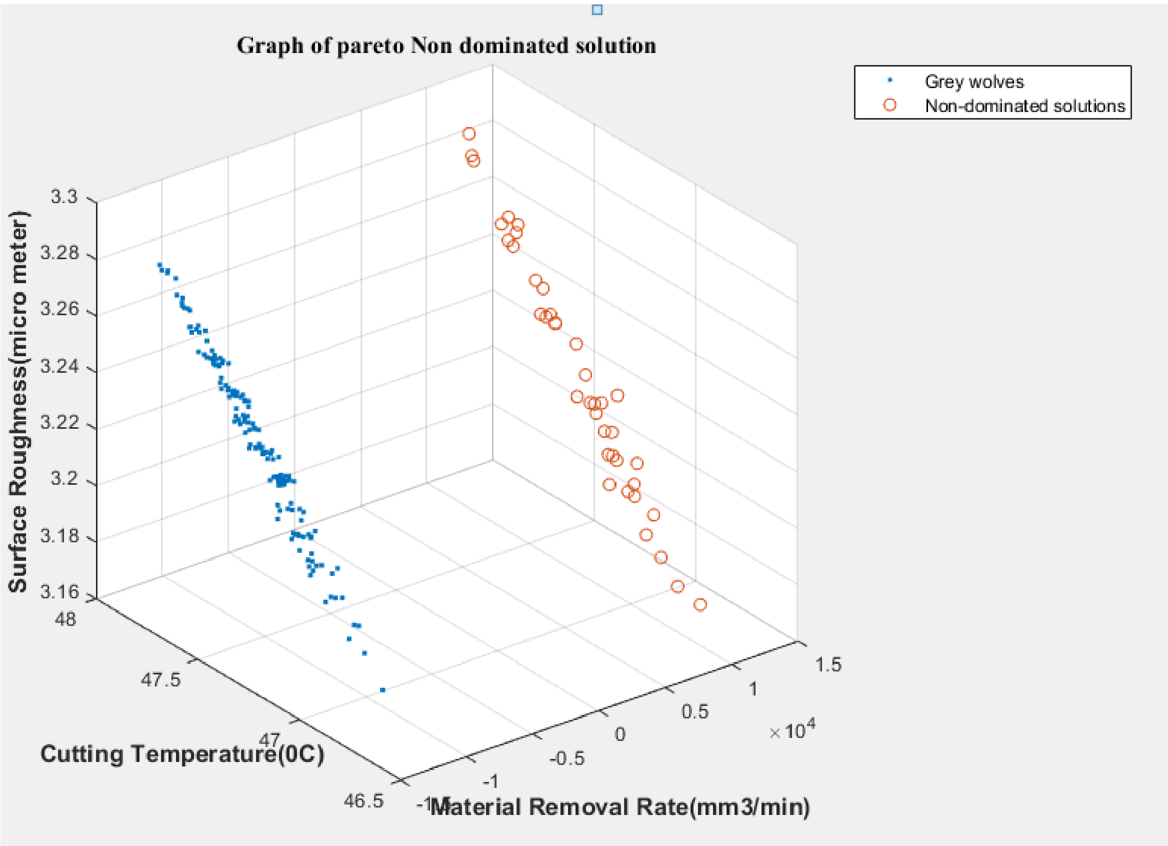

Figure 4.23: MOGWO output of obtained Pareto front for (MRR, SR and CT)

The set of non-dominated solutions that were listed in the Pareto sets are intended maximize material removal rate while minimize surface roughness and cutting temperature at the same time. Surface roughness has optimal values in the Pareto front that range between 1.79 µm and 4.90µm, material removal has optimum values between 5230.299 (mm^3/min) and 18912.52(mm^3/min), and cutting temperature has optimal values between 36.48821 (^{0}C)and 54.74071(^{0}C). For data sets of (69.87(m/min), 0.082(mm/rev), and 1.10(mm)), the Pareto front's lowest surface roughness is 1.79 µm, however the Material removal rate for these combinations is relatively low 6342.847(mm^3/min). From derived real Pareto front shown in Figure 4.23, it can be seen that Pareto front is quite close to the true Pareto front.

4.10 Using VIKOR method to select best solution

Any of the solutions in the Pareto optimum set are feasible because none of them is superior to any other. One option might be preferred over another depending on the requirements of the process engineer. It is important to point out that all of the solutions are feasible choice, and you can use any combination of input parameters to get the required responses. The Pareto front considers the distribution of responses to be at a point where it is impossible to improve one response without affecting another response. However, by using additional

Multi-Criteria Decision Making (MCDM) methods such as VIKOR techniques, it is possible to choose best solution from Pareto non dominated solutions as per requirement. As a result, the VIKOR method was utilized because additional Multi-Criteria Decision Making (MCDM) methods must be coupled with MOGWO to identify the required optimal solution per given requirements.

In utilizing VIKOR method and nearly all of the responses were given the same relative weight. Hence, weights criteria for Cutting temperature, surface roughness and material removal rate were assigned as w_{1}= 0.33, w_{2}= 0.34 and w_{3}= 0.33 respectively. W_i are the weights of criteria, expressed by the decision maker (DM) preference as the relative importance criteria to choose best solution. Therefore it is up to decision maker to choose relative importance between all criteria. The normalized out values of VIKOR techniques were calculated by using steps described in chapter three. The normalized values of the outputs for the VIKOR technique that was used are shown in Table 4.17. The group's best strategy is used to calculate the utility measure, individual regret scores are used to calculate the regret measure, and steps listed in chapter three are used to calculate the VIKOR measure.

The best and worst solutions are chosen. The solution with the lowest VIKOR value (64.60768m/min, 0.14834mm/rev and 1.237477mm) and the equivalent output is (11859.85 mm^3/min, 45.2^{0}C, and 3.70616µm) is the best one. The results of the confirmatory test are presented in Table 4.18 at the values that were obtained. The percentage errors between predicted and experimental value for surface roughness and cutting temperature were 6.48 and 2.9% respectively.

Table 4.17: VIKOR computations

NO	MRR	CT	Ra	Si	Ri	Qi	Rank
1	0.348283	0.227886	0.295773017	1.01	0.67	0.5	28
2	0.096319	0.151901	0.136128399	0.708766	0.378766	0.515429	29
3	0.116807	0.185394	0.108446092	0.756201	0.453034	0.464228	22
4	0.261235	0.1976	0.258643389	0.847674	0.583082	0.388102	10
5	**0.218405**	**0.188209**	**0.223612322**	**0.738327**	**0.535447**	**0.293987**	**1**
6	0.199691	0.210564	0.171469747	0.830623	0.56813	0.386345	9
7	0.150775	0.168063	0.186958767	0.727985	0.469306	0.390903	12
8	0.151431	0.168751	0.190032726	0.734762	0.476943	0.388694	11
9	0.143536	0.169715	0.171936631	0.727875	0.459716	0.407191	15
10	0.115007	0.172342	0.119509554	0.722001	0.416478	0.471975	23
11	0.11137	0.173885	0.11386945	0.728499	0.418211	0.479451	26
12	0.222542	0.189668	0.234786228	0.778805	0.556241	0.323401	3
13	0.143696	0.189052	0.138623163	0.755292	0.487343	0.403864	14
14	0.134121	0.169142	0.158505556	0.726314	0.445824	0.428529	18
15	0.140377	0.185598	0.138357574	0.748064	0.475768	0.41211	16
16	0.156038	0.186243	0.155829777	0.74071	0.488925	0.377691	8
17	0.107069	0.159024	0.128574521	0.699174	0.383254	0.492295	27
18	0.26176	0.208465	0.242860857	0.856306	0.603207	0.367437	6
19	0.270504	0.218212	0.233198019	0.91506	0.618348	0.435957	19
20	0.11413	0.164048	0.132709	0.710441	0.403769	0.475198	24
21	0.265092	0.208924	0.250473906	0.869466	0.614311	0.369543	7
22	0.177034	0.195708	0.168150758	0.749769	0.525482	0.3295	4
23	0.173589	0.182946	0.186363438	0.733773	0.504974	0.338977	5
24	0.12836	0.187474	0.120077454	0.755734	0.467699	0.438301	20
25	0.208764	0.199968	0.195376841	0.766026	0.550948	0.311932	2
26	0.138171	0.174924	0.152972162	0.731827	0.456642	0.418826	17
27	0.263119	0.201334	0.262680185	0.876134	0.604432	0.397231	21
28	0.129708	0.16924	0.151104826	0.72527	0.439001	0.438565	21
29	0.112743	0.15262	0.155192299	0.702543	0.394055	0.479171	25

In addition to the best solution obtained, a confirmatory test was run using two randomly selected no dominated solution from the Pareto solution set. For the second confirmatory test conducted, the percentage errors between predicted and experimental value for surface roughness and cutting temperature were 4.9%, 6%, respectively. Percentage errors of 2.3 % and 5.7% were observed for the third confirmatory test. From confirmatory test it can be seen that, the MOGWO algorithm was used to enhance the machining system's performance indicators, and the outcomes were encouraging.

4.11 Confirmatory test

The best selected solution by using MCDM approach (VIKOR method) was used to conduct the confirmatory test. In addition to the best solution obtained, a confirmatory test was run using two randomly selected no dominated solution from the Pareto solution set. Table 4.18 shows, the predicted, experimental, and percentage errors values from confirmatory test. The predicted and experimental values error percentages are listed in the table 4.18 for each confirmatory test performed. From confirmatory test it can be seen that, the MOGWO algorithm was used to enhance the machining system's performance indicators, and the outcomes were encouraging.

Table 4.18: Result of Confirmatory experiments conducted at selected solution and two randomly selected solutions

Run no	Optimal values	Response	predicted	experimental	%error
1	V=64.60768m/min, f=0.14834mm/rev d=1.237477mm	CT(^{0}C)	45.2	43.87	2.9%,
		Ra(**μm**)	3.7	3.46	6.48%,
3	v=76.09(m/min),, f=0.16(mm/rev),, d= 1.21(mm)	CT(^{0}C)	50.67727	52.51	4.9%,
		Ra(**μm**)	3.941615	4.18	6%,
3	v=71.86(m/min),, f=0.115(mm/rev),, d= 1.17(mm)	CT(^{0}C)	47.01121	45.93	2.3%,
		Ra(**μm**)	2.786938	2.63	5.7%,

4.12 Analysis of Chip Morphology

The machining test chips were gathered and evaluated to some extent. The type of chip used in metal cutting processes is important because it influences product accuracy, tool life, surface quality, and operator safety. In general, the cutting conditions used during the machining procedure have a large impact on chip control. Experiments with turning revealed several chip morphologies. In this investigation, chips fabricated from C69300 lead-free copper were mainly either continuous chips or connected arc chips; however, discontinues chips were also produced. Figure 4.24 shows an overall view of all the chips produced by each combination of cutting conditions. The chips are sorted according to the results of the experiment. It was discovered that increasing the depth of cut and feed rate while maintaining the same cutting speed thickened the chip, resulting in a poorer surface finish than those with a lower depth of cut and feed rate.

Figure4.24 shows that throughout the investigated range of feed and depth of cut at constant cutting speed, there was small discernible effect on the generated chip type for this alloy. At constant cutting speed, the types of chips produced changed from continuous chip to discontinuous chip when both depth of cut and feed rate increased. In general, when both the depth of cut and the feed rate rise at all constant cutting speeds evaluated, chip thickness increases significantly and the chip type produced changes from continuous to discontinuous. All studies with higher feed rates, faster cutting speeds, and lower depths of cut created discontinuous chips, indicating that feed rate had a greater influence on the type of chip produced. Chip morphology investigation found that as feed rate increased rapidly in dry machining, chip size decreased and chip breakability increased. When the feed rate was increased from 0.05 mm/rev to 0.2 mm/rev, very short discontinuous and closely curled thick chips were produced. According to the results of this experimental study, the feed rate was the most critical parameter determining the chip size types of chip produced, and discontinuous chip were made at fed rates greater than 0.15 mm/rev.

The type of chip formed during machining varies from continuous long to continuous fragmented at low feed rates and high cutting speeds, which is explained by a reduction in contact width between chip segments induced by the accumulation of cutting bands that grow progressively intense. Localized deformation in the primary cutting zone becomes critical due to thermal stress created during temperature increase. Because of the creation of a plastic instability, the mechanical characteristics of the work piece surface change, resulting in rapid chip shear. Increased cutting speed during hard turning turns the chip from a continuous ribbon chip to a fragmented ribbon chip while utilizing moderate feed (average feed level). The greatest chip thickness was 0.58 mm at a feed rate of 0.2 mm/rev, while the smallest chip thickness was 0.09 mm at a feed rate of 0.05 mm/rev. Furthermore, the longest and shortest chip lengths were discovered to be 10.6 mm and 2 mm, respectively. This study also found that continuous chips were formed from experiments conducted at high cutting speed, low feed rate, and low depth of cut, indicating that cutting speed has a greater effect on the types of chips produced than depth of cut. Changing the cutting speed (v) also has a substantial influence, since the chip moves from discontinuous to continuous as the cutting speed increases. It should be mentioned that, due to lower production, slowing down the cutting speed to produce the necessary discontinuous chip type is not recommended. Chip morphology analysis further revealed that at high cutting speed and low feed rate, chip thickness increases. This is due to a huge contact area at low cutting speeds. In contrast, increased feed caused by significant compressive stresses generated upstream of the tool rake resulted in plastic deformation of a large volume of material, resulting in a thick chip.

The observed direct relationship between feed and surface roughness can be due to the formation of fracture type discontinuous chips, which causes machined surface roughness to increase. At high depths of cut, the form of chip produced during machining changes from continuous long to continuous fragmented at low feed rates and high cutting speeds, which is explained by a reduction in contact width between chip segments caused by the accumulation of cutting bands that become increasingly intense. Localized deformation in the primary cutting zone becomes critical due to thermal stress created during temperature increase. Because of the creation of a plastic instability, the mechanical characteristics of the work piece surface change, resulting in rapid chip shear. Increased cutting speed during hard turning turns the chip from a continuous ribbon chip to a fragmented ribbon chip while utilizing moderate feed (average feed level). As the cutting speed increases with a high feed rate, the chip shape changes from a thin long ribbon to a continuous non-fractured ribbon.

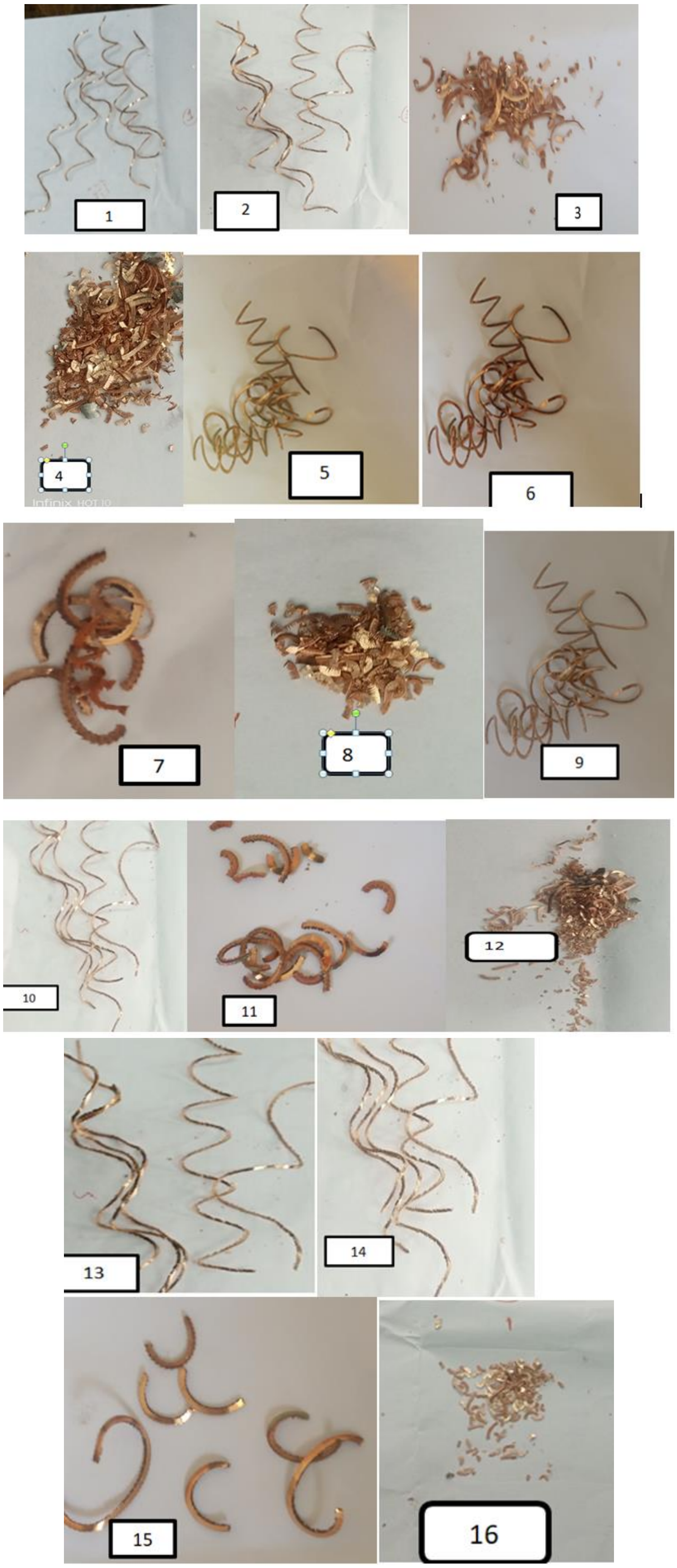

Figure 4.24: Chips collected from each experiment

CHAPTER FIVE

5. CONCLUSION AND RECOMMENDATION

5.1 Conclusions

The current study focuses on the simultaneous multi-objective optimization of machining parameters during dry turning of the C69300 lead-free copper alloy. The optimum cutting parameter setting for the best response performance was obtained by effectively implementation of multi-objective grey wolf algorithm together with VIKOR method. ANOVA was used to determine most significant parameter on the considered responses (Cutting temperature, surface roughness, material removal rate).

The following conclusions were drawn from the study:

1. From the Analysis of variance (ANOVA) for surface roughness, the most significant cutting parameter that affects surface roughness was feed rate followed by cutting speed and depth of cut. When this result is compared with that of leaded copper alloy, the result was different. According to different literature, cutting speed has the biggest influence on the Surface roughness followed by feed rate and depth of cut during the machining of leaded copper alloy. Therefore, the machining characteristics of lead-free copper alloys are different from that of leaded copper alloy.
2. The influence of cutting parameters on cutting temperature was ranked as following order: cutting speed in the 1st place, feed rate in the 2nd place and depth of cut in the 3rd place in this study. When compared to the outcome of the leaded copper alloy supported by the literature, this result was different once again. According to different literature, the influence of cutting parameters on cutting temperature was ranked in the following order: cutting speed in the 1st place, depth of cut in the 2nd place and feed rate in the 3rd place. Again this outcome shows, the machining characteristics of lead-free copper alloy is different from that of leaded copper alloy.
3. The factor that had the greatest influence on the material removal rate was feed rate, which contributed 56.73%, followed by the depth of cut and cutting speed, which contributed equally 18.18%.
4. From this experimental test it was concluded that, as three cutting parameters were increased, cutting temperature and the achievable surface roughness also increased. This increment in the cutting parameters also markedly increases the rate at which material was removed from the work piece. This makes it obvious that there is a the

trade-off between the positive and negative effects of the process parameters, requiring the use of multi-objective optimization algorithms to increase process productivity while minimizing the other two responses, namely cutting temperature and surface roughness.

5. The proposed method (i.e., the coupling of MOGWO with VIKOR) shows that it can be used in machining applications where the development of many outputs is necessary and optimal parameter combinations are required. Additionally, heuristic methods like MOGWO search responses within the boundaries of the experiments and provide several responses findings for VIKOR's optimality check.
6. The full range of objective functions is covered by MOGWO, and the produced Pareto front is quite close to the real Pareto front. Twenty-nine alternatives set of non-dominated solutions were obtained by MOGWO and any of the solutions in the Pareto optimum set are feasible because none of them is superior to any other. One option might be preferred over another depending on the requirements of the process engineer.
7. Using the MCDM technique (VIKOR method), the best choice from the Pareto solution set was selected based on the higher-level information. Higher level information was implemented by giving equal preference for three responses and the obtained solution was given as: surface roughness 3.70616µm, Cutting temperature 45.2^{0}C and material removal rates 11859.85 mm^3/min. The corresponding input cutting parameters were cutting speed 64.6 m/min, Feed rate 0.15 mm/rev and depth of cut 1.23 mm.
8. Three confirmatory tests were conducted and the results were compared to the predicted value. The results obtained from conducted experiment was, Surface roughness of 3.46 µm, 4.18µm and 2.63 µm for confirmatory test 1, 2 and 3 respectively. The results were in close agreement with predicted values obtained from optimization. The values of Cutting temperature for optimum combination were 43.87(^{0}C), 52.51(^{0}C) and 45.93 (^{0}C) for confirmatory test 1, 2 and 3 respectively. Again, these results were in close agreement with predicted values obtained from optimization. Material removal rate was 5230.299 (mm^3/min), 14069.11 (mm^3/min) and 9613.309 (mm^3/min) for confirmatory test 1, 2 and 3 respectively. As a result of the positive study results, the hybrid optimization technique (VIKOR and MOGA) is promising and can be used to solve further machining-related difficulties. Furthermore, from confirmatory tests conducted, it was concluded that the obtained

real Pareto front solutions were encouraging in improving machining performance during dry turning of C69300 lead-free copper alloy.

5.2 Recommendation

The approach employed in this study is limited to the parameters, equipment, and the work piece material C69300 lead-free copper alloy. This is its fundamental limitation. However, because the methodology is completely generalized and universal, it can be modified to different machining operations, work piece materials and machining circumstances with extra experimental investigation. Furthermore, future studies should thoroughly examine all sorts of cutting tool wear mechanisms and chip morphology. Generally, the following points are recommended for further investigation:

- Future studies could be focused on a greater number of input and output process variables. This will help to optimize the process by taking into account a greater number of factors.
- In this study, the effect of cutting parameters such as feed rate, depth of cut, and cutting speed was investigated. Future research could take into account additional aspects such as nose radius, cutting tool geometry, material coating, lubricants, chip breakers, and so on.
- An advanced multi-objective intelligent algorithm following the behavior and social activity of grey wolves was applied to optimize the process parameters. As a major future perspective it is recommended that, further investigation is required by using soft computing methods and several intelligent algorithms for optimizing the turning of C69300 lead-free copper alloy. The reason behind this is, due to different performance of intelligent algorithms in generating optimized solution.

SPECIAL AKCKOWLEDGEMENT

This research work is funded by Adama Science and Technology University under the grant number ASTU/SM-R/907/23, Adama, Ethiopia.

REFERENCE

Abbas, A. T., Al-abduljabbar, A. A., Rayes, M. M. El, Benyahia, F., Abdelgaliel, I. H., & Elkaseer, A. (2023). *Multi-Objective Optimization of Performance Indicators in Turning of AISI 1045 under Dry Cutting Conditions*. 1–22.

Abbas, A. T., Pimenov, D. Y., Erdakov, I. N., Taha, M. A., El Rayes, M. M., & Soliman, M. S. (2018). Artificial intelligence monitoring of hardening methods and cutting conditions and their effects on surface roughness, performance, and finish turning costs of solid-state recycled aluminum alloy 6061 chips. *Metals*, *8*(6). https://doi.org/10.3390/met8060394

Adineh, M., & Doostmohammadi, H. (2021). A hybrid approach based on artificial neural network and cuckoo algorithm for optimization of the main cutting force during turning of Si brass alloys. *SN Applied Sciences*, *3*(1), 1–15. https://doi.org/10.1007/s42452-020-04075-1

Adineh, M., Doostmohammadi, H., & Raiszadeh, R. (2019). Effect of Si and Al on the microstructure, mechanical properties and machinability of 65Cu-35Zn brass. *Iranian Journal of Materials Science and Engineering*, *16*(2), 21–32. https://doi.org/10.22068/ijmse.16.2.21

Amaral, L., Quinta, R., Silva, T. E., Soares, R. M. B., Castellanos, S. D., & de Jesus, A. M. P. (2018). Effect of lead on the machinability of brass alloys using polycrystalline diamond cutting tools. *Journal of Strain Analysis for Engineering Design*, *53*(8), 602–615. https://doi.org/10.1177/0309324718796384

Arun Vikram, K., Ratnam, C., Sankara Narayana, K., & Satish Ben, B. (2015). Assessment of surface roughness and MRR while machining brass with HSS tool and carbide inserts. *Indian Journal of Engineering and Materials Sciences*, *22*(3), 321–330.

Besharatnia, F., Talebpour, A., & Aliakbary, S. (2022). An Improved Grey Wolves Optimization Algorithm for Dynamic Community Detection and Data Clustering. *Applied Artificial Intelligence*, *36*(1). https://doi.org/10.1080/08839514.2021.2012000

Chruściński, M., Szkudelski, S., Borowski, J., Meller, A., & Suszyński, M. (2021). New copper alloys used to make products intended for contact with drinking water. *Materials*, *14*(21). https://doi.org/10.3390/ma14216301

Dietz, E. J., Mendenhall, W., & Sincich, T. (1997). A Second Course in Statistics: Regression Analysis. *Journal of the American Statistical Association*, *92*(438), 797. https://doi.org/10.2307/2965740

Doostmohammadi, H., & Moridshahi, H. (2015). Effects of Si on the microstructure, ordering transformation and properties of the Cu60Zn40 alloy. *Journal of Alloys and Compounds*, *640*, 401–407. https://doi.org/10.1016/j.jallcom.2015.03.228

Ebrahim, K. T., Jiru, M. G., & Sisay, A. (2020). *Optimization of Cutting Parameters for Free Cutting Brass (CuZn35Pb3) Using Optimization of Cutting Parameters for Free Cutting Brass (CuZn35Pb3) Using Taguchi Method*. *September*.

https://doi.org/10.20372/ejssdastu

Fountas, N., Kechagias, J. D., & Vaxevanidis, N. M. (2019). *implementing Grey Wolf algorithm*. *50*, 584–594. https://doi.org/10.3221/IGF-ESIS.50.49

Gaitonde, V. N., Karnik, S. R., & Davim, J. P. (2008). Selection of optimal MQL and cutting conditions for enhancing machinability in turning of brass. *Journal of Materials Processing Technology*, *204*(1–3), 459–464. https://doi.org/10.1016/j.jmatprotec.2007.11.193

Johansson, J., Alm, P., M'Saoubi, R., Malmberg, P., Ståhl, J. E., & Bushlya, V. (2022). On the function of lead (Pb) in machining brass alloys. *International Journal of Advanced Manufacturing Technology*, *120*(11–12), 7263–7275. https://doi.org/10.1007/s00170-022-09205-0

Klocke, F., Nobel, C., & Veselovac, D. (2016). Influence of Tool Coating, Tool Material, and Cutting Speed on the Machinability of Low-Leaded Brass Alloys in Turning. *Materials and Manufacturing Processes*, *31*(14), 1895–1903. https://doi.org/10.1080/10426914.2015.1127944

Kumar, P., Rajesh, K., & Verma, K. (2022). Exploration of nature inspired Grey wolf algorithm and Grey theory in machining of multiwall carbon nanotube / polymer nanocomposites. *Engineering with Computers*, *38*(2), 1127–1148. https://doi.org/10.1007/s00366-020-01103-x

Laakso, S. V. A., Hokka, M., Niemi, E., & Kuokkala, V. T. (2013). Investigation of the effect of different cutting parameters on chip formation of low-lead brass with experiments and simulations. *Proceedings of the Institution of Mechanical Engineers, Part B: Journal of Engineering Manufacture*, *227*(11), 1620–1634. https://doi.org/10.1177/0954405413492732

Makhadmeh, S. N., Alomari, O. A., Mirjalili, S., Al-Betar, M. A., & Elnagar, A. (2022). Recent advances in multi-objective grey wolf optimizer, its versions and applications. *Neural Computing and Applications*, *34*(22), 19723–19749. https://doi.org/10.1007/s00521-022-07704-5

Mardani, A., Zavadskas, E. K., Govindan, K., Senin, A. A., & Jusoh, A. (2016). VIKOR technique: A systematic review of the state of the art literature on methodologies and applications. *Sustainability (Switzerland)*, *8*(1). https://doi.org/10.3390/su8010037

Marler, R. T., & Arora, J. S. (2004). Survey of multi-objective optimization methods for engineering. *Structural and Multidisciplinary Optimization*, *26*(6), 369–395. https://doi.org/10.1007/s00158-003-0368-6

Mirjalili, S., Mirjalili, S. M., & Lewis, A. (2014). Grey Wolf Optimizer. *Advances in Engineering Software*, *69*, 46–61. https://doi.org/10.1016/j.advengsoft.2013.12.007

Ni, H., & Alpas, A. T. (2003). Sub-micrometer structures generated during dry machining of copper. *Materials Science and Engineering A*, *361*(1–2), 338–349. https://doi.org/10.1016/S0921-5093(03)00530-6

Nobel, C., Hofmann, U., Klocke, F., & Veselovac, D. (2016). Experimental investigation of chip formation, flow, and breakage in free orthogonal cutting of copper-zinc alloys. *International Journal of Advanced Manufacturing Technology*, *84*(5–8), 1127–1140. https://doi.org/10.1007/s00170-015-7749-z

Oishi, K., Goto, H., Suzaki, K., Oka, T., & Mori, H. (2023). *Development of Next-Generation Lead-Free Free-Cutting ¡ + ¢ Brass + 1 . 64*(1), 191–195.

Optimization, S., Toulfatzis, A. I., Pantazopoulos, G. A., Id, D. S. S., & Paipetis, A. S. (2018). Machinability of Eco-Friendly Lead-Free Brass Alloys : *Toulfatzis*, 1–18. https://doi.org/10.3390/met8040250

Pantazopoulos, G. (2002). Leaded brass rods C 38500 for automatic machining operations: A technical report. *Journal of Materials Engineering and Performance, 11*(4), 402–407. https://doi.org/10.1361/105994902770343926

Rajabi, Z., & Doostmohammadi, H. (2018). Effect of addition of tin on the microstructure and machinability of α-brass. *Materials Science and Technology (United Kingdom)*, *34*(10), 1218–1227. https://doi.org/10.1080/02670836.2018.1435484

Rao, K. V. (2019). *A Novel Approach for Minimization of Tool Vibration and Surface Roughness in Orthogonal Turn Milling of Silicon Bronze Alloy*. 691–701.

Rojananan, S., Suksongkarm, P., & Rojananan, S. (2017). Using recycled bismuth-tin solder in novel machinable lead-free brass. *Materials Transactions*, *58*(12), 1754–1760. https://doi.org/10.2320/matertrans.M2017227

Schultheiss, F., Johansson, D., Bushlya, V., Zhou, J., Nilsson, K., & Ståhl, J. E. (2021). Comparative study on the machinability of lead-free brass. *Journal of Cleaner Production*, *149*, 366–377. https://doi.org/10.1016/j.jclepro.2017.02.098

Schultheiss, F., Windmark, C., Sjöstrand, S., Rasmusson, M., & Ståhl, J. E. (2018). Machinability and manufacturing cost in low-lead brass. *International Journal of Advanced Manufacturing Technology*, *99*(9–12), 2101–2110. https://doi.org/10.1007/s00170-018-1866-4

Seçgin, Ö. (2021). Multi-objective Optimization of Ms58 Brass Machining Operation by Multi-axis CNC Lathe. *Arabian Journal for Science and Engineering*, *46*(3), 2133–2145. https://doi.org/10.1007/s13369-020-04984-8

Shape, C., & Alloys, B. (2023). *Effect of Wear on Vibration Amplitude and Chip Shape Characteristics during Machining of Eco-Friendly and Leaded Brass Alloys*.

Speed, H., Of, M., & Rod, B. (2019). *HSM2019-108 HIGH SPEED MACHINING OF BRASS ROD ALLOYS*. *1269*, 3277–3284. https://doi.org/10.17973/MMSJ.2019

Stoddart, C. T. H., Lea, C., Dench, W. A., Green, P., & Pettit, H. R. (1979). Relationship between lead content of Cu–40Zn, machinability, and svvarf surface composition determined by Auger electron spectroscopy. *Metals Technology*, *6*(1), 176–184. https://doi.org/10.1179/030716979803276435

Subbaiah, V. V. K. L. K. V. (2022). Eco - Friendly Machining of Ti - 6Al - 4V Alloy : Optimization Using a Hybrid Algorithm (Grey Wolf Algorithm and VIKOR Algorithm). *Journal of The Institution of Engineers (India): Series C*, *103*(5), 1111–1124.

https://doi.org/10.1007/s40032-022-00871-3

Taha, M. A., El-Mahallawy, N. A., Hammouda, R. M., Moussa, T. M., & Gheith, M. H. (2012). Machinability characteristics of lead-free-silicon brass alloys as correlated with microstructure and mechanical properties. *Ain Shams Engineering Journal*, *3*(4), 383–392. https://doi.org/10.1016/j.asej.2012.05.004

Tam, P. L., Schultheiss, F., Ståhl, J. E., & Nyborg, L. (2016). Residual stress analysis of machined lead-free and lead-containing brasses. *Materials Science and Technology (United Kingdom)*, *32*(17), 1789–1793. https://doi.org/10.1080/02670836.2016.1223266

Tesfay Reda, A., Zhang, D., Xu, X., Pan, M., Chang, C., Muhire, C., Liu, X., & Jiayi, S. (2021). Bismuth-impregnated aluminum/copper oxide-pillared montmorillonite for efficient vapor iodine sorption. *Separation and Purification Technology*, *270*(February), 118848. https://doi.org/10.1016/j.seppur.2021.118848

Toulfatzis, A. I., Pantazopoulos, G. A., David, C. N., Sagris, D. S., & Paipetis, A. S. (2018). Final heat treatment as a possible solution for the improvement of machinability of pb-free brass alloys. *Metals*, *8*(8), 1–14. https://doi.org/10.3390/met8080575

Toulfatzis, A. I., Pantazopoulos, G. A., & Paipetis, A. S. (2016). Microstructure and properties of lead-free brasses using post-processing heat treatment cycles. *Materials Science and Technology (United Kingdom)*, *32*(17), 1771–1781. https://doi.org/10.1080/02670836.2016.1221493

Vilarinho, C., Davim, J. P., Soares, D., Castro, F., & Barbosa, J. (2005). Influence of the chemical composition on the machinability of brasses. *Journal of Materials Processing Technology*, *170*(1–2), 441–447. https://doi.org/10.1016/j.jmatprotec.2005.05.035

Yadu Krishnan, J., Poorna Sundar, S., Karthikeyan, L., Veera Ajay, C., & Manisekar, K. (2020). Experimental optimization of cutting parameters in turning of brass alloy using Taguchi method. *Materials Today: Proceedings*, *42*(xxxx), 377–382. https://doi.org/10.1016/j.matpr.2020.09.561

Yang, C., Ding, Z., Tao, Q. C., Liang, L., Ding, Y. F., Zhang, W. W., & Zhu, Q. L. (2018). High-strength and free-cutting silicon brasses designed via the zinc equivalent rule. *Materials Science and Engineering A*, *723*(December 2017), 296–305. https://doi.org/10.1016/j.msea.2018.03.055

Zhao, H., Liu, L., Wu, Y., & Hu, W. (2007). Investigation on wear and corrosion behavior of Cu-graphite composites prepared by electroforming. *Composites Science and Technology*, *67*(6), 1210–1217. https://doi.org/10.1016/j.compscitech.2006.05.013

APPENDIX

a) Pseudo code of the MOGWO algorithm

Initialize the grey wolf population Xi (i = 1, 2, ..., n)
Initialize a, A, and C
Calculate the objective values for each search agent
Find the non-dominated solutions and initialized the archive with them
Xα=Select Leader(archive)
Exclude alpha from the archive temporarily to avoid selecting the same leader
Xβ= Select Leader(archive)
Exclude beta from the archive temporarily to avoid selecting the same leader
Xδ= Select Leader(archive)
Add back alpha and beta to the archive
t=1;
***while** (t < Max number of iterations)*
***for** each search agent*
Update the position of the current search agent by equations (3.5)-(3.11)
end for
Update a, A, and C
Calculate the objective values of all search agents
Find the non-dominated solutions
Update the archive with respect to the obtained non-dominated solutions
***If** the archive is full*
Run the grid mechanism to omit one of the current archive members
Add the new solution to the archive
end if
***If** any of the new added solutions to the archive is located outside the hypercube*
Update the grids to cover the new solution(s)
end if
Xα=Select Leader(archive)
Exclude alpha from the archive temporarily to avoid selecting the same leader
Xβ= Select Leader(archive)
Exclude beta from the archive temporarily to avoid selecting the same leader
Xδ= Select Leader(archive)
Add back alpha and beta to the archive
t=t+1
end while
*return **archive***

b) Matlab R2000 code for MOGWO

➡Note that, in this case: y1 is MRR,Y2 is Cutting temperature and Y3 is surface roughness whereas, x1 is cutting speed, X2 is feed rate and X3 is depth of cut.

➡ Creating Function name

```
function fobj = cec09(name)
    switch name
      case 'UF8'
            fobj = @UF8;
       end
end
function y = UF8(x)
 y(1,:)= -1000*x(1,:)*x(2,:)*x(3,:);
 y(2,:)=   -6.47+   0.81447*x(1,:)    +   69.2*x(2,:)    +   0.78*x(3,:)   -
0.002172*x(1,:)^2  - 0.324*x(1,:)*x(2,:);
 y(3,:)=   1.15   -   0.0579*x(1,:)    +   29.1*x(2,:)    +   0.059   *x(3,:)
+0.000387*x(1,:)^2-25.5*x(2,:)^2+ 0.089 *x(1,:)*x(2,:);
    clear Y;
end
```

➡ CreateEmptyParticle

```
function particle=CreateEmptyParticle(n)
    if nargin<1
        n=1;
    end
    empty_particle.Position=[];
    empty_particle.Velocity=[];
    empty_particle.Cost=[];
    empty_particle.Dominated=false;
    empty_particle.Best.Position=[];
    empty_particle.Best.Cost=[];
    empty_particle.GridIndex=[];
    empty_particle.GridSubIndex=[];
    particle=repmat(empty_particle,n,1);

end
```

➡ CreateHypercubes

```
function G=CreateHypercubes(costs,ngrid,alpha)
    nobj=size(costs,1);
    empty_grid.Lower=[];
    empty_grid.Upper=[];
    G=repmat(empty_grid,nobj,1);
    for j=1:nobj
         min_cj=min(costs(j,:));
        max_cj=max(costs(j,:));
        dcj=alpha*(max_cj-min_cj);
        min_cj=min_cj-dcj;
        max_cj=max_cj+dcj;
        gx=linspace(min_cj,max_cj,ngrid-1);
        G(j).Lower=[-inf gx];
        G(j).Upper=[gx inf];
    end
end
```

➡ DeleteFromRep

```
function rep=DeleteFromRep(rep,EXTRA,gamma)
```

```
    if nargin<3
        gamma=1;
    end
    for k=1:EXTRA
        [occ_cell_index occ_cell_member_count]=GetOccupiedCells(rep);
        p=occ_cell_member_count.^gamma;
        p=p/sum(p);
        selected_cell_index=occ_cell_index(RouletteWheelSelection(p));
        GridIndices=[rep.GridIndex];
        selected_cell_members=find(GridIndices==selected_cell_index);
        n=numel(selected_cell_members);
        selected_memebr_index=randi([1 n]);
        j=selected_cell_members(selected_memebr_index);
        rep=[rep(1:j-1); rep(j+1:end)];
    end
end
```

➡ **DetermineDomination**

```
function pop=DetermineDomination(pop)
    npop=numel(pop);
   for i=1:npop
        pop(i).Dominated=false;
        for j=1:i-1
            if ~pop(j).Dominated
                if Dominates(pop(i),pop(j))
                    pop(j).Dominated=true;
                elseif Dominates(pop(j),pop(i))
                    pop(i).Dominated=true;
                    break;
                end
            end
        end
    end
end

function dom=Dominates(x,y)
    if isstruct(x)
        x=x.Cost;
    end
    if isstruct(y)
        y=y.Cost;
    end
    dom=all(x<=y) && any(x<y);
end
```

➡ **GetCosts**

```
function costs=GetCosts(pop)
    nobj=numel(pop(1).Cost);
    costs=reshape([pop.Cost],nobj,[]);
end
```

➡ **GetGridIndex**

```
function [Index SubIndex]=GetGridIndex(particle,G)
    c=particle.Cost;
    nobj=numel(c);
    ngrid=numel(G(1).Upper);
    str=['sub2ind(' mat2str(ones(1,nobj)*ngrid)];
    SubIndex=zeros(1,nobj);
    for j=1:nobj
        U=G(j).Upper;
        i=find(c(j)<U,1,'first');
```

```
        SubIndex(j)=i;
        str=[str ',' num2str(i)];
    end
    str=[str ');'];
    Index=eval(str);
end
```

➡ GetNonDominatedParticles

```
function nd_pop=GetNonDominatedParticles(pop)
    ND=~[pop.Dominated];
    nd_pop=pop(ND);
end
```

➡ GetOccupiedCells

```
function [occ_cell_index occ_cell_member_count]=GetOccupiedCells(pop)
    GridIndices=[pop.GridIndex];
    occ_cell_index=unique(GridIndices);
    occ_cell_member_count=zeros(size(occ_cell_index));
    m=numel(occ_cell_index);
    for k=1:m
        occ_cell_member_count(k)=sum(GridIndices==occ_cell_index(k));
    end
end
```

➡ RouletteWheelSelection

```
function i=RouletteWheelSelection(p)
    r=rand;
    c=cumsum(p);
    i=find(r<=c,1,'first');
end
```

➡ SelectLeader

```
function rep_h=SelectLeader(rep,beta)
    if nargin<2
        beta=1;
    end
    [occ_cell_index occ_cell_member_count]=GetOccupiedCells(rep);
    p=occ_cell_member_count.^(-beta);
    p=p/sum(p);
    selected_cell_index=occ_cell_index(RouletteWheelSelection(p));
    GridIndices=[rep.GridIndex];
    selected_cell_members=find(GridIndices==selected_cell_index);
    n=numel(selected_cell_members);
    selected_memebr_index=randi([1 n]);
    h=selected_cell_members(selected_memebr_index);
    rep_h=rep(h);
end
```

➡ Variables boundary

```
function range = xboundary(name,dim)
    range = ones(dim,2);
    switch name
        case {'UF8'}
            range(1,1)  = 40;
            range(1,2)  = 100;
            range(2,1)  =  0.05;
            range(2,2)  =  0.2;
            range(3,1)  =  0.5;
            range(3,2)  =  1.25;
    end
end
```

➡Mail Program

```
clear all
clc
drawing_flag = 1;
TestProblem='UF8';
nVar=3;
fobj = cec09(TestProblem);
xrange = xboundary(TestProblem, nVar);
lb=xrange(:,1)';
ub=xrange(:,2)';
VarSize=[1 nVar];
GreyWolves_num=30;
MaxIt=1000;
Archive_size=50;
alpha=0.1;
nGrid=10;
beta=4;
gamma=2;
GreyWolves=CreateEmptyParticle(GreyWolves_num);
for i=1:GreyWolves_num
    GreyWolves(i).Velocity=0;
    GreyWolves(i).Position=zeros(1,nVar);
    for j=1:nVar
        GreyWolves(i).Position(1,j)=unifrnd(lb(j),ub(j),1);
    end
    GreyWolves(i).Cost=fobj(GreyWolves(i).Position')';
    GreyWolves(i).Best.Position=GreyWolves(i).Position;
    GreyWolves(i).Best.Cost=GreyWolves(i).Cost;
end
GreyWolves=DetermineDomination(GreyWolves);
Archive=GetNonDominatedParticles(GreyWolves);
Archive_costs=GetCosts(Archive);
G=CreateHypercubes(Archive_costs,nGrid,alpha);
for i=1:numel(Archive)
    [Archive(i).GridIndex
Archive(i).GridSubIndex]=GetGridIndex(Archive(i),G);
end
for it=1:MaxIt
    a=2-it*((2)/MaxIt);
    for i=1:GreyWolves_num

        clear rep2
        clear rep3
        Delta=SelectLeader(Archive,beta);
        Beta=SelectLeader(Archive,beta);
        if size(Archive,1)>1
            counter=0;
            for newi=1:size(Archive,1)
                if sum(Delta.Position~=Archive(newi).Position)~=0
                    counter=counter+1;
                    rep2(counter,1)=Archive(newi);
                end
            end
            Beta=SelectLeader(rep2,beta);
        end
        if size(Archive,1)>2
            counter=0;
            for newi=1:size(rep2,1)
                if sum(Beta.Position~=rep2(newi).Position)~=0
                    counter=counter+1;
```

```
                    rep3(counter,1)=rep2(newi);
                end
            end
            Alpha=SelectLeader(rep3,beta);
        end
        c=2.*rand(1, nVar);
        D=abs(c.*Delta.Position-GreyWolves(i).Position);
        A=2.*a.*rand(1, nVar)-a;
        X1=Delta.Position-A.*abs(D);
        c=2.*rand(1, nVar);
        D=abs(c.*Beta.Position-GreyWolves(i).Position);
        A=2.*a.*rand()-a;
        X2=Beta.Position-A.*abs(D);
        c=2.*rand(1, nVar);
        D=abs(c.*Alpha.Position-GreyWolves(i).Position);
        A=2.*a.*rand()-a;
        X3=Alpha.Position-A.*abs(D);
        GreyWolves(i).Position=(X1+X2+X3)./3;
        GreyWolves(i).Position=min(max(GreyWolves(i).Position,lb),ub);
        GreyWolves(i).Cost=fobj(GreyWolves(i).Position')';
    end
    GreyWolves=DetermineDomination(GreyWolves);
    non_dominated_wolves=GetNonDominatedParticles(GreyWolves);
    Archive=[Archive
        non_dominated_wolves];
    Archive=DetermineDomination(Archive);
    Archive=GetNonDominatedParticles(Archive);
    for i=1:numel(Archive)
        [Archive(i).GridIndex
Archive(i).GridSubIndex]=GetGridIndex(Archive(i),G);
    end
    if numel(Archive)>Archive_size
        EXTRA=numel(Archive)-Archive_size;
        Archive=DeleteFromRep(Archive,EXTRA,gamma);
                Archive_costs=GetCosts(Archive);
        G=CreateHypercubes(Archive_costs,nGrid,alpha);
    end
    disp(['In iteration ' num2str(it) ': Number of solutions in the
archive = ' num2str(numel(Archive))]);
    save results
    costs=GetCosts(GreyWolves);
    Archive_costs=GetCosts(Archive);
    if drawing_flag==1
        hold off
        plot3(costs(1,:),costs(2,:),costs(3,:),'.');
        hold on
        plot3(-
Archive_costs(1,:),Archive_costs(2,:),Archive_costs(3,:),'o');
        legend('Grey wolves','Non-dominated solutions');
        drawnow
    end
    y= -Archive_costs(:,1);
end
```

c) Result of composition of materials from spectroscopy

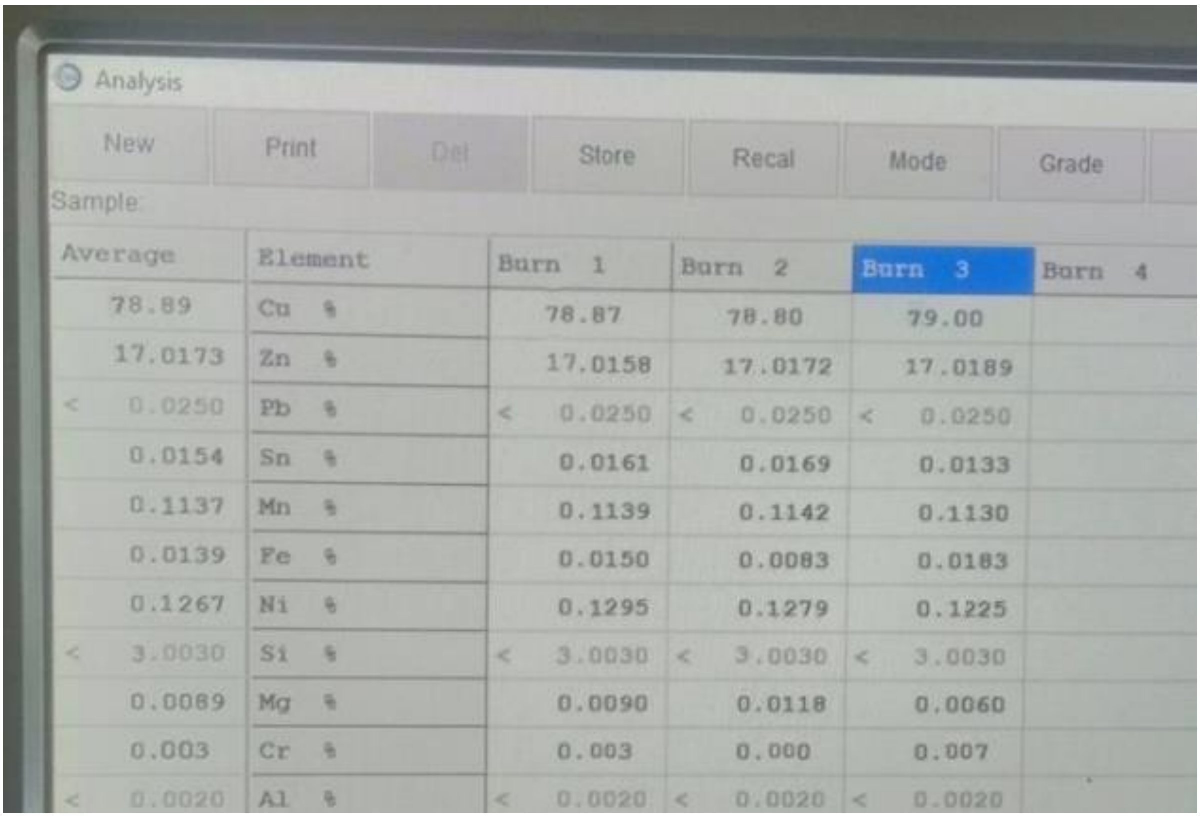

Average	Element	Burn 1	Burn 2	Burn 3	Burn 4
78.89	Cu %	78.87	78.80	79.00	
17.0173	Zn %	17.0158	17.0172	17.0189	
< 0.0250	Pb %	< 0.0250	< 0.0250	< 0.0250	
0.0154	Sn %	0.0161	0.0169	0.0133	
0.1137	Mn %	0.1139	0.1142	0.1130	
0.0139	Fe %	0.0150	0.0083	0.0183	
0.1267	Ni %	0.1295	0.1279	0.1225	
< 3.0030	Si %	< 3.0030	< 3.0030	< 3.0030	
0.0089	Mg %	0.0090	0.0118	0.0060	
0.003	Cr %	0.003	0.000	0.007	
< 0.0020	Al %	< 0.0020	< 0.0020	< 0.0020	

d) Steps Of Vikor Method Computation

			Normalization of the responses						
v	f	d	MRR	CT	Ra	sj	rj	Qj	Rank
82.62032	0.183127	1.25	0.348283321	0.227886167	0.295773017	0.34	0.34	0.5	29
53.12969	0.0966	1.019093	0.096318511	0.151900799	0.136128399	0.33	0.33	0.537124	28
69.87453	0.082449	1.10098	0.116806619	0.185394152	0.108446092	0.303167	0.303167	0.636739	22
67.22859	0.169221	1.246924	0.261234507	0.197599832	0.258643389	0.264591	0.264591	0.779944	12
64.60768	0.14834	1.237477	0.218404971	0.188209404	0.223612322	0.20288	0.20288	1.00904	1
79.89106	0.113354	1.197401	0.199690974	0.210564431	0.171469747	0.262493	0.262493	0.787734	11
57.29791	0.126899	1.126029	0.150774547	0.168062874	0.186958767	0.258679	0.258679	0.801895	10
57.45348	0.128782	1.111374	0.151430823	0.1687513	0.190032726	0.257819	0.257819	0.805086	9
58.9111	0.118143	1.11988	0.143535726	0.169714893	0.171936631	0.268159	0.268159	0.766699	14
62.96019	0.08865	1.118908	0.115006981	0.172341876	0.119509554	0.305524	0.305524	0.627989	23
63.99755	0.08563	1.10355	0.111369539	0.173885122	0.11386945	0.310288	0.310288	0.610303	26
64.7004	0.155225	1.20326	0.222542332	0.189668427	0.234786228	0.222564	0.222564	0.935965	3
70.08904	0.098652	1.128509	0.143696224	0.189051542	0.138623163	0.267949	0.267949	0.767479	13
59.40567	0.110395	1.110542	0.134121186	0.169142423	0.158505556	0.28049	0.28049	0.720924	18
68.35536	0.098761	1.129152	0.140376666	0.185597663	0.138357574	0.272297	0.272297	0.751339	16
67.68958	0.108496	1.153744	0.156037853	0.186243454	0.155829777	0.251785	0.251785	0.827486	6
56.4844	0.092936	1.107562	0.107068601	0.159024282	0.128574521	0.315921	0.315921	0.589392	27
74.29801	0.156652	1.221258	0.261760284	0.208464921	0.242860857	0.253099	0.253099	0.822609	7
80.68575	0.147422	1.234894	0.270503771	0.218212084	0.233198019	0.296713	0.296713	0.660698	21
58.48961	0.095606	1.108284	0.114129922	0.164048266	0.132709	0.306672	0.306672	0.623725	24
74.09645	0.161362	1.20397	0.265091743	0.208924454	0.250473906	0.255155	0.255155	0.814976	8
71.85993	0.114512	1.168245	0.177033776	0.195708158	0.168150758	0.224287	0.224287	0.92957	4
64.31781	0.126367	1.159778	0.173589022	0.182946389	0.186363438	0.228798	0.228798	0.912821	5
70.289	0.088584	1.119438	0.128359631	0.187473836	0.120077454	0.288036	0.288036	0.692911	20

e) Percentage of the F Distribution: F0.05, V1, V2 (F0.05, 3, 6=8.94)

$\nu_1 \backslash \nu_2$	1	2	3	4	5	6	7	8	9	10
1	161.5	199.5	215.7	224.6	230.2	234.0	236.8	238.9	240.5	241.9
2	18.51	19.00	19.16	19.25	19.30	19.33	19.35	19.37	19.38	19.40
3	10.13	9.55	9.28	9.12	9.01	8.94	8.89	8.85	8.81	8.79
4	7.71	6.94	6.59	6.39	6.26	6.16	6.09	6.04	6.00	5.96
5	6.61	5.79	5.41	5.19	5.05	4.95	4.88	4.82	4.77	4.74
6	5.99	5.14	4.76	4.53	4.39	4.28	4.21	4.15	4.10	4.06
7	5.59	4.74	4.35	4.12	3.97	3.87	3.79	3.73	3.68	3.64
8	5.32	4.46	4.07	3.84	3.69	3.58	3.50	3.44	3.39	3.35
9	5.12	4.26	3.86	3.63	3.48	3.37	3.29	3.23	3.18	3.14
10	4.96	4.10	3.71	3.48	3.33	3.22	3.14	3.07	3.02	2.98
11	4.84	3.98	3.59	3.36	3.20	3.09	3.01	2.95	2.90	2.85
12	4.75	3.89	3.49	3.26	3.11	3.00	2.91	2.85	2.80	2.75
13	4.67	3.81	3.41	3.18	3.03	2.92	2.83	2.77	2.71	2.67
14	4.60	3.74	3.34	3.11	2.96	2.85	2.76	2.70	2.65	2.60
15	4.54	3.68	3.29	3.06	2.90	2.79	2.71	2.64	2.59	2.54
16	4.49	3.63	3.24	3.01	2.85	2.74	2.66	2.59	2.54	2.49
17	4.45	3.59	3.20	2.96	2.81	2.70	2.61	2.55	2.49	2.45
18	4.41	3.55	3.16	2.93	2.77	2.66	2.58	2.51	2.46	2.41
19	4.38	3.52	3.13	2.90	2.74	2.63	2.54	2.48	2.42	2.38
20	4.35	3.49	3.10	2.87	2.71	2.60	2.51	2.45	2.39	2.35
21	4.32	3.47	3.07	2.84	2.68	2.57	2.49	2.42	2.37	2.32
22	4.30	3.44	3.05	2.82	2.66	2.55	2.46	2.40	2.34	2.30
23	4.28	3.42	3.03	2.80	2.64	2.53	2.44	2.37	2.32	2.27
24	4.26	3.40	3.01	2.78	2.62	2.51	2.42	2.36	2.30	2.25
25	4.24	3.39	2.99	2.76	2.60	2.49	2.40	2.34	2.28	2.24
30	4.17	3.32	2.92	2.69	2.53	2.42	2.33	2.27	2.21	2.16
40	4.08	3.23	2.84	2.61	2.45	2.34	2.25	2.18	2.12	2.08
50	4.03	3.18	2.79	2.56	2.40	2.29	2.20	2.13	2.07	2.03
100	3.94	3.09	2.70	2.46	2.31	2.19	2.10	2.03	1.97	1.93